



UNIVERSITY OF LEEDS

This is a repository copy of *End Permian to Middle Triassic plant species richness and abundance patterns in South China: Coevolution of plants and the environment through the Permian–Triassic transition*.

White Rose Research Online URL for this paper:

<https://eprints.whiterose.ac.uk/191441/>

Version: Accepted Version

---

**Article:**

Xu, Z, Hilton, J, Yu, J et al. (7 more authors) (2022) End Permian to Middle Triassic plant species richness and abundance patterns in South China: Coevolution of plants and the environment through the Permian–Triassic transition. *Earth-Science Reviews*, 232. 104136. p. 104136. ISSN 0012-8252

<https://doi.org/10.1016/j.earscirev.2022.104136>

---

© 2022 Elsevier B.V. All rights reserved. This manuscript version is made available under the CC-BY-NC-ND 4.0 license <http://creativecommons.org/licenses/by-nc-nd/4.0/>.

**Reuse**

This article is distributed under the terms of the Creative Commons Attribution-NonCommercial-NoDerivs (CC BY-NC-ND) licence. This licence only allows you to download this work and share it with others as long as you credit the authors, but you can't change the article in any way or use it commercially. More information and the full terms of the licence here: <https://creativecommons.org/licenses/>

**Takedown**

If you consider content in White Rose Research Online to be in breach of UK law, please notify us by emailing [eprints@whiterose.ac.uk](mailto:eprints@whiterose.ac.uk) including the URL of the record and the reason for the withdrawal request.



[eprints@whiterose.ac.uk](mailto:eprints@whiterose.ac.uk)  
<https://eprints.whiterose.ac.uk/>

1 End Permian to Middle Triassic plant species richness and  
2 abundance patterns in South China: coevolution of plants and  
3 the environment through the Permian–Triassic transition

4

5 Zhen Xu<sup>a,c</sup>, Jason Hilton<sup>b</sup>, Jianxin Yu<sup>a,\*</sup>, Paul B. Wignall<sup>c</sup>, Hongfu Yin<sup>a</sup>, Qing Xue<sup>a</sup>,  
6 Weiju Ran<sup>a</sup>, Hui Li<sup>d</sup>, Jun Shen<sup>e</sup>, Fansong Meng<sup>f</sup>

7

8 <sup>a</sup> *School of Earth Sciences, State Key Laboratory of Biogeology and Environmental Geology, China*  
9 *University of Geosciences, Wuhan, Hubei 430074, PR China*

10 <sup>b</sup> *School of Geography, Earth and Environmental Sciences and Birmingham Institute of Forest*  
11 *Research, University of Birmingham, Edgbaston, Birmingham B15 2TT, UK*

12 <sup>c</sup> *School of Earth and Environment, University of Leeds, Leeds, LS2 9JT, UK*

13 <sup>d</sup> *Jiangxi Key Laboratory of Mass Spectrometry and Instrumentation, East China University of*  
14 *Technology, Nanchang, Jiangxi 330105, PR China*

15 <sup>e</sup> *State Key Laboratory of Geological Processes and Mineral Resources, China University of*  
16 *Geosciences, Wuhan, Hubei 430074, PR China*

17 <sup>f</sup> *Wuhan Geological Survey Center (Yichang Base), China Geological Survey, Yichang, Hubei 443005,*  
18 *PR China*

19

20 \* Corresponding author. Tel: +86 18986112835; fax: +86 27 67882345.

21 E-mail address: yujianxin@cug.edu.cn (J. Yu)

22

23

24 ABSTRACT This study reviews plant species richness and abundance change from  
25 the End Permian to Middle Triassic in South China and examines the co-evolutionary  
26 relationship between the flora and the environment through this critical interval in the  
27 history of terrestrial biotas. A normalized macro-fossil plant record, that considers  
28 only one taxon per whole plant, is produced. This identifies four broad phases of plant  
29 evolution. Phase 1 is marked by pre-extinction floras that demonstrate a long-term  
30 decline of species richness beginning in the Late Permian (lower Changhsingian) that  
31 culminates in the distinct End Permian Plant Crisis (EPPC) at the end of the  
32 Changhsingian. Other evidence for the health of the flora, including palynology,  
33 biomarkers, wildfire proxies, soil erosion and weathering proxies show a drastic loss  
34 of plant abundance (biomass) and increase of wildfire frequency (suggestive of  
35 increasing seasonal aridity) during the EPPC. A Phase 2 survival interval, during the  
36 Changhsingian–Griesbachian transition, has a severely impoverished plant  
37 assemblage consisting of opportunistic lycopods and a short-lived holdover flora.  
38 Phase 3 (Late Griesbachian–Smithian) saw the modest recovery of species richness as  
39 several groups began to radiate, notably conifers and ferns. Diversity increases  
40 substantially and persistently during the succeeding Phase 4 and sees the dominant  
41 lycopods/herbaceous bryophytes of Phase 3 replaced by conifer-dominated floras.  
42 Plant abundance recovery began earlier than the resumption of coal formation which  
43 only initiated in the Anisian following its disappearance during the EPPC. Only in the  
44 Late Triassic did the flora recover to a level comparable to that seen in the Permian.  
45 The flora of South China thus took ~15 million years to completely recover from the  
46 profound environmental and climatic effects of the Permo-Triassic mass extinction.

47

48 *Keywords:* plant–environment coevolution, mass extinction, coal gap, Permo-Triassic  
49 and end-Permian, gigantopterids, lycopod

50

## 51 1. Introduction

52 The 60 million years from the Middle Permian to the end-Triassic was one of the  
53 most stressful in life’s history. It witnessed the Permo-Triassic Mass Extinction

54 (PTME), the most severe crisis of the Phanerozoic, together with the end-Triassic  
55 mass extinction and several lesser crises (e.g., Wignall, 2015). The result was a  
56 fundamental change of incumbents in both marine and terrestrial realms. Terrestrial  
57 tetrapod dynasties changed several times. The dinocephalians of the Middle Permian  
58 were a distant memory by the time dinosaurs rose to dominance in the Jurassic. The  
59 composition of plant communities also underwent fundamental overhaul during the  
60 Permian and Triassic but the nature of this transition and its relationship with other  
61 biosphere changes has long remained enigmatic (e.g., Knoll, 1984; Rees, 2002). In  
62 particular, it is unclear if plant communities underwent a series of abrupt mass  
63 extinctions, such as seen amongst the marine biota and tetrapods, or instead showed  
64 more gradual long-term changes (McElwain & Punyasena, 2007).

65 In an influential study, Knoll (1984) suggested that there was a protracted  
66 changeover from a Paleophytic to a Mesophytic flora separated by a transitional or  
67 mixed flora, but with no abrupt extinction event at the Permo-Triassic boundary.  
68 Subsequent work suggests that this distinction is between floras from different biomes  
69 and has no chronostratigraphic significance (DiMichele et al., 2008). Nonetheless, the  
70 idea that plants did not suffer mass extinction, even during the Permo-Triassic  
71 transition survives. Many studies based on literature compilations favour a non-  
72 catastrophic floral history at the end of the Permian (e.g., Rees, 2002; Ouyang and  
73 Zhu, 2007; Nowak et al., 2019), and some field studies also support the notion that  
74 there were relatively few losses at this time (e.g., Krassilov & Karasev, 2009; Hochuli  
75 et al., 2010; Xiong & Wang, 2011; Yang et al., 2021). In contrast, there is clear  
76 evidence for a major upheaval in plant communities at the end of the Permian,  
77 including the short-term proliferation of fungal spores (*Reduviasporonites*) at the  
78 expense of plant palynomorphs (Visscher et al., 1996), the abrupt loss of  
79 palynomorphs from woody species suggesting forest die-off (Looy et al., 1999) and  
80 the abrupt and prolonged disappearance of coals from the geological record: a 20 myr  
81 “coal gap” (Retallack, 1995, 1996). Clearly, something happened to plants at the end  
82 of the Permian (Yu et al., 2015).

83 Prior to the PTME, plants are divided into four main paleogeographic regions

84 (e.g., Hilton and Cleal, 2007) whilst low diversity survivors were similar after the  
85 crisis (Grauvogel-Stamm and Ash., 2005; Yu et al., 2015; Feng et al., 2020).  
86 Compositionally, the survivors consist of holdover elements of the late Permian floras,  
87 notably in South China, together with a few, new Triassic forms (Yao et al., 1980;  
88 Chen et al., 2011; Yu et al., 2015). Some have argued, based on the palynological  
89 record from South China, Xinjiang and Greenland, that the main plant crisis occurred  
90 at the end of the Griesbachian, the first substage of the Triassic (Qu et al., 1986;  
91 Zhang et al., 2004; Yu et al., 2008; Peng et al., 2009; Hochuli et al., 2016). If this  
92 proved to be a global phenomenon then the fortunes of plants would be fundamentally  
93 out of kilter with that of terrestrial tetrapods and the marine biosphere (cf. Stanley,  
94 2009; Sun et al., 2012; Song H.J. et al., 2018; Allen et al., 2020; Romano et al., 2020).  
95 It is notable that the onset of the “coal gap”, marking the loss of wetland peat-forming  
96 communities, coincided with the PTME and not the end of the Griesbachian.

97       Following the PTME, floras were of low diversity in the Early Triassic (e.g., Yu et  
98 al., 2015; Feng et al., 2020). Unlike the prosperous Late Triassic floras such as the  
99 Baoding, Jiuliang, Xujiache, Shazhenxi floras in South China, the Early to Middle  
100 floras are poorly understood (Li, 1964; Xu et al., 1979; Huang and Lu, 1992; Meng et  
101 al., 1994; Li et al., 1995). Recent discoveries of Early to Middle Triassic floras have  
102 helped fill in the blanks at this time (Meng et al., 1995; Broutin et al., 2020). Clearly,  
103 we have yet to achieve a full understanding of the dynamics of terrestrial recovery  
104 following the PTME, and questions still remain: were plants marching to a different  
105 beat compared to the marine biota or are the major differences caused by a poor  
106 understanding of the floral record, and why is there a “coal gap” during the Early and  
107 much of the Middle Triassic?

108       To address these questions, we here present a comprehensive review of the  
109 Permian to Triassic fossil plant assemblages of South China supplemented with  
110 extensive additional data from our own field collecting. This region comprises the  
111 Kangdian Oldland to the west and the Cathaysia Oldland to the East that were  
112 separated by the upper Yangtze Platform. Intensive studies during the past few  
113 decades have provided a major increase in our understanding of the flora which have

114 substantially increased our knowledge of changes in low paleolatitudes. We also  
115 incorporate information from other proxies for the health of the terrestrial biosphere.  
116 These include levels of total organic carbon (TOC), weathering proxies, carbon  
117 isotopic variations and black carbon and charcoal concentrations (as wildfire  
118 indicators). Our synthesis of fossil plant occurrences is placed in a detailed  
119 stratigraphic framework and, where available, zircon-derived radiometric dating  
120 (Shen S.Z. et al., 1995, 2011; Burgess et al., 2014; He et al., 2017). Our synthesis of  
121 the floral species richness and abundance differs from previous analyses (e.g., Yu et  
122 al., 2015; Chu et al., 2016; Feng et al., 2020) by normalizing the plant fossil  
123 occurrences to remove duplications that are an artefact of paleobotanical systematics,  
124 preservational types, and taxon recording (see Hilton and Cleal, 2007; Cleal et al.,  
125 2021). This provides a more realistic measure of plant species richness in the fossil  
126 record and unsurprisingly produces a substantially lower estimate of floral species  
127 richness than previous accounts.

128

## 129 2. Materials and methods

130 We use a combination of approaches to evaluate plant species turnover from the  
131 Middle Permian to the early Late Triassic in South China. The successive floras are  
132 documented in stratigraphic order (Fig. 1) and for each we review their stratigraphical  
133 relationships and depositional sedimentary facies to provide a taphonomic context for  
134 the palaeobotanical occurrences.

135

### 136 2.1. *Sampling strategy*

137 Due to an absence of marine fauna and diachronism of plant-bearing units, we use  
138 the concept of an end-Permian plant crisis (EPPC) to represent the point of  
139 disappearance of plant macrofossils in the terrestrial South China successions. The  
140 EPPC is composed of two phenomena. One is the gradual alternation of plant  
141 assemblages during the Changhsingian associated with a gradual decline of species  
142 richness. The second phenomenon was a much more rapid extinction interval, at the

143 end of the Changhsingian, when many long-ranging elements disappeared, and plant  
144 abundance declined markedly.

145 For fossil plants we have adopted two different levels of stratigraphic  
146 resolution. For formations recording the EPPC of the Dalong, Xuanwei and Kayitou  
147 formations (Fig. 1), and its Lower to Middle Triassic aftermath in the Feixianguan,  
148 Lingwen and Badong formations (Fig. 1), we selected representative localities in  
149 terms of their fossil plant composition. For the Xuanwei Formation, we systematically  
150 collected plants from the Chahe and Chinahe sections in Guizhou and Yunnan  
151 provinces, for the Dalong Formation the Xinmin and Duanshan A, B sections in  
152 Guizhou Province, for the Feixianguan Formation the Chinahe, Tucheng and Mide  
153 sections in Yunnan and Guizhou provinces and the Pojiao and Lubei sections in  
154 Yunnan Province, for the Lingwen Formation the Lingwen Section in Hainan  
155 Province, and for the Badong Formation the Hongjiaguan and Furongqiao sections in  
156 Hunan Province. For each formation we have undertaken extensive fieldwork to  
157 identify and collect fossil plants *in situ* on a bed-by-bed basis to investigate them in  
158 stratigraphically high-resolution, with the floras of the Feixianguan being reported  
159 here in detail for the first time. For these formations all the fossils have been  
160 identified by the same individuals using reference materials such that the  
161 identifications are internally consistent and accurate, rather than being based solely on  
162 literature compilation. To reduce the influence of “Signor-Lipps” effect, all the  
163 published plant fossil records from each studied flora in South China are collected and  
164 used in calculating species richness and stratigraphical distributions. We have not  
165 applied statistical methods to correct for the Signor-Lipps effect (e.g. Marshall and  
166 Ward, 1996; Wang et al., 2014) due to the non-uniform rates of deposition,  
167 diachroneity, depositional hiatuses and taphonomic controls in terrestrial strata that  
168 affect fossil plant distribution and preservation. The location of all the included  
169 sections are marked on the paleogeographic map (Fig. 3, 8, 13).

170 For the floras of the Liangshan, Maokou and Longtan formations that predate the  
171 EPPC, and for the Upper Triassic floras of the Jiuligang, Daqiaodi and Dajing  
172 formations (Fig. 1), we have conducted lower-resolution investigations and have

173 summarized the sedimentology and floral compositions, but do not provide detailed  
174 stratigraphic ranges for individual species as that information is not presently  
175 available. Data collected from these sections can only be evaluated at stage level  
176 rather than to show origination and extinction rates within the respective formations.

177

## 178 2.2. *Evaluating fossil plant species richness and normalizing data occurrences*

179 While ideally our study would seek to identify species diversity, it is rarely  
180 possible to determine species evenness from the fossil plant record (Cleal et al., 2012,  
181 2021). Here we focus on species richness that denotes the number of species present  
182 in a particular bed, locality, formation or flora and is measurable from the plant fossil  
183 record (see supplementary dataset). To assess plant species richness, it is necessary to  
184 evaluate patterns of species change over time (e.g., Li et al., 1995; Peng et al., 2009;  
185 Yu et al., 2015; Chu et al., 2016; Feng et al., 2020). This is achieved by constructing  
186 stratigraphic range diagrams for each species showing their first appearance datum (=  
187 origination) and last appearance datum (= extinction) in each geological section, and  
188 then correlating using litho-, bio- or chemostratigraphic methods to compile  
189 stratigraphic range charts. From this information the total number of species can be  
190 determined at particular time intervals, and origination and extinction rates calculated  
191 noting these are when species originate and go extinct in South China within the  
192 dataset. We do not extend the range of plant fossils by calculating confidence intervals  
193 or interpolation due to the complexity of terrestrial stratal deposition and taphonomy,  
194 utilizing the the stratigraphic range of the raw, plant fossil occurrences as recorded in  
195 the field. In order to provide values for the Middle Permian Maokou Flora, we have  
196 also included data from the latest early Permian Qixia Flora to provide range-through  
197 data (e.g., Cleal et al., 2012, 2021). Likewise, to provide the same for the early Late  
198 Triassic Shazhenxi Flora, we have included data from latest Triassic (Rhaetian)  
199 Yangbaichong Flora (see supplementary data for additional details).

200 To meaningfully extract plant species richness patterns from the fossil data, it is  
201 important to eliminate duplicates that are an artefact of paleobotanical nomenclature  
202 (e.g., Hilton and Cleal, 2007; Cleal et al., 2012, 2021). A single reconstructed whole-



203 plant species in the fossil record includes numerous distinct organs (e.g., leaves, stems,  
204 roots, cones, seeds), each with their own generic and species name (see Chaloner,  
205 1986; Bateman and Hilton, 2009). The solution we have adopted is to normalize the  
206 data (see Cleal et al., 2012, 2021) and evaluate only those organs whose fossil  
207 taxonomy is most likely to reflect the original whole organism taxonomy. This  
208 represents the first time this approach has been applied to plant species richness  
209 through the Permo-Triassic interval including the EPPC and its Triassic recovery. All  
210 previous studies have artificially inflated species richness by including names of  
211 organs from the same plant species. Species richness estimates for normalized taxa  
212 uses only one organ for each viable whole plant. The organ selected for normalization  
213 varies depending on the composition of individual fossil plant assemblages and  
214 requires critical evaluation. The process identifies from each systematic group the  
215 organ that and can be reliably identified and is the most diverse, selecting it as the  
216 most representative rather than other organs.

217 Our approach includes omitting accounts of genera that lack species-level  
218 identifications (e.g., *Tomiostrobus* (= *Annalepis*) sp.) from assemblages in which one  
219 or more identified species of the same genus occurs (e.g., *Tomiostrobus* (= *Annalepis*)  
220 *augusta*, *T. (A.) brevicystis*). This assumes that the specimens identified as “sp.” are  
221 likely poorly preserved or incomplete examples of named species. We have also  
222 omitted from species richness estimates fertile organs including gymnosperm seeds  
223 when other organs of the same plants are present in the same assemblage; in all cases  
224 where seeds are present, they co-occur with one or more species of gymnosperm leaf  
225 from which it is assumed that the seeds belonged to one or more of these plants.  
226 Lycopsid rootstock (*Stigmaria*), sporophylls (*Lepidostrobohyllum*) and cones  
227 (*Lepidostrobus*) are also omitted because, in all instances, these co-occur with stems  
228 (*Lepidodendron*) that are more distinctive and are typically identified to the species  
229 level (see Table 1). However, Mesozoic lycopods lack the leafy stems and branches of  
230 Paleozoic arborescent species, while their sporophylls tend to be well-preserved,  
231 systematically distinctive and diverse and so represent the best organ to measure  
232 richness. For Paleozoic sphenophytes we use their leaves (including species of

233 *Annularia*) as they are systematically distinctive and the most diverse organ. However,  
234 leaves of Mesozoic sphenophytes are typically simpler, lack features to reliably  
235 distinguish species, and are of limited diversity so we use their stems and branches to  
236 measure richness as they are more readily distinguished from one another and more  
237 diverse. For “ferns” including members of the Marattiales, as well as gymnosperms  
238 including conifers, cycads and ginkgophytes, vegetative leaves have been used for  
239 normalization as they are reliably identified to species and genus level and in each  
240 case have the highest diversity. The only exceptions are rare instances where whole  
241 plants have been reconstructed in which, irrespective of whatever organ is selected for  
242 normalization, the name of the whole plant is used for that particular occurrence  
243 rather than the name of the isolated organ, following paleobotanical convention (see  
244 Bateman and Hilton, 2009). We accept that normalizing fossil plant data is, to some  
245 extent, subjective and cannot readily be tested for their robustness, but we consider  
246 these data to provide more realistic estimates of paleobotanical species richness than  
247 simple, raw-data based accounts. All data are presented in the supplementary dataset  
248 including information on normalization.

249

### 250 2.3. *Fossil plant abundance*

251 There is no robust method to quantitatively assess plant abundance in terrestrial  
252 settings (Cleal et al., 2021) unless fossil floras are preserved in-situ by obrution events  
253 such as volcanic ash-falls (e.g., Wang et al., 2012). In a broad sense, plant abundance  
254 may be indicated by a number of indirect measures including the number of locations  
255 that contain fossil plants as well as the paleobotanical richness in terms of numbers of  
256 specimens at each location, but these are subject to a variety of controls including  
257 collection intensity, spatial heterogeneity of plant distributions in contemporaneous  
258 settings, and a variety of physical (biostratigraphic, sedimentary) and chemical  
259 taphonomic processes (Bateman, 1991; Allison and Bottjer, 2010). Here we focus on  
260 relative measure of abundance as well as using specific environmental proxies that  
261 provide crude insights into plant abundance in the environment in which they lived.

262 Firstly, having undertaken extensive fieldwork and collections-based

263 investigations on Permian–Triassic plant bearing sedimentary successions from South  
264 China, it is obvious that plant abundance varies considerably. In order not to overlook  
265 evidence for plants, we have considered all plant material, from fragmented plant  
266 debris to intact fossil plant organs because we are interested in assessing the presence  
267 of plants in the sedimentary system. As a crude measure of plant abundance, we use  
268 the relative descriptors absent, very rare, rare, common, abundant and very abundant  
269 to describe the amount of plant fragments encountered in each section in terms of (a)  
270 plant fossils on individual beds, and (b) the number of beds containing fossil plants.

271 Secondly, as coals represent accumulated peat, we consider coals to indicate high  
272 plant abundance for an extended time period. In contrast, the studied interval includes  
273 the Triassic “coal gap” (Retallack et al., 1996). While it is possible that the coal gap  
274 could represent widespread adverse preservation conditions for fossil plants (e.g.,  
275 Vajda et al., 2020), in South China abundant waterlogged, fine grained paralic  
276 sedimentary facies occur in the early Triassic (Yu et al., 2008, 2010, 2015; Bercovici  
277 et al., 2015) that would have been suitable for preserving fossil plants if they were  
278 present in these settings. We therefore interpret the Triassic coal gap to indicate low  
279 plant abundance in paralic depositional sedimentary environments.

280 Thirdly, we consider environmental proxies related to soils on the basis that  
281 abundant vegetation cover is likely to bind soils together and diffuse water infiltration  
282 into the ground, thus having the net result of reducing surface water run-off (Zuazo  
283 and Pleguezuelo, 2009; Davies and Gibling, 2010). In contrast, bare, un-vegetated  
284 ground would be more susceptible to surface water run-off, physical weathering and  
285 erosion (Retallack, 2005; Algeo et al., 2011; Kaiho et al., 2016; Shen et al., 2015,  
286 2022). We therefore use the presence of physical weathering in terrestrial settings as a  
287 rough proxy for plant abundance in terms of ground cover, highlighting the co-  
288 evolution of plants and the environment. Finally, we consider Total Organic Carbon  
289 (TOC) levels in sediments as a crude proxy for terrestrial biomass and plant  
290 abundance with the caveat that it requires careful interpretation because of diagenetic  
291 controls on the value.

292

293 2.4. *Evaluating plant ecology*

294 The geological and paleoecological contexts in which fossil plants occur is  
295 important to their interpretation to provide links between fossil plants and the  
296 environment(s) in which they grew. It also allows greater understanding of the  
297 conditions in which extinction survivors lived, identifying features that may have  
298 contributed to their resilience as well as identifying the locations and environments of  
299 refugia.

300 Paleoecological assessments for plant taxa here come primarily from the available  
301 literature and is based on plant fossil anatomy and morphology and the sedimentary  
302 depositional environments in which they occur (Yao, 1978; Meyen, 1987; Bateman,  
303 1991; Yang, 1993; Yang, 1994; Taylor et al., 2009). Fossil plant specimens were  
304 evaluated for their shape, size and completeness to elucidate their taphonomy in terms  
305 of being transported long, medium or short distances from their growth environment.  
306 For example, entire or almost entire organs lacking signs of taphonomic  
307 fragmentation, abrasion or size-sorting were interpreted as having undergone minimal  
308 transportation. This included in-situ plants and fossil plants found in paleosols, e.g.,  
309 whole plants of *Lepacyclotes* (= *Annalepis*) in the Badong Formation (Meng, 1995).  
310 Greater levels of transport result in higher levels of fragmentation and size sorting and  
311 culminate in fine grained, well sorted plant debris beds such as layers of dispersed  
312 branches of *Neocalamites* in the Badong Formation (Meng, 1995). Depositional  
313 environments of the plant fossil were determined by sedimentary analysis and from  
314 the literature, as well as their paleogeographic location.

315

316 3. Fossil plant occurrences

317 3.1. *Qixia Flora (Artinskian, Cisuralian)*

318 This flora comes from the Liangshan Formation and other strata of the Qixia  
319 regional Stage in South China (Fig. 1), the age of which is roughly Artinskian (late  
320 Cisuralian, Shen S.Z. et al., 2019). Neither the Liangshan Formation nor its plant  
321 assemblage has received much study. This flora consists of a *Emplectopteris*  
322 *triangularis* - *Taeniopteris multinervis* assemblage but lacks gigantopterids,

323 representing the early stage of the Cathayian flora (Li et al., 1995).

324

### 325 3.2. *Maokou Flora (Wordian–Capitanian)*

326 The Maokou Flora (Fig. 1) comes from the Maokou regional Stage in China,  
327 the age of which is roughly Wordian to Capitanian in age (Li et al., 1995 and  
328 references therein). It mainly occurs in southeastern part of South China including  
329 Fujian, Guangxi, Guangdong and Jiangsu provinces and seldomly occurs in eastern  
330 parts of the Yangtze Platform. In the Maokouan (Capitanian Stage), the Cathaysian  
331 (*Gigantopteris*) flora started to develop across South China. The dominant species are  
332 *Gigantonoclea*, *Gigantopteris* and *Gigantopteridium*, while *Tingia*, *Asterophyllites*  
333 and *Cordaites* are common.

334

### 335 3.3. *Longtan Flora (Wuchiapingian)*

336 The Longtan flora (Fig. 1) from the Longtan Formation and lower Xuanwei  
337 Formation is of Wuchiapingian age (Li et al., 1995). It belongs to the Cathaysian  
338 (*Gigantopteris*) flora which steadily become more diverse and widespread during  
339 Wuchiapingian Stage (Li, 1997; Luo et al., 2021). In addition to southeastern parts of  
340 South China, the Cathaysian (*Gigantopteris*) flora spread to the west of the Yangtze  
341 massif including the Xizang (Tibet) and Qinghai areas in the Wuchiapingian.

342

### 343 3.4. *Xuanwei Flora (Changhsingian, latest Permian)*

344 The Xuanwei flora occurs in the upper part of the Xuanwei Formation that crops  
345 out in western Guizhou and Eastern Yunnan provinces (Figs 1–3). It occurs in  
346 siliclastic sediments and coals deposited in paralic settings (Li and Yao, 1980; Yu et  
347 al., 2015; Chu et al., 2016; Shen J. et al., 2019a). It rests stratigraphically on the  
348 Emeishan Basalt (Fig. 2) and is dated to the late Changhsingian (He et al., 2017). In  
349 the Chinahe section, in the Zhehai area (Fig. 2) ash bed zircons have yielded ages  
350  $252.4 \pm 4.1$  Ma and  $252.30 \pm 0.07$  Ma (He et al., 2017; Shen S.Z. et al., 2011; Chu et  
351 al., 2016). The Xuanwei Formation contains abundant fossil plants that represent the  
352 last occurrence of the Cathaysian tropical wetland flora (e.g., Shen G.L., 1995; Hilton

353 and Cleal, 2007; Feng et al., 2020). Of the 35 locations known to preserve fossil plant  
354 assemblages in the Xuanwei Formation (Yu et al., 2015), the sections at Chahe  
355 (Bercovici et al., 2015; Yu et al., 2015) and Chinahe (Fig. 3) are selected for study as  
356 they are amongst the most continuous successions and have been studied in detail.  
357 Fossil plant data from these sections provide statistical information on plant  
358 distribution and evolutionary patterns through the Changhsingian, but information on  
359 evolutionary rates also use data on all fossils from South China reported from this  
360 time interval (see supplementary dataset).

361

#### 362 3.4.1. *Chahe Section (Changhsingian, late Permian)*

363 The Chahe section in Weining County, western Guizhou Province (Figs. 3, 4) has  
364 been well studied (e.g., Yu et al., 2015; Chu et al., 2016). The section exposes the  
365 Xuanwei Formation (Beds 1–70) and overlying Kaiyitou Formation (Beds 71–89) (Fig.  
366 4) and is conformably overlain by the Dongchuan Formation. A zircon U-Pb date of  
367  $252.30 \pm 0.07$  Ma from volcanic ash near the top of the Xuanwei Formation indicates a  
368 latest Permian age (Shen S.Z. et al., 2011), suggesting the Permian–Triassic boundary  
369 (PTB) is in the basal Kayitou Formation. Two layers of volcanic ash, with an  
370 intervening layer of black mudstone, provide a common lithostratigraphic marker for  
371 a level immediately below the Permo-Triassic Boundary in non-marine sections (Chu  
372 et al., 2016).

373 The Xuanwei Formation at the Chahe section contains numerous plant fossils  
374 including the Cathaysian wetland genera *Gigantopteris*, *Lepidodendron*, *Pecopteris*,  
375 and *Fascipteris*. Plant fossils are abundant in the 31 plant-bearing layers (Fig. 4)  
376 before disappearing at Bed 69 in the latest Permian, with only *Peltaspermum* sp.  
377 persisting in Bed 70 above the EPPC level. Fossil plants are absent in the overlying  
378 Kayitou Formation in the Chahe section (Fig. 4).

379

#### 380 3.4.2. *Chinahe Section (Changhsingian, late Permian)*

381 The Chinahe section of eastern Yunnan Province (Fig. 3) starts with the Emeishan  
382 Basalt (Bed 0) and is unconformably overlain by terrestrial facies of the Xuanwei

383 Formation (Beds 1–25). Paralic gray–blue–green mudstone facies of the Kayitou  
384 Formation (Bed 26) conformably overly the Xuanwei Formation (Fig. 5) which in  
385 turn is overlain by the purple red Dongchuan Formation (Wignall et al., 2020).

386 The Xuanwei Formation in the Chinahe section commences with a thick layer of  
387 gray–black mudstone (Bed 1), that contains large amounts of well-preserved plant  
388 fossils (Fig. 5, 6). In Bed 1, *Lobatannularia*, *Pecopteris* and *Gigantopteris* are  
389 common, but the flora in this bed is diverse and also contains a range of sphenopsids  
390 (*Lobatannularia cathaysiana*, *L. heianensis*, *Paracalamites stenocostatus* and  
391 *Schizoneura amnchuriensis*), marattialean ferns (*Pecopteris (Asterotheca)*  
392 *guizhouensis*, *P. (A.) orientalis*, *P. (A.) hemotelioides*, *P. sahnii*, *Fascipteris sinensis*  
393 and *F. hallei*), gigantopterids (*Gigantonoclea guizhouensis*, *G. rosulata*, *Gigantopteris*  
394 *dictyophylloides* and *Gigantopteris nicotianaefolia*), ferns (*Cladophlebis permica*, *C.*  
395 *ozakii*) and occasional gymnosperm leaves (*Neuropteridium* sp., *Peltaspermum* sp.,  
396 *Taeniopteris multinervis*, *Rhipidopsis panii*). Above Bed 1, the lithology changes into  
397 gray yellow or gray green, thin-bedded muddy siltstone and thin coals, pale gray or  
398 gray blue, thin-bedded mudstone and yellow gray fine-grained sandstone (Bed 2–25).  
399 Thin-bedded mudstones developed above coals (in Beds 3, 12, 16, 25) contain some  
400 plants fragments that are not identifiable to species level, but include fragments of  
401 *Lepidostrobophyllum*, gigantopterids, *Compsopteris*, *Pecopteris* and *Taeniopteris*.  
402 Until Bed 25 there are more gray–black, medium bedded, siltstones mixed with shaly  
403 coals as well as gray yellow or green silty-mudstone. Above Bed 25, there are two  
404 gray, thin-bedded mudstones together with a black mudstone layer, which may be  
405 correlative with the sandwich-like lithologies seen in the Chahe section at the  
406 boundary of the Xuanwei and Kaiyitou formations. Above this “sandwich-like”  
407 mudstone layer, a gray–yellow, thin-bedded sandstone and a layer of black siltstone  
408 contains numerous of fragmentary specimens of *Peltaspermum*, *Lepidopteris*,  
409 *Pecopteris* and *Giantopteridium*. In the boundary of the Xuanwei and Kayitou  
410 formations (Bed 26), there is a monotypic layer of dispersed *Tomiostrobus*  
411 (= *Annalepis*) in the dark gray, thin-bedded siltstone (in the bottom of bed 26). After  
412 the layer of *Tomiostrobus* (= *Annalepis*) comes the blue to greenish blue, thick-bedded

413 siltstones of the Kayitou Formation, which contain no plants but abundant  
414 conchostraca and a few horizons of marine bivalves (Fig. 6).

415

### 416 3.5. *Dalong Flora (Changhsingian, late Permian)*

417 The Dalong Formation formed in the western part of the Yangtze shallow sea and  
418 is laterally equivalent to the Heshan Formation in eastern areas (Figs. 2). Fossil plants  
419 from the Dalong Formation were documented by Liu et al. (2007), Song et al. (2013,  
420 2015) and Li et al. (2019). The marine formation consists of thin-bedded cherts,  
421 siltstones, and clays (Shen J. et al., 2012a, 2013; Fig. 7). The chert beds contain both  
422 plant fossils and a marine biota including radiolarian, brachiopods, bivalves,  
423 conodonts, and foraminifera (Fig. 7) that enables correlation with the PTB GSSP at  
424 Meishan (Yin et al., 2007; Shen J. et al., 2012a; Li et al., 2019). Based on conodont  
425 occurrences, the Dalong Formation has been dated to the Changhsingian (Li et al.,  
426 2019). Although the Dalong and Heshan formations are of subtly different age (Figs.  
427 1, 2), they share similar plant fossils and so are discussed together here. From them,  
428 five locations contain plant fossils.

429 From the Dalong Formation we studied the plant fossils from three published  
430 sections: Xinmin, Duanshan A and Duanshan B sections (Fig. 7). In general, the  
431 gymnosperms are well-preserved while the typical Cathaysian floral elements are  
432 more fragmentary and abraded suggesting considerable transport into the depositional  
433 setting. Xinmin is the longest section and, based on the presence of the conodont  
434 *Hindeodus parvus*, is the only section where the Permian–Triassic boundary (PTB) is  
435 well defined (Zhang et al., 2014). In the following account, the Xinmin section is  
436 illustrated as the main section, with the Duanshan A and B sections providing  
437 additional data.

438

#### 439 3.5.1. *Xinmin Section*

440 The Xinmin section in Jiaozishan town, Anshun City, southern Guizhou  
441 Province is 105 km away from the Duanshan A and B sections of the Dalong  
442 Formation (Fig. 3). Lithologies in the Xinmin section (Fig. 7) comprise thin-bedded



443 chert and carbonates including micritic limestones, with siltstone interlayers and  
444 occasional thin, gray–green, volcanic tuff beds (Beds 1–6, Shen J. et al., 2012b; 2021).  
445 Plant fossils mainly come from the black, thin-bedded mudstone interlayers in the  
446 middle of Bed 2 and the top of Bed 4. These comprise large conifer branches  
447 including secondary or tertiary branches that can reach up to 50 cm long and  
448 *Taeniopteris* leaves with good cuticle, amongst smaller, fragmentary fossils of  
449 *Lepidostrobohyllum*, *Paracalamites*, *Pecopteris*, *Gigantopteris*, *Cordaites* and  
450 *Sphenobaiera* (Li et al., 2019). The conifers with well-preserved cuticles have been  
451 identified as *Anshuncladus xinminensis*, *A. contiguous*, *A. aduncatus*, *Pseudoullmania*  
452 *frumentarioides* and *Szecladia multinervis*. Li et al. (2019) interpreted the conifers to  
453 be preserved very close to where they grew, inhabiting coastal habitats, due to their  
454 completeness. These conifers are only preserved in the terrestrial-marine interbedded  
455 facies of the Dalong and Heshan formations and are absent in terrestrial facies rich in  
456 fossil plants (Liu et al., 2007, 2013; Li et al., 2019). In contrast, the fragmentary  
457 *Gigantopteris* and *Pecopteris* leaves in the Dalong Flora were likely transported  
458 greater distances.

459         Based on the presence of the conodont *Hindeodus parvus* in the Dalong  
460 Formation, the PTB is placed in the middle of the limestone at the bottom of Bed 5.  
461 Beds 1 to 6 contain a Permian–Triassic fauna (Fig. 7) including bivalves  
462 (*Hunanopecten exilis* - *H. qujiangensis* in the Permian and *Claraia liuqiaoensis* in the  
463 Triassic), ammonites (*Pseudotirolites* - *Sinoceltites* of the Permian and Triassic  
464 *Xenaspis*), and conodonts (*Clarkina changxingensis*, *C. yini* Permian and *C.*  
465 *meishanensis*, *Hindeodus changxingensis*, *H. parvus* Triassic assemblages) (Zhang et  
466 al., 2014; Yang, 2015; Li et al., 2019). The biostratigraphic evidence shows that this  
467 section is complete (Li et al., 2019).

468

### 469 3.5.2. Duanshan A Section

470         The Duanshan A section is in the same town as the Xinmin section in Huishui  
471 County, Guizhou province (Fig. 3), and the two sections share similar plant as well as  
472 marine faunal records. The section is lithologically divided into eight Beds (Fig. 7)

473 that comprise gray, siliceous mudstone, gray blue, thin-bedded micritic limestone,  
474 with gray black or gray–yellow mudstone interlayers. This is quite similar to the  
475 succession in the Xinmin section, except that Bed 3 is composed of gray yellow  
476 mudstone and white volcanic ash. Beds 1–2 and 4–6 contain the *Hunanopecten exilis*  
477 - *H. qujiangensis* bivalve assemblage, the *Pseudotirolites* - *Sinoceltites* ammonite  
478 assemblage, and the *Albaillella triangularis* - *A. yaoi* radiolarida assemblages (Fig. 7)  
479 and allow us to correlate Beds 3–8 in this section with the middle of Bed 3 to the top  
480 of Bed 4 in the Xinmin section (Fig. 7).

481

### 482 3.5.3. Duanshan B Section

483 The Duanshan B section is on the opposite side of the road to the Duanshan A  
484 section (Fig. 3) and is much shorter. It contains more grayish yellow mudstone and  
485 pelitic siltstone than Duanshan A and shares a similar plant fossil record (Fig. 7).  
486 According to the lithological successions and the location of the Duanshan A and B  
487 sections, Beds 1–6 of Duanshan B corresponds to Bed 3 in Duanshan A (Fig. 7).

488

### 489 3.6. Kayitou Flora (*Griesbachian interval, Permian–Triassic transition*)

490 The Kayitou Formation conformably overlies the Xuanwei Formation and  
491 represents paralic facies (Fig. 1). According to the plant fossils and conchostracan  
492 biostratigraphy and other criteria, the PTB occurs near the base of the Kayitou  
493 Formation (Yu et al., 2010; Chu et al., 2016; Wignall et al., 2020). The Kayitou Flora  
494 occurs in the bottom of the Kayitou Formation, but its exact age is contentious (Chen  
495 et al., 2011). The widespread appearance in south China of the lycopod *Tomiostrabus*  
496 (= *Annalepis*) has been suggested to coincide with the end of the EPPC and the  
497 beginning of Triassic (Yu et al., 2010, 2015). Six sections contain the Kayitou Flora in  
498 South China and have similar plant fossil compositions (Fig. 8). To eliminate the  
499 influence of diachroneity, representative sections containing datable marine biota and  
500 typical plant fossils are selected in this study: the Chinahe, Tucheng and Mide  
501 sections. In general, these sections contain limited occurrences of plant fossils,  
502 typically within single beds and abundance is low. This is noticeably different from

503 plant fossil occurrences prior to the EPPC.

504

### 505 3.6.1. Chinahe Section

506 The Chinahe section in Xuanwei City, eastern Yunnan Province (Figs. 8, 9)  
507 contains terrestrial facies of the Xuanwei Formation (Beds 1–25) and marine facies of  
508 the Kayitou Formation (Bed 26–29). At Chinahe, the EPPC is defined at the level of  
509 disappearance of the Xuanwei Flora together with the last coal line in Bed 25 and the  
510 appearance of *Tomiostrobus* (= *Annalepis*) (Fig. 9) between Beds 25 and 26 at the  
511 lithologic boundary between the Xuanwei and Kayitou formations. The last coal in  
512 the Xuanwei Formation marks the top of the Xuanwei Formation at Chinahe. Bed 26  
513 at the base of the Kayitou Formation contains *Tomiostrobus* (= *Annalepis*) *augusta*, *T.*  
514 (*A.*) *brevicystis*, *T. (A.) latiloba*, *T. (A.) zeilleri*, *T. (A.)* spp., *Sphenopteris tenuis*,  
515 *Fascipteris stena*, *Peltaspermum martinisii*, and fragmentary remains of  
516 *Gigantopteris* spp. and *Pecopteris (Asterotheca) orientalis* that extend their range  
517 from Beds 21 and 24 respectively (Fig. 9). Above this level, plant fossils are  
518 extremely rare and limited to fragments of *Tomiostrobus* (= *Annalepis*) in Bed 27,  
519 which occur above the first occurrence of the bivalve *Pteria variabilis* at this location.  
520 This bivalve also occurs above the EPPC boundary in the Tucheng and Mide sections  
521 (Figs 8, 9). According to the presence of the *Pteria variabilis*-*Promyalina schamarae*  
522 bivalve assemblage in Beds 26–28 (Song T. et al., 2018), the age of plant assemblage  
523 in Beds 26–27 from the Chinahe section is considered to be Griesbachian.

524

### 525 3.6.2. Tucheng Section

526 The Tucheng section in Panxian County, western Guizhou Province (Fig. 8)  
527 exposes a thick coal (Bed 16) of the Xuanwei Formation, and the overlying Kayitou  
528 Formation (Beds 17–23) (Fig. 9; Yu et al., 2015; Broutin et al., 2020). Beds 17–20 are  
529 gray-yellow, thin-bedded mudstone except for Bed 19, a gray-yellow sandstone.  
530 Fossil plants occur in the middle of Beds 17 and 18, and include *Lepidodendron* sp.,  
531 *Tomiostrobus* (= *Annalepis*) *zeilleri*, *T. (A.) brevicystis*, *Pecopteris* sp. and  
532 *Peltaspermum martini*. The upper part of Bed 21 is gray-green, medium-bedded

533 siltstone interbedded with thin beds of mudstone. Bed 22 is a gray-brown, medium-  
534 bedded siltstone, while Bed 23 changes into gray green siltstone and contains  
535 *Sphenopteris* sp., *Peltaspermum mattenii*, *P. lobutalum*, *P. sp.*, *Pecopteris* sp.,  
536 *Gigantonoclea guizhouensis*, *Gigantonoclea* sp., *Gigantopteris dictyophylloides* and  
537 *Gigantopteris* sp. (Fig. 9).

538 Beds 17–23 at Tucheng contain marine fossils including the bivalves *Unionites*  
539 *fassaensis*, *U. canalensis*, *U. sp.*, *Leviconcha orbicularis*, *L. praeorbicularis*, *Pteria*  
540 *ussurica variabilis* and *P. purchisoni leshanensis* (Fig. 9). Correlation with other  
541 sections (Fig. 9), places the termination of the EPPC in the lower middle of Bed 17,  
542 below the first appearance of *Tomiostrabus* (= *Annalepis*).

543

### 544 3.6.3. *Mide Section*

545 The Mide section in Xuanwei City, eastern Yunnan Province (Fig. 8) is  
546 composed of thin-bedded, gray green siltstone (Beds 15–17 and 24–26), while Bed 18  
547 is a thin, white volcanic ash (Fig. 9; Chen et al., 2011; Bercovici et al., 2015). Bed 19  
548 is a yellowish green sandstone and Bed 20 a gray-yellow siltstone. Beds 21–23 are  
549 pale yellow to gray-brown siltstone. Bed 16 contains *Paracalamites stenocoastatus*,  
550 *Gigantonoclea guizhouensis*, *Gigantopteris* sp. Beds 20 and 21 contain *Tomiostrabus*  
551 (= *Annalepis*) *zeilleri*, *T. (A) brevicystis*, *Peltaspermum martensii*, *P. sp.*, *Pecopteris* sp.  
552 and lycopsid roots of *Stigmaria*. Marine biota is abundant in Beds 18–25 (Fig. 9) and  
553 includes the bivalves *Unionites fassaensis*, *U. canalensis*, *U. sp.*, *Leviconcha*  
554 *orbicularia* and *L. praeorbicularis*, the ammonite *Ophiceras* sp. and the ostracod  
555 *Langdaia suboblonga* (Forel et al., 2020). The EPPC termination level occurs at the  
556 beginning of Bed 19 prior to the appearance of *Tomiostrabus* (= *Annalepis*) (Fig. 9).

557

### 558 3.7. *Feixianguan Flora (Dienerian or Smithian, Early Triassic)*

559 The lower part of Feixianguan Formation (Fig. 1) is correlative with the Triassic  
560 portion of the Kayitou Formation (Tong et al., 2019) and conformably overlies the  
561 Xuanwei Formation (Figs. 1, 2). Fossil plants occur at the top of the Feixianguan  
562 Formation one metre below the boundary with the overlying Yongningzhen Formation

563 (Fig. 10). Bivalve data indicate that the age of the fossil plant assemblage in the  
564 Feixianguan Formation is Dienerian or early Smithian (Yin et al., 1985; Gou et al.,  
565 1996; Tong et al., 2019). In South China, only the Feixianguan Formation in the  
566 Pojiao, Lubei sections and the Dongchuan Formation in one section near Lubei  
567 Village (Feng et al., 2018) contain plant fossils of this age and all yield the same flora.  
568 Due to the similar age and floristic composition of the sections of the Dongchuan and  
569 Feixianguan formations, we combine them as one Feixianguan Flora and focus on  
570 describing the Feixianguan sections as much less is known about the flora of the  
571 Dongchuan Formation. In general, the Pojiao and Lubei sections contain limited plant  
572 fossil layers, and each layer yields a few fossil plant fragments. The sedimentary  
573 facies of the Feixianguan Formation comprise interacting terrestrial and marine facies  
574 according to the lithological succession and marine bivalve fossil yielded in the lower  
575 beds below the plant fossil horizons.

576

### 577 3.7.1. *Pojiao Section*

578 The Pojiao section is located in Pojiao village, Huize County, northeastern  
579 Yunnan Province (Fig. 8). It exposes the Feixianguan Formation (Beds 1–9) that  
580 comprises cyclic beds of reddish purple and gray black sandstone (Fig. 10), and the  
581 overlying Yongningzheng Formation (Beds 10–11) that gradually change from gray  
582 green thick-bedded calcareous sandstone (Bed 10), into dark gray limestone (Bed 11).  
583 In the Feixianguan Formation, fossil plants occur in at the top of Bed 9 in two layers of  
584 thin-bedded siltstone interbedded with gray green thick sandstone. These comprise  
585 *Phyllothea* sp., *Neocalamites* sp., *Equisites* sp., *Cladophlebis* sp., *Todites* sp., *Voltzia*  
586 *heterophylla*, *Peltaspermum* sp., *Baiera* sp. and *Taeniopteris* sp. (Fig. 11). The Bed 9  
587 plants are abraded preventing species-level identifications with the exception of  
588 *Peltaspermum* and *Voltzia* from which an almost fertile shoot is known. In this flora  
589 there are abundant gymnosperm seeds, but these are not listed in the range diagram  
590 (Fig. 10) as they most likely represent the seeds of one (or more) of the other  
591 gymnosperms in the flora (i.e., *Voltzia*, *Peltaspermum*, *Baiera*, *Taeniopteris*). The  
592 bottom and middle parts of the Feixianguan Formation at Pojiao are mostly marine

593 facies and contain two bivalve assemblages with the lower *Claraia wangi* assemblage  
594 typical of the early Induan, and the upper *Eumorphotis multiformis* - *Claraia aurita* -  
595 *Claraia stachei* assemblage typical of middle–late Induan of Feixianguan Formation  
596 (Gou et al., 1996; Tong et al., 2019).

597

### 598 3.7.2. Lubei Section

599 The Lubei section in Lubei village, Huize County, northeastern Yunnan Province  
600 (Xu et al., 2017; Shen J. et al., 2019b) is close to Pojiao (Fig. 8). It exposes the late  
601 Permian Xuanwei Formation (Beds 1–3), the early Triassic Feixianguan Formation  
602 (Beds 4–8) and later Early Triassic Yongningzhen Formation (Beds 9–13) (Fig. 10).  
603 The Feixianguan Formation comprises purple red to gray green, thin to medium-  
604 bedded lithic sandstone and siltstone (Xu et al., 2017; Shen J. et al., 2019b). Fossil  
605 plants occur in Beds 5–6 and comprise *Phyllothea* sp., *Neocalamites* sp., *Equisites*  
606 *acanthodon*, *Equisites* sp., *Cladophlebis* sp., *Peltaspermum* sp., *Taeniopteris* sp. and  
607 *Voltzia* sp. (Fig. 11).

608

### 609 3.8. Lingwen Flora (Spathian, Early Triassic)

610 The Lingwen section in Hainan Province (Figs. 1, 8) was previously documented  
611 by Zhou et al. (1979) and Zhang et al. (1992), but the flora has not been investigated  
612 subsequently. Only one section contains the Lingwen Flora in South China. The  
613 Lingwen Flora is considered to have been deposited during the Olenekian based on  
614 plants and palynomorph assemblages that are similar to those from the French  
615 Buntsandstein (Gall and Grauvogel-Stamm, 2005). The flora at Lingwen contains  
616 elements including *Pleuromeia?* sp., *Todites shensiensis*, *Asterotheca szeiana*,  
617 *Ctenozamites cycadea*, *Leuthardtia ovalis*, *Vittaeohyllum* sp., *Albertia*, *Voltzia* and  
618 *Pelourdea* (= *Yuccites*) (See full fossil list in supplementary dataset; Fig. 12) that are  
619 also common in the lower part of the Badong Flora (see below). The sediments of the  
620 Lingwen Formation comprise terrestrial fluvio–lacustrine facies (Zhou et al., 1979;  
621 Zhang et al., 1992).

622

623 3.9. *Badong Flora (Anisian, Middle Triassic)*

624 Plant fossils in the Badong Formation (Fig. 1) were first reported by Ye et al.  
625 (1979) and systematically investigated by Meng et al. (1993, 1995, 1996, 1998). The  
626 Badong Formation has a widespread distribution across the Upper and Middle  
627 Yangtze area in South China (Fig. 13). It conformably overlies the Jialingjiang  
628 Formation (Figs. 1, 14) and comprises five members, but in most areas only three or  
629 four are present due to erosion during Ladinian regression. In Hunan Province, the  
630 Sangzhi County area yields the longest stratigraphic sections especially around the  
631 village of Hongjiaguan (Fig. 13) where an almost continuous section occurs, although  
632 it contains few plant fossils. In contrast, the nearby section in Furongqiao Village  
633 contains abundant plants but is less continuous. These two sections are correlated with  
634 each other and included as the combined Hongjiaguan and Furongqiao section (Fig.  
635 14).

636 Lithologically the Badong Formation comprises pale gray, yellow to gray green  
637 calcareous mudstone to siltstone in Member 1 above a gypsum-karst breccia at the top  
638 of Jialingjiang Formation, and purple red, thick-bedded siltstone to sandstone with  
639 interbedded blue mudstone to siltstone in Member 2 (Fig. 14). Member 3 comprises  
640 gray-yellow calcareous mudstone to siltstone and limestone, and Member 4 purple red,  
641 thick-bedded siltstone to sandstone, while Member 5 comprises gray blue to yellow,  
642 thin-bedded siltstone and gray black, thin-bedded limestone to calcareous siltstone. In  
643 the Hongjiaguan and Furongqiao section, only members 1 and 2 are present (Fig. 14).  
644 The boundary between members 4 and 5 contains the first coal in South China after  
645 the PTB, and thus represents the end of the “coal gap” (Meng et al., 1995; Retallack et  
646 al., 1996). The sedimentary facies of the Badong Formation are coastal or tidal in  
647 members 1, 2, 4 and 5 and the abundant marine biota preserved together with in-situ  
648 ‘mangrove-like’ plants of *Lepacyclotes* (= *Annalepis*) and *Pleuromeia* (Meng et al.,  
649 1995).

650 Fossil plants in the Badong Formation mostly come from the boundary of  
651 members 1 and 2 (Fig. 14), although less common and more poorly preserved fossils  
652 also occur in green blue interlayers in members 2 and 4. We found eight plant fossil

653 locations at Hongjiaguan with four locations combined as one, and four in Furongqiao  
654 Village (Fig. 15). The flora comprises *Lepacyclotes* (= *Annalepis*) *brevicystis*, *L. (A).*  
655 *zeilleri*, *L. (A).* *sangzhiensis*, *L. (A).* *angusta*, *Pleuromeia sanxiaensis*, *P. marginulata*, *P.*  
656 *hunanensis*, *Equisites gracilis*, *Neocalamites shanxiensis*, *Todites shensiensis*,  
657 *Peltaspermum multicostatum*, *P. miracarinum*, *Yuccites vogesiacus*, *Y. anastomosis*,  
658 *Yuccites* sp., *Voltzia heterophylla*, *V. curtifolia*, *V. sp.*, *Willsiostrobus cordiformis*,  
659 *Cardiocarpus triquestrus*, and *C. sp.* (Fig. 15).

660 In Member 1 of the Badong Formation, typical Anisian bivalves of the  
661 *Leptochondria - Myophoria goldfussi mansuyi* assemblage are preserved in siltstones–  
662 mudstones, whilst Member 3 contains the bivalves *Plagiostoma* sp., *Placunopsis* sp.,  
663 the conodonts *Neospathodus* sp. and *Enantiognathus* sp., and the ammonoid  
664 *Progonoceratites* sp. that indicates an Anisian age (Meng et al. 1995).

665

### 666 3.10. Carnian and Norian (Daqiodi and Shazhenxi) flora

667 Carnian and Norian floras are quite common in South China although the  
668 boundary between these stages is poorly constrained. The Carnian/Norian floras are  
669 known from the Daqiadi Formation at Yongren on the border between Yunnan and  
670 Sichuan Provinces, the Jiuligang Formation at Yuan'an in western Hubei Province,  
671 and the Japeila Formation in eastern Xizang Province (Tibet), collectively from over  
672 24 locations in South China; Xujiage Formation at Guangyuan in Sichuan Province,  
673 the Dajing Formation in the border area of Sichuan and Yunnan provinces, the  
674 Anyuan Formation in Hunan and Jiangxi provinces, the Bagong Formation in  
675 southern Fujian Province and the Malugou Formation at Tianqiaoling in Jilin province  
676 (Xu et al., 1979; Li et al., 1995; Liu et al., 2009). The age of this flora is determined  
677 by marine biostratigraphy (Li et al., 1995). The lower part of the flora comprises the  
678 *Abropteris - Pterophyllum longifolium* Assemblage that includes *Equisetites*  
679 *arenaceus*, *Abropteris cottonii*, *Mixopteris intercaearis*, *Pterophyllum longifolium*, *P.*  
680 *jaegeri*, *Angiopteris antiqua*, *Sagenopteris glossopteroides*, *Danaeopsis marantacea*,  
681 *Ctenozamites chinensis*, *Stenopteris bifurcata* and *Ctenozamites chinensis* and  
682 resembles the early Late Triassic Lettenkohle Flora in western Europe (Li et al.,



683 1995). The upper part of the flora comprises the *Dictyophyllum* - *Drepanozamites* or  
684 *Dictyophyllum* - *Cycadocarpidium* Assemblages, including *Dictyophyllum nathorstii*,  
685 *Clathropteris elegans*, *Reteophlebis simplex*, *Drepanozamites nilssonii*,  
686 *Doratophyllum hsuchiahoense*, *Anomozamites loczyi*, *Podozamites (Cycadocarpidium)*  
687 *gigantean*, *Cycadocarpidium swabii* and *Hausmannia ussuriensis*, and thus  
688 considered to be Norian (Li et al., 1995), comparable to the Nariwa Flora of Japan.

689

### 690 3.11. Rhaetian (Yangbaichong) flora

691 The Rhaetian Flora (Fig. 1) is represented by the plant assemblage from the  
692 Yangbaichong Formation at Hengyang in South Hunan province and comprises the  
693 *Ptilozamites* - *Anthrophyopsis* Assemblage. The plant assemblage in the Anyuan  
694 Formation probably belongs to this flora as well and comprises *Ptilozamites chinensis*,  
695 *Anthrophyopsis leeiana*, *Clathropteris meniscioides*, *Todites crenatus*, *Nilssoniopteris*  
696 *oligotricha*, *N. xuiana*, *Pterophyllum ptilum*, *Podozamites distans*, *Cycadocarpidium*  
697 *erdmannii* and *Stalagma samara* (Li et al., 1995). It is comparable to the *Lepidopteris*  
698 zone floras from eastern Greenland and Germany (Zhou et al., 1989), and is  
699 considered to be of Rhaetian age (Li et al., 1995).

700

701

## 702 4. Permo-Triassic vegetation change in South China

703 Artinskian (Middle Permian) to Rhaetian (Late Triassic) macro and micro-floral  
704 stratigraphic range data have been compiled to determine the complete range of plant  
705 taxa present during the End Permian to Middle Triassic before normalization (Figures  
706 18, 19). Then normalized data from the fossil plant ranges in South China from the  
707 Late Permian to the early Late Triassic are analyzed to show species richness and  
708 origination and extinction taxa number for the entire flora (Fig. 18), and origination,  
709 extinction rates of the entire flora together with the rates for individual plant group  
710 (Fig. 19). These data show an increase in total species richness from the Artinskian  
711 (late Cisuralian) and peak species richness in the Wuchiapingian, followed by a  
712 decrease culminating in a diversity lowpoint either side of the PTB (Fig. 18). There is

713 no evidence for a floral crisis in the Capitanian although this may be because our data  
714 is compiled at the stage level, whilst in the marine realm extinction many losses were  
715 intra-Captanian (Bond et al., 2010). The Lower Triassic saw low species richness  
716 (typically <20 species), with values only increasing during the Carnian and Norian  
717 (Upper Triassic) before declining again in the Rhaetian.

718 The plant diversity decline started from the lower Changhsingian with only  
719 species richness decline and flora alternation without apparent vegetation abundance  
720 reduction, characterized by the decline of gigantopterid flora in South China (Yu et al.,  
721 2015). The termination of the EPPC is marked by both these phenomena including the  
722 notable and abrupt drop of species together with cessation of coal formation, marking  
723 the collapse of terrestrial ecosystems (Fig. 22). The low-diversity survivors in the  
724 Kayitou Formation represents a holdover subset of the Cathaysian Flora including  
725 *Lepidodendron*, *Paracalamites*, *Pecopteris*, *Sphenopteris*, *Fasciapteris*, *Gigantopteris*  
726 and *Gigantonoclea*, mixed with the opportunistic lycopod *Tomiostrabus* (= *Annalepis*).  
727 This floral assemblage is only present in the basal-most part of the Kayitou formation  
728 suggesting only a short survival interval. In this regard, they are closely comparable  
729 with the numerous, short-ranging holdover taxa in the marine record which thrived  
730 between two extinction pulses in the early Griesbachian (Song et al., 2012). Previous  
731 analyses of species richness within Paleozoic floras suggest Pennsylvanian wetlands  
732 of Europe (Cleal et al., 2012) had local standing diversity typically in the region of  
733 40–60 species, but with regular species originations and extinctions (Cleal and  
734 Thomas, 2004; Cleal et al., 2012). From our analyses, species richness has been  
735 calculated using data compiled in stage-level time bins and from the pre-EPPC  
736 Xuanwei Flora values and is more comparable to Pennsylvanian regional-scale  
737 richness of the Variscan Foreland with standing diversity of >70 species (Cleal et al.,  
738 2012). Although not from the Permian, these data suggest a standing diversity of the  
739 pre-EPPC Longtan and Xuanwei floras was comparable to Euramerican  
740 Carboniferous peat forming communities, but the early Triassic diversity is  
741 significantly below this level (Fig. 18) and more comparable to diversity of the  
742 Devonian Rhyniophytic and Eophytic evolutionary floras (Cleal and Cascales-Miñana,

743 2014).

744 The species origination rate began to exceed the extinction rate in the Early  
745 Triassic Feixianguan Formation, representing the earliest stage of the species richness  
746 recovery following the EPPC. This interval is characterized by plant populations with  
747 low abundances and an absence of coals. The first post-EPPC coals in South China  
748 are in the Anisian, and their reappearance coincides with that of terrestrial herbivores  
749 (*Lotosaurus*) in Member 2 of the Badong Formation (Meng et al., 1995; Hagen et al.,  
750 2018). In the Upper Triassic, more floras are reported (Li et al., 1995) demonstrating  
751 the continued diversification in humid conditions. Peak Triassic species richness  
752 occurs in the Carnian and Norian when diversity attained a comparable level to that of  
753 the Late Permian (Fig. 18).

754 Overall, late Permian to middle Triassic plant evolution patterns can be resolved  
755 into four distinct phases according to the macro plant fossil data, palynology data,  
756 biomarker and wildfire proxies (Fig. 22). Phase 1 occurred during the Changhsingian  
757 and terminated at the end of the EPPC. Phase 2 consists of the holdover Permian flora  
758 found in the Permian–Triassic transitional Kayitou Formation, including the Chinahe,  
759 Tucheng and Mide sections (Changhsingian–Griesbachian interval). Phase 3  
760 represents the recovery of species richness during the late Induan in the upper part of  
761 the Feixianguan section. Finally, Phase 4 represents substantial recovery after the  
762 Olenekian, as seen in floras of the Lingwen Formation at Lingwen and the Badong  
763 Formation, including the Hongjiaguan and Furongqiao sections.

764

#### 765 4.1. Phase 1: Pre-extinction floras and the EPPC

766 The Changhsingian flora at Chahe (Fig. 3) and Chinahe (Fig. 4) has a typical  
767 Cathaysian character. The fragmented plant assemblage shows considerable turnover  
768 of short-ranging taxa and a final, rapid loss of almost all taxa, including long-ranging  
769 taxa, at the end of the phase. Plant taxa ranges vary between the sections. The minor  
770 losses during the initial episode of the EPPC can be considered a turnover of short-  
771 ranging taxa while the disappearance of long-ranging taxa marks a severe crisis. For  
772 example, the long-ranging elements both in the Chahe and Chinahe sections including

773 *Lobatannularia multifolia*, *Pecopteris orientalis*, *P. arcuata*, *P. gracilenta*, *P.*  
774 *taiyuanensis*, *Rajahia guizhouensis*, *Fasciapteris sinensis*, *Compsopteris contracta*, *C.*  
775 *punctinervis*, *Gigantopteris nicotianaefolia*, *Gigantonoclea largrelii*, *Gigantopteris*  
776 *dictyophylloides* and *Neuropteridium* were common in every layer bearing fossil  
777 plants, until their disappearance at the end of the EPPC marked a dramatic ecological  
778 crisis.

779 Floral assemblages from the Chahe and Chinahe sections lack conifer  
780 macrofossil remains. This phenomenon is quite common in South China with  
781 Guadalupian–Cisuralian floras lacking conifers in terrestrial or terrestrial-marine  
782 sections. Conifers are only found in the fully marine facies of the Dalong Formation  
783 which yields both conifers and the cycadophyte *Taeniopteris* with well-preserved  
784 cuticles (Li et al., 2019). This pattern is in marked contrast to contemporaneous floras  
785 from Europe and North China where conifers occur in terrestrial and terrestrial-  
786 marine facies (Wang et al., 1985, 1996). According to taphonomic features of the  
787 fossils and the sedimentology, the conifers in the Dalong Formation are likely to have  
788 lived in coastal settings or on islands. Species of conifer in the Dalong Formation all  
789 disappear before or during the EPPC and do not reappear in the Triassic. Mesozoic-  
790 type conifers *Voltzia* and *Albertia* appear in South China after the EPPC. Due to lack  
791 of understanding of the evolutionary relationships within Paleozoic and Mesozoic  
792 conifers as whole plants, it is unknown whether stratigraphically younger Triassic  
793 conifers are closely related to the Late Permian conifers from South China.

794 The abrupt abundance reduction of the terminal EPPC is caused by elevated  
795 extinction and declining origination rates that are seen in the entire flora and amongst  
796 each plant group (Fig. 19). Most of the plants from Cathaysian floral communities  
797 disappeared during this event, including Paleozoic lycopods, noeggerathialean  
798 progymnosperms and cordaitalean coniferophytes, leaving only a few survivors. Five  
799 sections from different sedimentary facies allow the details of the plant evolution  
800 pattern to be deciphered: terrestrial facies from the Chahe section in the Xuanwei  
801 Formation, terrestrial-marine transitional facies from the Chinahe section in the  
802 Xuanwei Formation, and marine facies from the Xinmin and Duanshan A and B

803 sections in the Dalong Formation.

804 The EPPC record is that of coal-swamp flora rather than upland taxa (Yu et al.,  
805 2015). Xeric upland taxa took over the empty space after the extinction of coal-  
806 swamp taxa a trend that began slightly before the terminal crisis, as shown by the  
807 gradually increasing proportion of pollen before the EPPC (Yu et al., 2008). Moreover,  
808 the palynological record from the Changhsingian paralic Kayitou Formation in  
809 Yunnan Province (Ouyang, 1991) is similar to the marine Yinkeng Formation in  
810 Meishan section of Zhejiang Province, and other sections in South China (Zhang et al.,  
811 2004). There were few fungal/algal spores before the lithological boundary of the  
812 Permian and Triassic. The palynological record from before the crisis in terrestrial  
813 locations in Xinjiang differs from that in South China, being mainly composed of  
814 gymnosperm pollen, thereby showing an earlier transition from Paleophytic to  
815 Mesophytic flora in this northern area (Qu et al., 1986) (Fig. 22). The crisis in the  
816 Guodikeng Formation in Xinjiang was coupled with an abundance of lycopod spores  
817 (Qu et al., 1986; Chu et al., 2015).

818 Black carbon (BC) content and biomarkers for combustion process such as  
819 polynuclear aromatic hydrocarbons (PAHs) are useful tools for indicating wildfires  
820 (Shen W.J. et al., 2011, 2012; Xie et al., 2007; Chu et al., 2020). In the paralic  
821 Chinahe section, charcoal content peaks in the upper part of Bed 25 to Bed 26 with a  
822 similar peak also seen in the coeval beds 23–24 at Meishan (Fig. 20), although PAHs  
823 peak later in Bed 26 in Meishan (Xie et al., 2007; Shen W.J. et al., 2011) suggesting  
824 there was still fuel for combustion, after the main plant crisis, albeit for a short period  
825 of time (Shen W.J. et al., 2011).

826

#### 827 4.2. Phase 2: Griesbachian interval extinction and survival

828 The Griesbachian plant assemblage from the Kayitou Formation is characterized  
829 by pioneering or opportunistic taxa comprising Mesozoic-type lycopods *Tomiostrobus*  
830 (= *Annalepis*), mixed with holdover taxa including lycopods (*Lepidodendron*),  
831 sphenophytes (*Paracalamites*), ferns (*Pecopteris*) and gigantopterids  
832 (*Gigantopteridium*). This composition is mirrored in palynological data and marked

833 as a distinct, Permian–Triassic transitional flora (Chen et al., 2011; Yu et al., 2015).  
834 The palynological record in the Dalongkou section in Xingjiang (NW China) also  
835 comprises a transitional assemblage, with a mix of Permian and Triassic species, but it  
836 differs from the South China record in having a higher percentage of gymnosperm  
837 pollen (Qu et al., 1986; Ouyang, 1991, 2007). Although holdover elements persist into  
838 the Kayitou Formation, they rarely range more than 30 m above the base in all  
839 sections, whilst most disappear within 5 m. The palynology record confirms the short  
840 duration of survival of the holdover elements, whilst the pioneers persisted for much  
841 longer into the Late Triassic (Ouyang, 1991; Grauvogel-Stamm and Ash., 2005; Yu et  
842 al., 2008, 2010). The survival elements are restricted to refuges, for instance swamp  
843 facies preserved in the paralic Kayitou Formation (Li et al., 1995; Grauvogel-Stamm  
844 and Ash., 2005; Yu et al., 2008).

845 Post EPPC opportunistic plant species abruptly occupied empty niches but  
846 disappeared shortly afterwards following the initial stages of ecosystem recovery. In  
847 addition to holdover and opportunist taxa, the early Induan flora also includes the  
848 surviving seed fern *Peltaspermum* that rapidly recovered after the EPPC in terms of  
849 both its species richness and abundance, together with conifers that gradually radiated  
850 (Whittaker & Goodman, 1979; Huston and Smith, 1987; Glenn-Lewin et al., 1992;  
851 Ren et al., 2001). The success of *Peltaspermum* and conifers marks forest ecosystem's  
852 re-establishment and shows spatial and ecological species richness, such as those from  
853 the late Early Triassic Feixianguan and Lingwen Floras that contain various conifers  
854 (Zhang et al., 1992; Li et al., 1995).

855 Following the dominance of spores over pollen in the early Griesbachian  
856 substage, the percentage of pollen increases in the South China palynological record  
857 (Zhang et al., 2004; Yu et al., 2008; Ouyang and Zhu, 2007). Although there is only a  
858 single, rare megafossil species of *Peltaspermum* in the Kayitou Formation,  
859 palynology indicates the widespread presence of seed plant groups that are absent  
860 from the macrofossil record (Fig. 17).

861 The majority of the plant taxa in Phase 2 are inherited from the Permian  
862 suggesting the Kayitou Flora belongs to the survival stage rather than the recovery

863 stage. Wildfire proxies, such as black carbon, show that wildfires were still prevalent  
864 during this interval (Xie et al., 2007; Shen W.J. et al., 2011, 2012; Yin et al., 2012; Fig.  
865 20),

866 During Phase 2 in the Kayitou Formation, the plant extinction rate is higher than  
867 the origination rate, due to the demise of holdover taxa. This is followed by an  
868 absence of plants fossils from the middle Kayitou Formation to the middle of the  
869 Dongchuan Formation (Feng et al., 2018) (Fig. 1).

870

#### 871 4.3. Phase 3: Late Griesbachian–Smithian species richness recovery

872 Phase 3 marks the start of the post-EPPC recovery and is recorded in the  
873 Dienerian-Smithian Feixianguan Formation. The Feixianguan Formation contains 16  
874 genera and 17 species, thus with low species numbers within individual genera. The  
875 origination rate in the Feixianguan Formation exceeds the extinction rate for the first  
876 time since the EPPC, although extinctions still occurred but at low levels (< 20  
877 species extinctions per time bin). Within individual plant groups (Fig. 19), the  
878 origination rate of Mesozoic lycopod, sphenophyte, cycads, ferns and conifers  
879 noticeably exceeds their extinction rates, whilst the origination rates of seed plants for  
880 example seed ferns, ginkgophytes and some gymnosperms, such as *Pelourdea*  
881 (= *Yuccites*), are similar to the extinction rates.

882 Plant taxa in the Feixianguan Formation consists of small numbers of Mesozoic-  
883 type lycopods, abundant sphenophyll branches (including *Neocalamites* and  
884 *Equisites*), and includes Mesozoic-type ferns (*Todites* spp., *Anomopteris*,  
885 *Dictyophyllum* (= *Thaumatopteris*)), seed ferns (*Peltaspermum* sp.), cycads  
886 (*Taeniopteris* sp.), ginkgophyte (*Baiera* sp., *Sphenobaiera* sp.) and some conifers  
887 (*Albertia* sp., *Voltzia heterophylla*, *Voltzia* sp.) (Zhou et al., 1979; Figs. 10). Most of  
888 the plants, especially *Peltaspermum* and the conifers, are considered to be floral  
889 elements adapted to dry and hot climates based on their thick cuticles (Poort and Kerp,  
890 1990; Huang and Lu, 1992; Taylor et al., 2009).

891 Early Triassic (Late Griesbachian to Smithian) palynological data from South  
892 China is absent whilst the Xinjiang record from North China is derived from from the

893 Jiucaiyuan and Shaofanggou formations (Qu et al., 1986). Spores dominate over  
894 pollen in both formations although the younger levels of the Shaofanggou Formation  
895 have slightly higher pollen content (Qu et al., 1986). The abundance of the Triassic  
896 lycopod spore *Lundbladispora* in those two formations denotes the success of  
897 lycopods during the Griesbachian and Smithian (Qu et al., 1986). Using biomarker  
898 proxies for plant abundance, retene, simonellite and dehydroabietane, which are likely  
899 to be derived from herbaceous rather than woody plants because of low C/N ratios  
900 (<10), suggests recovery was underway during the Smithian (Saito et al., 2013).  
901 Nonetheless, plant fossils are rare and coal formation is still absent during Phase 3.

902

#### 903 4.4. Phase 4: Spathian abundance recovery

904 The Spathian Lingwen flora and the Anisian Badong flora are dominated by  
905 Mesozoic-type lycopods *Lepacyclotes* (= *Annalepis*) and *Pleuromeia* alongside  
906 sphenopsids (*Equisites* and *Neocalamites*), while gymnosperms (*Taeniopteris*,  
907 *Peltaspermum* (*Vittaeophyllum*), *Pelourdea* (= *Yuccites*) and the conifer *Voltzia*) are  
908 common (Figs. 14, 15). Diversity within the Lingwen and Badong formations are  
909 broadly similar to that of the Early Triassic Feixianguan Formation with 22 genera  
910 and 29 species in Lingwen flora and 17 genera and 27 species in Badong flora present.  
911 However, plant abundance is much higher in the Badong Formation, as reflected by  
912 fossil abundance and the development of peat (Meng et al., 1995). Significantly,  
913 Member 2 of the Badong Formation yields the terrestrial tetrapod *Lotosaurus* (Figs.  
914 14, 15), showing there was sufficient vegetation to support large herbivores (Hagen et  
915 al., 2018).

916 According to palynological data in South China, gymnosperm pollen is the major  
917 constituent, especially in the Spathian Lingwen Formation (Zang et al. 1992; Meng et  
918 al. 1995). In the Xinjiang area, gymnosperm pollen content slightly exceeds that of  
919 spores in the Shaofanggou Formation and is increasingly common in the Karamay  
920 Formation of the Xinjiang Dalongkou section. This is similar with the Badong  
921 Formation of South China in the Hongjiaguan section (Qu et al., 1990; Meng et al.,  
922 1995) and indicates progressive vegetation changes during the Spathian. Increased



923 abundance of the conifer derived biomarker pimarane during the Spathian in South  
924 China denotes a vegetation change from the Griesbachian to Smithian  
925 lycophytes/herbaceous bryophytes to conifer-dominated floras (Saito et al., 2013) and  
926 correlates well with gymnosperm pollen dominance of over 90% in Lingwen flora  
927 (Zhang et al., 1992) (Fig. 22). In addition, rapid increases of C/N ratios (>10, reaching  
928 28) after the Smithian-Spathian boundary in South China from the Chaohu section,  
929 reveals the flourishing of vascular land plants (Saito et al., 2013). Plant macro fossils,  
930 palynology and biomarker data all record species richness and abundance recovery  
931 happened after the Spathian.

932

## 933 5. Discussion

### 934 5.1 *Distinctions between macro- and micro-floral (palynology) data*

935 In paleobotanical studies across the PTB in South China, the study of Xiong and  
936 Wang (2011) stands out for documenting a gradual, stepwise loss in plant megafossil  
937 species richness in the run up to the EPPC while concurrent palynological records  
938 only recorded a minor fluctuation in species richness. Their study was based on an  
939 uncritical compilation of data from literature with identifications that were not  
940 verified by examination of original materials, and species were not collected in a  
941 detailed, bed-by-bed stratigraphic framework as undertaken here for the EPPC  
942 interval. In our study, as well as having the extinction level, our megafossil data also  
943 shows a gradual, stepwise loss of megafossil species richness (Figs. 4, 5, 7, 9),  
944 presumably related to gradual facies and/or environmental changes (MacLeod, 1997;  
945 Stevens et al., 2011) in the run up to the extinction level. These environmental or  
946 facies changes adversely affected plants in wetland, peat forming clastic settings (e.g.,  
947 Wang et al., 2011; Yan et al., 2019; Feng et al., 2020), but they do not provide insights  
948 into the vegetation from contemporaneous upland, extrabasinal settings (see  
949 DiMichele et al., 2020) such as the Khangdian Oldland in South China (Fig. 1; Wang  
950 et al., 2020).

951 We consider this is a probable consequence of taphonomic megabias in which the  
952 microfossil record potentially samples a larger geographical source area including

953 uplands compared to megafossil assemblages that are extensively restricted to  
954 lowland depositional settings (e.g., Looy et al., 2004; Neregato et al., 2016;  
955 DiMichele et al., 2020; Cleal et al., 2021). Support for this comes from the  
956 characteristically Mesozoic palynomorphs *Wilsonisporites* (unknown affinity),  
957 *Neoraistrickia* (putative isoetalian lycopsid; Singh 1971) and *Pteruchipollenites*  
958 (corystosperm gymnosperm) found in conglomerates from the basal Xuanwei  
959 Formation (Neregato et al., 2016) whilst the plants that produced them are absent  
960 from the megaflora. This shows their parent plants persisted in South China outside  
961 the coastal wetlands preservation window and survived the EPPC in this region. In  
962 addition, xerophyte palynomorphs recorded in the Chahe section (Yu et al., 2008) are  
963 distinct from the contemporaneous wetland megaflora and include disaccate striatiti  
964 (*Coniferopsida*), *Protohaploxylinus* and *Vittatina* (*Peltaspermales*, *Ginkgopsida*;  
965 Balme, 1995), *Lueckisporites* (*Majonicaceae*, *Coniferopsida*; Clement-Westerhof,  
966 1974), *Striatopodocarpidites* (*Glossopteridales*, *Ginkgopsida*; Pant, 1977; Balme,  
967 1995) and *Taeniaesporites* (= *Lunatisporites*: *Podocarpaceae*, *Coniferopsida*; Clement-  
968 Westerhof, 1974). While first appearing in the late Permian Xuanwei Formation, these  
969 palynomorphs became dominant in the Early Triassic Kayitou Formation where they  
970 played significant roles in post-EPPC floras and the EPPC recovery (Fig. 17).

971 In the Changhsingian, spore producing plants including lycopods, sphenophytes  
972 and ferns were dominant in the megafossil record, while Paleozoic lycopod spores are  
973 absent from the palynology record (Fig. 16, 17). This discrepancy indicates that to  
974 fully characterize the flora information from both sources are required. Palynological  
975 data likely samples flora from a wider setting than just the lowland depositional  
976 environments of the Xuanwei Formation but has limits in reconstructing the affinity  
977 diversity and abundance as it is often hard to correlate palynological species with  
978 parent plants. In contrast, plant macrofossil data tends to record more localized areas  
979 in the Xuanwei Formation in detail, but it does not necessarily represent the  
980 vegetation from the entire basin. The combined macro- and micro-floral data indicates  
981 that the end Permian Changhsingian lowlands of the Xuanwei Formation were  
982 occupied by Paleozoic lycopods, sphenophytes, fern, progymnosperms gigantopterids

983 and seed ferns while the uplands were dominated by other gymnosperms including  
984 conifers, ginkgophytes, cycads and peltaspermalean seed ferns. The proliferation of  
985 fungal spores indicates a widespread land ecosystem crisis in South China during the  
986 EPPC. After the EPPC, lowland floras were left with only a few Paleozoic holdover  
987 taxa and pioneering Triassic lycopods growing in coastal areas, while the uplands saw  
988 the persistence of gymnosperm-like peltasperms, cycadophytes, ginkgophytes and  
989 conifers: a Permo-Triassic transitional flora. Soon after the early Griesbachian, the  
990 survival flora died out in lowland areas, and gymnosperms previously occupying  
991 upland habitats gradually occupied the empty niches and formed what became typical  
992 Mesozoic gymnosperm-dominated floras (Fig. 17). The palynological record shows  
993 this transformation may have started in the late Changhsingian, although it is only  
994 seen in the macrofloral record after the Griesbachian (Fig. 16, 17).

995       Ouyang (1991) noted that about 30–50% of palynology species from the  
996 Permian–Triassic transitional flora at the bottom of the Kayitou Formation in Yunnan  
997 province were holdovers from Permian or older ages and comprised exclusively of  
998 gymnosperm pollen. Of these only 15–17% extended into the later Early Triassic (Fig.  
999 17). We consider these gymnosperm pollen as Methuselah taxa (see Looy et al., 2004;  
1000 Blomenkemper et al., 2018; DiMichele et al., 2020) with unexpectedly early  
1001 stratigraphic occurrences that were living outside the preservationally biased wetland  
1002 settings in ecological niches such as upland fluvial and lacustrine systems less  
1003 affected by the EPPC extinction mechanisms. Further study is required to evaluate the  
1004 taphonomic nature of late Permian palynofloras to confidently identify Methuselah  
1005 taxa, and where possible, match the dispersed spore and pollen accounts to plant  
1006 groups to characterize in detail for the first time the composition of these cryptic  
1007 upland floras.

1008

## 1009 5.2 *Permian–Triassic extinction on land and in ocean*

1010       As to the age of the terminal phase of the EPPC, the Hg/TOC spikes and the  
1011 carbon isotope trends in China and many other terrestrial sections can be correlated  
1012 with the marine GSSP at Meishan (Shen J. et al., 2019b; Chu et al., 2020): a peak of

1013 Hg/TOC was recorded in Meishan Bed 24, and in Bed 26 at Chinahe (Fig. 20). The  
1014 former records the first, severe phase of the marine mass extinction but at Chinahe the  
1015 main plant mass extinction occurs below this in Bed 25 indicating an earlier terrestrial  
1016 crisis. The pioneer lycopod genus *Tomiostrabus* (= *Annalepis*) occurs immediately  
1017 below the Hg/TOC peak and maybe used for correlation due to its stratigraphically  
1018 short-ranging and geographically widespread distribution in South China (Yu et al.,  
1019 2010). Further evidence for this earlier crisis comes from radiometric dating at the  
1020 Chahe section, where the loss of plants occurs in Bed 69. This level is constrained by  
1021 a zircon age from Bed 68 of  $252.30 \pm 0.07$  Ma. This is close to the age of  $252.104 \pm$   
1022  $0.089$  Ma in Bed 22 and  $251.941 \pm 0.037$  Ma in Bed 25 at Meishan (Shen S.Z. et al.,  
1023 2011; Burgess et al., 2014). The first phase of the marine extinction at Meishan  
1024 therefore lagged behind the floral crisis by tens to hundreds of thousands of years (Fig.  
1025 20; Yin et al., 2012; Cui et al., 2017; Dal Corso et al., 2022; Wang Y. et al., 2022).  
1026 This conclusion is supported by the two fungal spore peaks in Bed 66 and 68, and the  
1027 proliferation of gymnosperm pollen in Bed 70 and 78 of the Chahe section (Yu et al.,  
1028 2008). In the marine facies of the Meishan Section, the end Permian to early  
1029 Griesbachian palynological record is more continuous and shows the increasing  
1030 dominance of gymnosperm pollen from Bed 27 (Yu et al., 2008; Zhang et al., 2004)  
1031 after the Permian–Triassic Boundary in the early Griesbachian.

1032 Based on moretane/hopane ( $C_{29}\text{-M}/C_{30}\text{-HP}$ ,  $C_{30}\text{-M}/C_{30}\text{-HP}$ ) ratios and the  
1033 biomarker DBF index ( $\text{DBF}/(\text{DBF}+\text{DBT}+\text{F})$ ), anomalously high terrestrial organic C  
1034 inputs occurred in the latest Permian (Beds 25–26) at Meishan, before gradually  
1035 decreasing in the Early Triassic (Beds 27–30) before increasing again in Bed 34 (Xie  
1036 et al., 2007, 2009; Wang, 2007). According to this timescale, the marine faunal  
1037 extinction episode at the base of Bed 25 at Meishan (Fig. 20) and the marine  
1038 productivity decline before Bed 25 (Song et al., 2012; Shen J. et al., 2015) occurs  
1039 after the terrestrial EPPC, whilst plant abundance declined to its lowest level after  
1040 Meishan Bed 24.

1041

1042 5.3 *Plant and environment co-evolution*

1043 To evaluate the paleoenvironmental influences of the floral changes evaluated  
1044 here, a timescale for environmental events has been compiled through the end  
1045 Permian to Middle Triassic. This is divided into two phases: the Changhsingian to  
1046 Griesbachian interval set against the timescale of the marine Meishan section from  
1047 which precise zircon ages have been determined (Fig. 20), and, with lower  
1048 stratigraphic resolution, the Induan to Anisian interval (Fig. 22).

1049 The EPPC is thought to coincide with a long-term aridification associated with  
1050 the formation of Pangaea beginning in the Middle Permian (Kidder et al., 2004;  
1051 Roscher et al., 2011; Benton et al., 2014; Blomenkemper et al., 2018). Rising  
1052 extinction rates in South China began in the Changhsingian and coincide the start of a  
1053 trend that saw pollen percentages climb (see supplementary dataset for the macro and  
1054 micro spore and pollen plant percentage from Wuchiapingian to Ladinian) (Figs. 16,  
1055 19). Increased charcoal concentrations in the latest Changhsingian suggest aridity  
1056 intensified, likely seasonally, as the climax of the EPPC developed (Shen W.J. et al.,  
1057 2011; Yan et al., 2019; Chu et al., 2020; Cai et al., 2021). The increase of the chemical  
1058 weathering index (CIA) in South China at the same time (e.g. Xu et al., 2017) could  
1059 reflect the loss of plant cover. The increase of fungi could also be caused by more  
1060 prolonged arid episodes (Berdugo et al., 2020).

1061 Increasing drought and climbing temperature could all have weakened the  
1062 gigantopterid (Cathaysian) flora in South China and lead to the the mass extinction  
1063 that marked the culmination of the EPPC. Whether this was a culmination of stresses  
1064 that began in the early Changxingian or if the terminal EPPC was a distinct event,  
1065 with a separate causation, can be debated. However, prior to the rapid warming of  
1066 equatorial, ocean surface-waters in the latest EPPC, temperatures were stable and  
1067 rather cool during the Changxingian (Joachimski et al. 2020) which argues against the  
1068 notion of progressive temperature rise reaching a lethal threshold at the end of the  
1069 EPPC. Instead, the effect of rapid warming appears to have been impact a South  
1070 China flora that was already experiencing diversity decline perhaps due to increasing  
1071 seasonal aridity. Siberian volcanism is generally apportioned the blame for the rapid  
1072 warming episode and other consequences of the eruptions may have been acid rain

1073 and depletion of the ozone layer resulting in increased UVB radiation (Benca et al.,  
1074 2018; Black et al., 2018; Cai et al., 2021; Fig. 21).

1075 Volcanism-induced weathering on land and increasing terrestrial inputs play  
1076 significant role to the marine ecosystem (e.g., Shen J. et al., 2022; Huang et al., 2022).  
1077 Modelling of factors such as volcanism, tectonism, marine redox and acidification,  
1078 cannot explain the extreme hothouse climate in Early Triassic without including the  
1079 terrestrial biome (Mills et al., 2021, Fig. 21). We inferred the enhancement of climate  
1080 instability, seasonal aridity and following loss of lowland peat vegetation during  
1081 EPPC caused the drop of terrestrial biomass storage, probably contributing to the  
1082 carbon cycle fluctuation, while this requires further study of land biomass and global  
1083 carbon cycle.

1084 Wildfire proxies probably indicate the disappearance of the Griesbachian  
1085 interval vegetation after the early Griesbachian (Fig. 20). The initial loss of the  
1086 holdover flora might result in a temporary increase of soil erosion (Fig. 20). The flora  
1087 of this interval was dominated by the herbaceous lycopods *Tomiostrubus* (= *Annalepis*)  
1088 and *Pleuromeia* which, with their shallow rooting systems (Retallack et al., 1975; Yu  
1089 et al., 2010), were likely insufficient to effectively bind soils (Algeo et al., 2011;  
1090 Boyce et al., 2016; Fig. 22).

1091 From our data, plant species richness recovery occurred during the  
1092 Griesbachian to the Smithian stage, while plant abundance indicated by the  
1093 palynology data, biomarkers, TOC and C/N ratio data this aspect began to recover in  
1094 the Spathian (Saito et al., 2013). The first post-EPPC herbivorous tetrapods appeared  
1095 and coal accumulation re-commenced in the Anisian, indicating a return of diverse  
1096 and productive terrestrial ecosystems. The soil erosion proxy also indicates the re-  
1097 stabilization of land surface system after Spathian (Algeo et al., 2011). Diverse marine  
1098 ecosystems were also reestablished at Anisian but full recovery to a pre-extinction  
1099 level was not until the Late Triassic (Song H.J. et al., 2018).

1100

1101 *5.4 Comparison of floristic patterns between low latitude South China and other*  
1102 *geographical areas*

1103 Both the North and South China plates occupied low–middle latitude positions  
1104 during the Late Permian and experienced tropical–subtropical climates (Nowak et al.,  
1105 2020). The Late Permian vegetation from North China was a mixed Cathaysian,  
1106 Euramerican and Angara flora, whilst a typical Cathaysian flora occupied South China  
1107 (Wang et al., 1985; Yu et al., 2015; Wu et al., 2021). In North China terrestrial  
1108 depositional facies have made identification and correlation of the PTB and PTME  
1109 difficult, with recent investigations using radiometric ages from ash beds to confirm  
1110 the End Permian Plant Crisis predates the PTME which concludes with the PTB in the  
1111 uppermost Sunjiagou Formation from the Liujiang Coalfield (Wu et al., 2021; Wang Y.  
1112 et al., 2022). The terrestrial ecosystem collapse in North China commenced  
1113 approximately  $270\pm 150$  kyrs before the marine crisis (Guo et al., 2022), but occurs  
1114 approximately 310 kry later than the terrestrial crisis in high southern latitudes in  
1115 Australia (Lu et al. 2022). Prior to the PTME, the plant macrofossil extinction and  
1116 origination rates in North China are comparable to those of South China and indicate  
1117 significant floral turnover (Xiong et al., 2021). In both areas plant extinction rates  
1118 exceeded origination rate before the EPPC, but in North China the severest plant crisis  
1119 event, which is shown by the biggest value difference between extinction and  
1120 origination rates, occurred before the PTB boundary and may be earlier than South  
1121 China (Xiong et al., 2021), although Lu et al. (2022) considered they may be  
1122 synchronous. After the terrestrial plant crisis and PTME, the earliest Triassic flora in  
1123 North China comprised similar pioneering Triassic isoetalean and Pleuromeia  
1124 lycopods and later in the early Triassic conifer dominated floras (Yu et al., 2015;  
1125 Xiong et al., 2021).

1126 The fossil record from Australia in high latitude Gondwana reveals that the  
1127 *Glossopteris* flora suffered abrupt extinction due to rapid warming and increased  
1128 seasonality somewhat before the Permian–Triassic Boundary (Vajda et al., 2020;  
1129 Frank et al., 2021; Fielding et al., 2022). This ecological disaster reset Paleozoic  
1130 terrestrial phytogeographic provincialism and marked the end to the former separation  
1131 of floras into the low-mid latitude Euramerican and Cathaysian floras and the high-  
1132 latitude Gondwana floras. The peak of plant species richness decline, last coal seam,

1133 and ecosystem collapse indicated by fungal spike in Australia, South and North China  
1134 all denote the onset and main peak of the land plant crisis occurred tens of thousands  
1135 of years before the marine crisis (Yu et al., 2008, 2015; Xiong et al., 2021; Fielding et  
1136 al., 2022). Spikes of fungal spores are common in Australia, South China, and the  
1137 Karoo Basin where they occur at several levels at this time (Visscher et al., 1996;  
1138 Steiner et al., 2003; Ouyang and Zhu, 2007; Yu et al., 2008; Fielding et al., 2022).  
1139 Early Triassic floras from low to high latitudes comprised a uniform lycopod  
1140 dominated flora (e.g. in Australia and South and North China).

1141 In the Kuznetsk Basin in Russia, increased aridity may have affected the  
1142 composition of the Angaran flora, but this region saw floral turnover and migration in  
1143 response to changing climate rather than an extinction event (Davydov et al., 2021).  
1144 The regional extinction of the humidity-adapted, cordaites-dominated flora happened  
1145 approximately 820 kyrs earlier than the PTME marine extinction event in South China  
1146 (Davydov et al., 2021). Following the floral turnover, plants subsequently diversified  
1147 across the Permian–Triassic transition when mixed fern (*Cladophlebis*,  
1148 *Kovuntschania*, *Katasiopteris*, *Kchonomakidium*, *Todites*, *Kedroviella* and  
1149 *Prynadaeopteris*), sphenophyte (*Neokoretrophyllites*, *Schizoneura*, *Paracalamites*)  
1150 peltasperm (*Lepidopteris*), seed fern (*Tersiella* and *Madygenia*), cycad (*Tomia* and  
1151 *Glossozamites*), Ginkgoales (*Rhipidopteris* and *Glossophyllum*), conifer  
1152 (*Quadrocladus*) and Triassic lycopods (*Tomiostrabus*, *Mesenterihyllum*) characterized  
1153 the flora (Davydov et al., 2021).

1154 Comparison between floras in different latitudes and in various distances from  
1155 continental interiors shows that climate instability and expansion of seasonal aridity  
1156 was a significant control on floral composition and distribution through the Permian  
1157 and Triassic transition. The plant mass extinction level occurred over wide areas with  
1158 only the Siberian region recording a diverse flora in the aftermath of the crisis and  
1159 turnover (Davydov et al., 2021). Given the proximity of this region to the flood  
1160 basalts of the Siberian Traps it is ironic that the flora of the Phase 2 interval was so  
1161 diverse. It could be argued that factors that are at their most intense adjacent to  
1162 volcanism, such as acid rain, may not therefore have been an important factor in the



1163 floral mass extinction. Other factors such as a relatively muted temperature rise, in the  
1164 high northern Siberian latitudes, and a persistent humid climate may all have favoured  
1165 this region as a refuge.

1166 In tropical areas such as South China, a rapid temperature rise of over 15°C  
1167 proved fatal, resulting in ocean surface temperatures > 35°C degrees, and possibly >  
1168 42°C on land; such levels are likely to have been directly responsible for the  
1169 extinction losses (Sun et al., 2012). In higher latitudes, the peak temperatures would  
1170 have been lower whilst still exceeding the tolerance of indigenous plants (Fielding et  
1171 al., 2022), although perhaps not in the Siberian region (Davydov et al., 2021). Plants  
1172 living in higher altitudes may also have been more resilient to extreme temperatures  
1173 due to temperatures typically decreasing adiabatically with height. Consequently,  
1174 upland floras were able to colonize lowland settings after the EPPC once competition  
1175 pressures (and temperatures) in these settings were lower following extinction.

1176

## 1177 6. Conclusions

1178 Investigation of plant macrofossil occurrences from the Artinskian to Rhaetian in  
1179 South China has shown that floral species richness declined after the Wuchiapingian  
1180 and experienced a distinct species richness and abundance drop in the Changhsingian  
1181 that we term the End Permian Plant Crisis (EPPC). During the EPPC plant extinction  
1182 rates overtook origination rates, with this scenario continuing into the early Triassic  
1183 although the gap narrowed after the EPPC. The culmination of the EPPC was marked  
1184 by a major extinction with losses of coal-swamp taxa including tree lycopods  
1185 (*Lepidodendron*), sphenopsids (*Lobatannularia*, *Annularia*), Noeggerathiales  
1186 progymnosperms (*Tingia*), Marattiales ferns (*Pecopteris*), gigantopterids  
1187 (*Gigantopteris*) and cordaites gymnosperms (*Cordaites*) which flourished during the  
1188 Late Paleozoic (Phase 1). There seems to have been a hidden upland gymnosperm-  
1189 dominated flora at this time which is not preserved in the macrofossil record but is  
1190 evident in palynological data. Other evidence of terrestrial plants, such as wildfire and  
1191 terrestrial input proxies obtained from marine sections, indicate the climax of the  
1192 terrestrial EPPC predated the marine PTME extinction.

1193 In the early Triassic Kayitou Flora, surviving end-Permian elements were mixed  
1194 with Triassic opportunist herbaceous lycopods with low species richness and  
1195 abundance. We term this the Griesbachian interval flora (Phase 2). Origination rates  
1196 only began to exceeded extinction rates in the late Induan, and this trend continued  
1197 into the Olenekian. The recovery of abundant plant biomass happened later than the  
1198 diversity recovery, and probably commenced during the Spathian as indicated by  
1199 increasing conifer biomarker concentrations and C/N ratios, and continued into the  
1200 Anisian. Triassic floras only attained a comparable species richness in South China to  
1201 the pre-EPPC flora after the Carnian (early Late Triassic). According to the  
1202 origination and extinction rates of each plant family, the flora overall changed from a  
1203 Paleozoic Cathaysian peat forming type into Mesozoic seed plant-dominant type  
1204 which likely reflects an adaption to drier climate.

1205

#### 1206 Declaration of Competing Interest

1207 The authors declare they have no known competing financial interests or  
1208 personal relationships that could have appeared to influence the work reported in this  
1209 paper.

1210

#### 1211 Acknowledgements

1212 We thank Xiao Shi, Wenchao Shu, Meijia Zhang, Xujie Wang, Yuyang Tian  
1213 for fieldwork assistance, Professor Jean Broutin and Qisheng Huang for the plant  
1214 fossil identifications, and Christopher J. Cleal for discussion on methods and species  
1215 richness, and Jiri Bek for discussion on pollen and spore affinities, and Xin Sun,  
1216 Bethany J. Allen for discussion on paleontology diversity method. The manuscript  
1217 benefited from reviews by constructive reviews from Christopher Fielding, Mike  
1218 Benton and two anonymous reviewers. This research was financially supported by the  
1219 NSFC (grants 92055201), the 111 Project (grant BP0820004) and Natural  
1220 Environment Research Council (UK) Biosphere Evolution, Transition and Resilience  
1221 (BETR) program (grant NE/P0137224/1)

1222

1223 References

- 1224 Algeo, T.J., Chen, Z.Q., Fraiser, M.L., Twitchett, R.J., 2011. Terrestrial–marine  
1225 teleconnections in the collapse and rebuilding of Early Triassic marine  
1226 ecosystems. *Palaeogeogr. Palaeoclimatol. Palaeoecol.* 308(1–2), 1–11  
1227 <https://doi.org/10.1016/j.palaeo.2011.01.011>.
- 1228 Allen, B.J., Wignall, P.B., Hill, D.J., Saupe, E.E., Dunhill, A.M., 2020. The latitudinal  
1229 diversity gradient of tetrapods across the Permo-Triassic mass extinction and  
1230 recovery interval. *Proc. R. Soc. Bull.* 287(1929), 20201125  
1231 <https://doi.org/10.1098/rspb.2020.1125>.
- 1232 Allison, P.A., Bottjer, D.J., 2010. *Taphonomy: Process and bias through time* (Second  
1233 Edition). Springer [https://doi.org/10.1007/978-90-481-8643-3\\_1](https://doi.org/10.1007/978-90-481-8643-3_1).
- 1234 Balme, B.A., 1995. Fossil in situ spores and pollen grains: an annotated catalogue.  
1235 *Rev. Palaeobot. Palynol.* 87, 81–323 [https://doi.org/10.1016/0034-](https://doi.org/10.1016/0034-6667(95)93235-X)  
1236 [6667\(95\)93235-X](https://doi.org/10.1016/0034-6667(95)93235-X).
- 1237 Bateman, R.M., 1991. Palaeoecology, in: Cleal, C.J. (Ed.), *Plant Fossils in Geological*  
1238 *Investigation: The Palaeozoic*. Ellis Horwood, London, pp. 34–116.
- 1239 Bateman, R.M., & Hilton, J.M., 2009. Palaeobotanical systematics for the  
1240 phylogenetic age: applying organspecies, form-species and phylogenetic species  
1241 concepts in a framework of reconstructed fossil and extant whole-plants. *Taxon*  
1242 58(4), 1254–1280 <https://doi.org/10.1002/tax.584016>.
- 1243 Bek, J., 2017. Paleozoic in situ spores and pollen. *Lycopsida. Palaeontographica Abt.*  
1244 B 296(1–6), 1–111 <https://doi.org/10.1127/palb/296/2017/1>.
- 1245 Benca, J.P., Duijnste, I., Looy, C.V., 2018. UV-B–induced forest sterility:  
1246 Implications of Ozone shield failure in Earth’s largest extinction. *Sci. Adv.* 4(2),  
1247 e1700618 <https://doi.org/10.1126/sciadv.1700618>.
- 1248 Benton, M.J., Newell, A.J., 2014. Impacts of global warming on Permian–Triassic  
1249 terrestrial ecosystems. *Gond. Res.* 25(4), 1308–1337  
1250 <https://doi.org/10.1016/j.gr.2012.12.010>.
- 1251 Bercovici, A., Cui, Y., Forel, M., Yu, J.X., Vajda, V., 2015. Terrestrial  
1252 paleoenvironment characterization across the Permian–Triassic boundary in

1253 South China. *J. Asian Earth Sci.* 98, 225–246  
1254 <https://doi.org/10.1016/j.jseaes.2014.11.016>.

1255 Black, B.A., Neely, R.R., Lamarque, J., Elkins-Tanton, L.T., Kiehl, J.T., Shields, C.A.,  
1256 Mills, M.J., Bardeen, C., 2018. Systemic swings in End-Permian climate from  
1257 Siberian Traps carbon and sulfur outgassing. *Nat. Geosci.* 11(12), 949–954  
1258 <https://doi.org/10.1038/s41561-018-0261-y>.

1259 Blomenkemper, P., Kerp, H., Hamad, A.A., Dimichele, W.A., Bomfleur, B., 2018. A  
1260 hidden cradle of plant evolution in Permian tropical lowlands. *Science* 362,  
1261 1414–1416 <https://doi.org/10.1126/science.aau4061>.

1262 Bond, D.P.G., Hilton, J.M., Wignall, P.B., Stevens, L.G., Ali, J.R., Sun, Y.D., and Lai,  
1263 X. L., 2010. The Middle Permian (Capitanian) mass extinction on land and in the  
1264 oceans. *Earth-Sci. Rev.* 102, 100–116  
1265 <https://doi.org/10.1016/j.earscirev.2010.07.004>.

1266 Boyce, C.K., Dimichele, W.A., 2016. Arborescent lycopsid productivity and lifespan:  
1267 constraining the possibilities. *Rev. Palaeobot. Palynol.* 227, 97–110  
1268 <https://doi.org/10.1016/j.revpalbo.2015.10.007>.

1269 Broutin, J., Yu, J.X., Shi, X., Shu, W.C., & Xue, Q., 2020. Terrestrial palaeofloral  
1270 succession across the Permian–Triassic boundary in the north and south china  
1271 blocks: a brief review. *Paläontologische Zeitschrift* 94(1), 1–12  
1272 <https://doi.org/10.1007/s12542-020-00511-0>.

1273 Berdugo, M., Delgado-Baquerizo, M., Soliveres, S., Hernández-Clemente, R., Zhao,  
1274 Y.C., Gaitán, J. J., Gross, N., Saiz, H., Maire, V., Lehmann, A., Rilling, M.C.,  
1275 Solé, R.V., Maestre, F.T., 2020. Global ecosystem thresholds driven by aridity.  
1276 *Science* 367(6479), 787–790 <https://doi.org/10.1126/science.aay5958>.

1277 Burgess, S.D., Bowring, S., Shen, S.Z., 2014. High-precision timeline for earth's most  
1278 severe extinction. *Proc. Natl. Acad. Sci. USA* 111(9), 3316–3321  
1279 <https://doi.org/10.1073/pnas.1317692111>.

1280 Cai, Y.F., Zhang, H., Cao, C.Q., Zheng, Q.F., Jin, C.F., Shen, S.Z., 2021. Wildfires and  
1281 deforestation during the Permian–Triassic transition in the southern Junggar  
1282 Basin, Northwest China. *Earth-Sci. Rev.* 218, 103670

1283 <https://doi.org/10.1016/j.earscirev.2021.103670>.

1284 Chaloner, W.G., 1986. Reassembling the whole fossil plant, and naming it. Pages 67–  
1285 78 in Spicer R.A., Thomas, B.A. (Eds), Systematic and taxonomic approaches in  
1286 palaeobotany. Systematics Association Special, Vol 31. Oxford: Oxford  
1287 University Press.

1288 Chen, J.H., Yu, J.X., Huang, Q.S., Broutin, J., Song, Q.Q., Chen, B., 2011. New  
1289 research progress on the paleoflora in the earliest Triassic of western Guizhou  
1290 and eastern Yunnan, South China. Earth Sci. J. China Uni. Geosci. 36(3), 500–  
1291 510 (In Chinese with English abstract).

1292 Chu, D.L., Grasby, S.E., Song, H.J., Corso, J.D., Wang, Y., Mather, T.A., Wu, Y., Song,  
1293 H.Y., Shu, W.C., Tong, J.N., Wignall, P.B., 2020. Ecological disturbance in  
1294 tropical peatlands prior to marine Permian–Triassic mass extinction. Geology 48,  
1295 288–292 <https://doi.org/10.1130/G46631.1>.

1296 Chu, D.L., Tong, J.N., Song, H.J., Benton, M.J., Song, H.Y., Yu, J.X., Qiu, X.C.,  
1297 Huang, Y.F., Tian, L., 2015. Lilliput effect in freshwater ostracods during the  
1298 Permian–Triassic extinction. Palaeogeogr. Palaeoclimatol. Palaeoecol. 435, 38–  
1299 52 <https://doi.org/10.1016/j.palaeo.2015.06.003>.

1300 Chu, D.L., Yu, J.X., Tong, J.N., Benton, M.J., Song, H.Y., Huang, Y.F., Song, T., Tian,  
1301 L., 2016. Biostratigraphic correlation and mass extinction during the Permian–  
1302 Triassic transition in terrestrial-marine siliciclastic settings of South China. Glob.  
1303 Planet. Change 146, 67–88 <https://doi.org/10.1016/j.gloplacha.2016.09.009>.

1304 Cleal, C.J., Cascales-Miñana, B., 2014. Composition and dynamics of the great  
1305 Phanerozoic evolutionary floras. Lethia 47, 469–484  
1306 <https://doi.org/10.1111/let.12070>.

1307 Cleal, C.J., Pardoe, H.S., Berry, C.M., Cascales-Miñana, B., Davis, B.A.S., Diez, J.B.,  
1308 Filipova-Marinova, M.V., Giesecke, T., Hilton, J.M., Ivanov, D.A., Kustatscher,  
1309 E., Leroy, S.A.G., McElwain, J.C., Opluštil, S., Popa, M.E., Seyfullah, L.J. Stolle,  
1310 E., Thomas, B.A., Uhl, D., 2021. Palaeobotanical experiences of plant diversity  
1311 in deep time. 1: How well can we identify past plant diversity in the fossil record?  
1312 Palaeogeogr. Palaeoclimatol. Palaeoecol. 576, 110481

1313 <https://doi.org/10.1016/j.palaeo.2021.110481>.

1314 Cleal, C.J., Thomas, B.A., 2004. Late Carboniferous palaeobotany of the upper  
1315 Bideford Formation, north Devon: a coastal setting for a Coal Measures flora.  
1316 Proc. Geol. Assoc. 115(3), 267–281 [https://doi.org/10.1016/S0016-](https://doi.org/10.1016/S0016-7878(04)80007-5)  
1317 [7878\(04\)80007-5](https://doi.org/10.1016/S0016-7878(04)80007-5).

1318 Cleal, C.J., Uhl, D., Cascales-Miñana, B., Thomas, B.A., Bashforth, A.R., King, S.C.,  
1319 Zodrow, E.L., 2012. Plant biodiversity changes in Carboniferous wetlands.  
1320 Earth-Sci. Rev. 114, 124–155 <https://doi.org/10.1016/j.earscirev.2012.05.004>.

1321 Clement-Westerhof, J.A., 1974. In situ pollen from gymnospermous cones from the  
1322 Upper Permian of the Italian Alps—A preliminary account. Rev. Palaeobot.  
1323 Palynol. 17(1–2), 63–73 [https://doi.org/10.1016/0034-6667\(74\)90092-X](https://doi.org/10.1016/0034-6667(74)90092-X).

1324 Cui, Y., Bercovici, A., Yu, J.X., Kump, L.R., Freeman, K. H., Su, S.G., Vajda, V.,  
1325 2017. Carbon cycle perturbation expressed in terrestrial Permian–Triassic  
1326 boundary sections in South China. Glob. Planet. Change 148, 272–285  
1327 <https://doi.org/10.1016/j.gloplacha.2015.10.018>.

1328 Dal Corso, J., Song, H.J., Callegaro, S., Chu, D.L., Sun, Y.D., Hilton, J., Grasby, S.E.,  
1329 Joachimski, M.M., Wignall, P.B., 2022. Environmental crises at the Permian–  
1330 Triassic mass extinction. Nature Rev. Earth Environ. 1–18  
1331 <https://doi.org/10.1038/s43017-021-00259-4>.

1332 Davies, N.R., Gibling, M.R., 2010. Cambrian to Devonian evolution of alluvial  
1333 systems: the sedimentological impact of the earliest land plants. Earth-Sci. Rev.  
1334 98, 171–200 <https://doi.org/10.1016/j.earscirev.2009.11.002>.

1335 Davydov, V.I., Karasev, E.V., Nurgalieva, N.G., Schmitz, M.D., Budnikov, I.V.,  
1336 Biakov, A.S., Kuzina, D.M., Silantiev, V.V., Urazaeva, M.N., Zharinova, V.V.,  
1337 Zorina, S.O., Gareev, B., Vasilenko, D.V., 2021. Climate and biotic evolution  
1338 during the Permian-Triassic transition in the temperate Northern Hemisphere,  
1339 Kuznetsk Basin, Siberia, Russia. Palaeogeogr. Palaeoclimatol. Palaeoecol. 573,  
1340 110432 <https://doi.org/10.1016/j.palaeo.2021.110432>.

1341 DiMichele, W.A., Bashforth, A.R., Falcon-Lang, H.J., Lucas, S.G., 2020. Uplands,  
1342 lowlands, and climate: Taphonomic megabiases and the apparent rise of

1343 xeromorphic, drought-tolerant flora during the Pennsylvanian–Permian transition.  
1344 *Palaeogeogr. Palaeoclimatol. Palaeoecol.* 559, 109965  
1345 <https://doi.org/10.1016/j.palaeo.2020.109965>.

1346 DiMichele, W.A., Kerp, H., Tabor, N.J., Looy, C.V., 2008. The so-called  
1347 "Paleophytic–Mesophytic" transition in equatorial Pangea—multiple biomes and  
1348 vegetational tracking of climate change through geological time. *Palaeogeogr.*  
1349 *Palaeoclimatol. Palaeoecol.* 268(3), 152–163  
1350 <https://doi.org/10.1016/j.palaeo.2008.06.006>.

1351 Feng, Z., Wei, H.B., Guo, Y., Bomfleur, B., 2018. A conifer-dominated Early Triassic  
1352 flora from Southwest China. *Sci. Bull.* 63, 1462–1463  
1353 <https://doi.org/10.1016/j.scib.2018.09.011>.

1354 Feng, Z., Wei, H.B., Guo, Y., He, X.Y., Sui, Q., Zhou, Y., Liu, H.Y., Gou, X.D., Lv, Y.,  
1355 2020. From rainforest to herbland: New insights into land plant responses to the  
1356 End-Permian Mass Extinction. *Earth-Sci. Rev.* 204, 103153  
1357 <https://doi.org/10.1016/j.earscirev.2020.103153>.

1358 Fielding, C.R., Frank, T.D., Savatic, K., Mays, C., McLoughlin, S., Vajda, V., Nicoll,  
1359 R.S., 2022. Environmental change in the late Permian of Queensland, NE  
1360 Australia: The warmup to the end-Permian Extinction. *Palaeogeogr.*  
1361 *Palaeoclimatol. Palaeoecol.* 594, 110936  
1362 <https://doi.org/10.1016/j.palaeo.2022.110936>.

1363 Forel, M., Bercovici, A., Yu, J.X., 2020. Ostracods after the End-Permian extinction in  
1364 South China: insights into non-microbial survival. *Micropaleont.* hal–03098322f.

1365 Frank, T.D., Fielding, C.R., Winguth, A.M.E., Savatic, K., Tevyaw, A., Winguth, C.,  
1366 McLoughlin, S., Vajda, V., Mays, C., Nicoll, R., Bocking, M., Crowley, J.L.,  
1367 2021. Pace, magnitude, and nature of terrestrial climate change through the end-  
1368 Permian extinction in southeastern Gondwana. *Geology* 49(9), 1089–1095  
1369 <https://doi.org/10.1130/G48795.1>.

1370 Gall, J.C., Grauvogel-Stamm, L., 2005. The early Middle Triassic 'Grès à Voltzia'  
1371 Formation of eastern France: a model of environmental refugium. *C. R. Palevol.*  
1372 4, 637–652 <https://doi.org/10.1016/j.crpv.2005.04.007>.

- 1373 Glenn-Lewin, D.C., Peet, R.K., Veblen, T.T. (Eds.), 1992. Plant succession: theory  
1374 and prediction. Chapman and Hall, London, ss 352.
- 1375 Gou, Z.H., Lin, M.B., 1996. The bivalve fauna of Feixianguan Formation in Majiaoba  
1376 area, Jiangyou, Sichuan. J. Chengdu Inst. Tech. 23(4), 80–84 (In Chinese with  
1377 English abstract).
- 1378 Grauvogel-Stamm, L., Ash, S.R., 2005. Recovery of the Triassic land flora from the  
1379 End-Permian life crisis. Comptes. Rendus. Palevol. 4(6–7), 593–608  
1380 <https://doi.org/10.1016/j.crpv.2005.07.002>.
- 1381 Grice, K., Twitchett, R.J., Alexander, R., Foster, C.B., & Looy, C., 2005. A potential  
1382 biomarker for the Permian–Triassic ecological crisis. Earth Planet. Sci. Lett.  
1383 236(1–2), 315–321 <https://doi.org/10.1016/j.epsl.2005.05.008>.
- 1384 Guo, W.W., Tong, J.N., He, Q., Hounslow, M.W., Song, H.J., Dal Corso, J., Wignall,  
1385 P.B., Ramezani, J., Tian, L., Chu, D.L., 2022. Late Permian–Middle Triassic  
1386 magnetostratigraphy in North China and its implications for terrestrial-marine  
1387 correlations. Earth Planet. Sci. Lett. 585, 117519  
1388 <https://doi.org/10.1016/j.epsl.2022.117519>.
- 1389 Hagen, C.J., Roberts, E.M., Sullivan, C., Liu, J., Wang, Y., Owusu Agyemang, P.C.,  
1390 Xu, X., 2018. Taphonomy, geological age, and Paleobiogeography of *Lotosaurus*  
1391 *Adentus* (Archosauria: Poposauroida) from the Middle–Upper Triassic Badong  
1392 Formation, Hunan, China. Palaios 33(3), 106–124  
1393 <https://doi.org/10.2110/palo.2017.084>.
- 1394 He, B.H., Liu, S.F., Wu, P., 2017. LA-ICP-MS U-Pb geochronology and its geological  
1395 implications of the detrital Zircons from the lower strata of Upper Permian  
1396 Xuanwei Formation in Zhehai Town, Eastern Yunnan Province. North China  
1397 Geol. 40(2), 126–133 (In Chinese with English abstract)  
1398 <https://doi.org/10.3969/j.issn.1672-4135.2017.02.006>.
- 1399 Hilton, J.M., and Cleal, C.J., 2007. The relationship between Euramerican and  
1400 Cathaysian tropical floras in the Late Palaeozoic: palaeobiogeographical and  
1401 palaeogeographical implications. Earth-Sci. Rev. 85(3–4), 85–116  
1402 <https://doi.org/10.1016/j.earscirev.2007.07.003>.



1403 Hochuli, P.A., Hermann, E., Vigran, J.O., Bucher, H., Weissert, H., 2010. Rapid  
1404 demise and recovery of plant ecosystems across the End-Permian extinction  
1405 event. *Glob. Planet. Change* 74(3–4), 144–155  
1406 <https://doi.org/10.1016/j.gloplacha.2010.10.004>.

1407 Hochuli, P.A., Sanson-Barrera, A., Schneebeili-Hermann, E., Bucher, H., 2016.  
1408 Severest crisis overlooked—Worst disruption of terrestrial environments  
1409 postdates the Permian–Triassic Mass Extinction. *Sci. Rep.* 6(1), 28372  
1410 <https://doi.org/10.1038/srep28372>.

1411 Huang, Q.S., Lu, S.M., 1992. The primary studies on the palaeoecology of the Late  
1412 Triassic Xujiahe Flora in eastern Sichuan. *Earth Sci. J. China Uni. Geosci.* 17(3),  
1413 329–335.

1414 Huang, Y.F., He, W.H., Liao, W., Wang, Y.B., Yi, Z.X., Yang, H., Li, G.S., 2022. Two  
1415 pulses of increasing terrestrial input to marine environment during the Permian–  
1416 Triassic transition. *Palaeogeogr. Palaeoclimatol. Palaeoecol.* 586, 110753  
1417 <https://doi.org/10.1016/j.palaeo.2021.110753>.

1418 Huston, M., Smith, T., 1987. Plant succession: life history and competition. *Am. Nat.*  
1419 130(2), 168–198.

1420 Jin, Y.X., Shang, Q.H., Hou, J.P., Li, L., Wang, Y.J., Zhu, Z.L., Fei, S.Y., 2000.  
1421 Stratigraphical lexicon of China: Permian System. *Geol. Publ. Beijing* (In  
1422 Chinese).

1423 Joachimski, M.M., Alekseev, A.S., Grigoryan, A., Gatovsky, Y.A., 2020. Siberian Trap  
1424 volcanism, global warming and the Permian-Triassic mass extinction: New  
1425 insights from Armenian Permian-Triassic sections. *Geol. Soc. Am. Bull.* 132(1-  
1426 2), 427–443 <https://doi.org/10.1130/B36214.1>.

1427 Kaiho, K., Saito, R., Ito, K., Miyaji, T., Chen, Z.Q., 2016. Effects of soil erosion and  
1428 anoxic–euxinic ocean in the Permian–Triassic marine crisis. *Heliyon* 2(8), e00137  
1429 <https://doi.org/10.1016/j.heliyon.2016.e00137>.

1430 Kidder, D.L., Worsley, T.R., 2004. Causes and consequences of extreme Permo-  
1431 Triassic warming to globally equable climate and relation to the Permo-Triassic  
1432 extinction and recovery. *Palaeogeogr. Palaeoclimatol. Palaeoecol.* 203(3–4),

1433 207–237 [https://doi.org/10.1016/S0031-0182\(03\)00667-9](https://doi.org/10.1016/S0031-0182(03)00667-9).

1434 Knoll, A.H., 1984. Patterns of extinction in the fossil record of vascular plants, in:

1435 Nitecki, M.H. (Ed.), *Extinctions*. University of Chicago Press, Chicago, pp. 1–68.

1436 Krassilov, V., Karasev, E., 2009. Paleofloristic evidence of climate change near and

1437 beyond the Permian–Triassic boundary. *Palaeogeogr. Palaeoclimatol. Palaeoecol.*

1438 284(3–4), 326–336 <https://doi.org/10.1016/j.palaeo.2009.10.012>.

1439 Li, H., Yu, J.X., McElwain, J.C., Yiotis, C., Chen, Z.Q., 2019. Reconstruction of

1440 atmospheric CO<sub>2</sub> concentration during the late Changhsingian based on fossil

1441 conifers from the Dalong Formation in South China. *Palaeogeogr. Palaeoclimatol.*

1442 *Palaeoecol.* 519, 37–48 <https://doi.org/10.1016/j.palaeo.2018.09.006>.

1443 Li, P.J., 1964. Fossil plant from the Hsuchiaho Series of Kwangyuan, northern

1444 Szechuan. *Mem. Inst. Geol. Palaeont. Acad. Sin.* 3, 101–78.

1445 Li, X.X., Zhou, Z.Y., Cai, C.Y., Sun, G., Ouyang, S., Deng, L.H., 1995. Fossil floras

1446 in China through the geological ages (English edition). Guangdong Sci. Tech.

1447 Press, Guangzhou, pp. 1–695 <http://ir.nigpas.ac.cn/handle/332004/7973>.

1448 Li, X.X., 1997. The origin, evolution and distribution of the Cathaysian flora in East

1449 Asia. *Acta Palaeontol. Sin.* 36(4), 411–422 (In Chinese and English).

1450 Li, X.X., Yao, Z.Q., 1980. Permian coal-bearing formations in South China. *J. Stratigr.*

1451 4, 241–255 (In Chinese).

1452 Liu, D.D., Yang, Z.R., Yang, Y.D., Bao, Y.Y., Liu, B., 2009. Characteristic of the flora

1453 in the Zhenzhuchong Formation and the Jurassic–Triassic boundary in the

1454 Sichuan Basin. *J. Earth Sci. Environ.* 31(3), 254–259 (In Chinese with English

1455 abstract).

1456 Liu, L.L., Yao, Z.Q., 2013. The conifer-remains from the Permian of South China.

1457 *Acta Palaeontol. Sin.* 52(2), 182–201.

1458 Liu, L.J., Yao, Z.Q., 2007. Plant megafossils from the Permian Changhsingian marine

1459 deposits of Fusui, Guangxi, China. *Acta Palaeontol. Sin.* 46(2), 195–212.

1460 Looy, C.V., Brugman, W.A., Dilcher, D.L., Visscher, H., 1999. The delayed

1461 resurgence of equatorial forests after the Permian–Triassic ecologic crisis. *Proc.*

1462 *Natl. Acad. Sci. USA* 96(24), 13857–13862

1463 <https://doi.org/10.1073/pnas.96.24.13857>.

1464 Looy, C., Kerp, H., Duijnste, I., DiMichele, B., 2014. The late Paleozoic ecological-  
1465 evolutionary laboratory, a land-plant fossil record perspective. *Sedimentary Rec.*  
1466 12(4), 4–18 <https://doi.org/10.2110/sedred.2014.4>.

1467 Lu, J., Wang, Y., Yang, M.F., Zhang, P.X., Bond, D.P.G., Shao, L., Hilton, J. 2022.  
1468 Diachronous end-Permian terrestrial ecosystem collapse caused by catastrophic  
1469 wildfires. *Palaeocol. Palaeogeog. Palaeoclimatol.* 594, 110960  
1470 <https://doi.org/10.1016/j.palaeo.2022.110960>.

1471 Luo, C.K., Yang, R.D., Gao, L., Wang, L.B., Zhou, D.F. 2021. Systematics and  
1472 palaeoecology of fossil plants from the Upper Permian Longtan Formation in  
1473 western Guizhou Province, southwest China. *Hist. Biol.* 1–13  
1474 <https://doi.org/10.1080/08912963.2021.1884244>.

1475 MacLeod, N., Rawson, P.F., Forey, P.L., Banner, F.T., Boudagher-Fadel, M.K., Bown,  
1476 P.R., Burnett, J.A., Chambers, P., Culver, S., Evans, S.E., Jeffery, C., Kaminski,  
1477 M.A., Lord, A.R., Milner, A.C., Milner, A.R., Morris, N., Owen, E., Rosen, B.R.,  
1478 Smith, A.B., Taylor, P.D., Urquhart, E., & Young, J.R., 1997. The Cretaceous–  
1479 Tertiary biotic transition. *J. Geol. Soc.* 154, 265–293  
1480 <https://doi.org/10.1144/gsjgs.154.2.0265>.

1481 Marshall, C.R., Ward, P.D., 1996. Sudden and gradual molluscan extinctions in the  
1482 latest Cretaceous of Western European Tethys. *Science* 274, 1360–1363  
1483 <https://doi.org/10.1126/science.274.5291.1360>.

1484 McElwain, J.C., & Punyasena, S.W., 2007. Mass extinction events and the plant fossil  
1485 record. *Trends Ecol. Evol.* 22(10), 548–557  
1486 <https://doi.org/10.1016/j.tree.2007.09.003>.

1487 Meng, F.S., 1993. The *Annalepis–Pleuromeia* plant assemblage in South China and  
1488 the significance of it. *Chinese Sci. Bull.* 38(18), 1686–1688 (In Chinese).

1489 Meng, F.S., 1994. Discovery of *Pleuromeia–Annalepis* flora in South China and its  
1490 significance. *Chinese Sci. Bull.* 02, 44–48.

1491 Meng, F.S., 1996. Floral palaeoecological environment of the Badong Formation in  
1492 the Yangtze Gorges area. *Geol. Miner. Resour. South China* 4, 1–13 (In Chinese)

- 1493 with English abstract).
- 1494 Meng, F.S., 1998. Studies on *Annalepis* from Middle Triassic along the Yangtze River  
1495 and its bearing on the origin of *Isoetes*. Acta Bot. Sin. 40(8), 768–774.
- 1496 Meng, F.S., Xu, A.W., Zhang, Z.L., Lin, J.M., Yao, H.Z., 1995. Nonmarine biota and  
1497 sedimentary facies of the Badong Formation in the Yangtze and its neighbouring  
1498 areas. China Uni. Geosci. Press, Wuhan, pp. 1–76 (In Chinese with English  
1499 abstract).
- 1500 Meyen, S.V., 1987. Fundamentals of palaeobotany. Chapman and Hall, London.
- 1501 Mills, B.J.W., Tennenbaum, S., Schwartzman, D., 2021. Exploring multiple steady  
1502 states in Earth's long-term carbon cycle. Am. J. Sci. 321(7), 1033–1044  
1503 <https://doi.org/10.2475/07.2021.01>.
- 1504 Neregato, R., D'Apolito, C., Glasspool, I.J., Wang, S.J., Liu, F., Windslow, P., Lu, J.,  
1505 Shao, L.Y., Hilton, J., 2016. Palynological constraints on the provenance and  
1506 stratigraphic range of a Lopingian (Late Permian) inter-extinction floral  
1507 lagerstätte from the Xuanwei Formation, Guizhou Province, China. Int. J. Coal  
1508 Geol. 162, 139–150 <https://doi.org/10.1016/j.coal.2016.06.005>.
- 1509 Nowak, H., Schneebeil-Hermann, E., Kustatscher, E., 2019. No mass extinction for  
1510 land plants at the Permian–Triassic transition. Nat. Commun. 10(1), 1–8  
1511 <https://doi.org/10.1038/s41467-018-07945-w>.
- 1512 Nowak, H., Vérard, C., Kustatscher, E., 2020. Palaeophytogeographical patterns  
1513 across the Permian–Triassic boundary. Front. Earth Sci. 8, 609  
1514 <https://doi.org/10.3389/feart.2020.613350>.
- 1515 Ouyang, S., 1991. Transitional palynofloras from basal lower Triassic of China and  
1516 their ecological implications, with special reference to Paleophyte/Mesophyte  
1517 problems. Palaeoecology of China 1. Nanjing Uni. Press, Nanjing, pp. 168–196  
1518 <http://ir.nigpas.ac.cn/handle/332004/9027>.
- 1519 Ouyang, S., Zhu, H.C., 2007. Query the assumption of "End-Permian Fungal Spike  
1520 Event", with special reference to the Permo-Triassic transitional palynofloras.  
1521 Acta Palaeontol. Sin. 46(4), 394–410.
- 1522 Peng, Y., Shi, G.R., 2009. Life crises on land across the Permian–Triassic boundary in

- 1523 South China. *Glob. Planet. Change* 65, 155–165  
1524 <https://doi.org/10.1016/j.gloplacha.2008.10.016>.
- 1525 Poort, R.J., Kerp, J.H.F., 1990. Aspects of Permian palaeobotany and palynology. XI.  
1526 On the recognition of true peltasperms in the Upper Permian of Western and  
1527 Central Europe and a reclassification of species formerly included in  
1528 *Peltaspermum* Harris. *Rev. Palaeobot. Palynol.* 63(3–4), 197–225  
1529 [https://doi.org/10.1016/0034-6667\(90\)90100-W](https://doi.org/10.1016/0034-6667(90)90100-W).
- 1530 Qu, L.F., 1990. Palynological assemblages of Middle and Late Triassic in Sangzhi,  
1531 Hunan, and their stratigraphical significance. *J. Strati. Paleotol.* 23, 81–95 (In  
1532 Chinese with English abstract).
- 1533 Qu, L.F., Wang, Z., 1986. Triassic spores and pollen, in: Zhou, H.Q. (Ed.), Permian  
1534 and Triassic strata and fossil assemblages in the Dalongkou area of Jimsar,  
1535 Xinjiang. Geological Publ. Beijing, pp. 113–173 (in Chinese with English  
1536 summary).
- 1537 Rees, P.M., 2002. Land-plant diversity and the End-Permian Mass Extinction.  
1538 *Geology* 30(9), 827–830 [https://doi.org/10.1130/0091-](https://doi.org/10.1130/0091-7613(2002)030<0827:LPDATE>2.0.CO;2)  
1539 [7613\(2002\)030<0827:LPDATE>2.0.CO;2](https://doi.org/10.1130/0091-7613(2002)030<0827:LPDATE>2.0.CO;2).
- 1540 Ren, H., Cai, X.A., Rao, X.Q., Zhang, Q.M., Liu, S.Z., 2001. The theory on  
1541 succession of plant community. *Ecol. Sci.* 20(4), 59–67 (In Chinese with English  
1542 Abstract).
- 1543 Retallack, G.J., 1975. The life and time of a Triassic lycopod. *Alcheringa* 1, 3–29  
1544 <https://doi.org/10.1080/03115517508619477>.
- 1545 Retallack, G.J., 1995. Permian–Triassic life crisis on land. *Science* 267(5194), 77–80  
1546 <https://doi.org/10.1126/science.267.5194.77>.
- 1547 Retallack, G.J., 2005. Earliest Triassic claystone breccias and soil-erosion crisis. *J.*  
1548 *Sed. Res.* 75, 663–679 <https://doi.org/10.2110/jsr.2005.055>.
- 1549 Retallack, G.J., Veevers, J.J., Morante, R., 1996. Global coal gap between Permian–  
1550 Triassic extinction and Middle Triassic recovery of peat-forming plants. *Geol.*  
1551 *Soc. Am. Bull.* 108(2), 195–207 [https://doi.org/10.1130/0016-](https://doi.org/10.1130/0016-7606(1996)108<0195:GCGBPT>2.3.CO;2)  
1552 [7606\(1996\)108<0195:GCGBPT>2.3.CO;2](https://doi.org/10.1130/0016-7606(1996)108<0195:GCGBPT>2.3.CO;2).

- 1553 Romano, M., Bernardi, M., Petti, F.M., Rubidge, B., Hancox, J., Benton, M.J., 2020.  
1554 Early Triassic terrestrial tetrapod fauna: a review. *Earth-Sci. Rev.* 210, 103331  
1555 <https://doi.org/10.1016/j.earscirev.2020.103331>.
- 1556 Roscher, M., Stordal, F., Svensen, H., 2011. The effect of global warming and global  
1557 cooling on the distribution of the latest Permian climate zones. *Palaeogeogr.*  
1558 *Palaeoclimatol. Palaeoecol.* 309, 186–200  
1559 <https://doi.org/10.1016/j.palaeo.2011.05.042>.
- 1560 Saito, R., Kaiho, K., Oba, M., Takahashi, S., Chen, Z.Q., Tong, J.N., 2013. A  
1561 terrestrial vegetation turnover in the middle of the Early Triassic. *Glob. Planet.*  
1562 *Change* 105, 152–159 <https://doi.org/10.1016/j.gloplacha.2012.07.008>.
- 1563 Shen, G.L., 1995. Permian foras, in: Li, X.X. (Ed.), *Fossil Floras of China Through*  
1564 *the Geological Ages (English Edition)*. Guangdong Science and Technology  
1565 Press, Guanzhou, pp. 127–223.
- 1566 Shen, J., Algeo, T.J., Zhou, L., Feng, Q.L., Yu, J.X., Ellwood, B., 2012a. Volcanic  
1567 perturbations of the marine environment in South China preceding the latest  
1568 Permian mass extinction and their biotic effects. *Geobiol.* 10, 82–103  
1569 <https://doi.org/10.1111/j.1472-4669.2011.00306.x>.
- 1570 Shen, J., Algeo, T.J., Hu, Q., Zhang, N., Zhou, L., Xia, W., Xie, S.C., Feng, Q.L.,  
1571 2012b. Negative C-isotope excursions at the Permian–Triassic boundary linked  
1572 to volcanism. *Geology* 40 (11), 963–966 <https://doi.org/10.1130/G33329.1>.
- 1573 Shen, J., Lei, Y., Algeo, T.J., Feng, Q.L., Servais, T., Yu, J.X., & Zhou, L., 2013.  
1574 Volcanic effects on microplankton during the Permian–Triassic transition  
1575 (Shangsi and Xinmin, South China). *Palaios* 28(8), 552–567  
1576 <https://doi.org/10.2110/palo.2013.p13-014r>.
- 1577 Shen, J., Schoepfer, S.D., Feng, Q., Song, H.Y., 2015. Marine productivity changes  
1578 during the End-Permian crisis and Early Triassic recovery. *Earth-Sci. Rev.* 149,  
1579 136–162 <https://doi.org/10.1016/j.earscirev.2014.11.002>.
- 1580 Shen, J., Chen, J., Algeo, T.J., Yuan, S.L., Feng, Q.L., Yu, J.X., Zhou, L., O’Connell,  
1581 B., Planavsky, N.J., 2019a. Evidence for a prolonged Permian–Triassic  
1582 Extinction interval from global marine mercury records. *Nat. Commun.* 10, 1563

1583 <https://doi.org/10.1038/s41467-019-09620-0>.

1584 Shen, J., Yu, J.X., Chen, J.B., Algeo, T.J., Xu, G.Z., Feng, Q.L., Shi, X., Planavsky,  
1585 N.J., Shu, W.C., Xie, S.C., 2019b. Mercury evidence of intense volcanic effects  
1586 on land during the Permian-Triassic transition. *Geology* 47(12), 1117-1121  
1587 <https://doi.org/10.1130/G46679.1>.

1588 Shen, J., Chen, J.B., Algeo, T.J., Feng, Q.L., Yu, J.X., Xu, Y.G., Xu, G.Z., Lei Y.,  
1589 Planavsky, N.J., Xie, S.C., 2021. Mercury fluxes record regional volcanism in  
1590 the South China craton prior to the end-Permian mass extinction. *Geology* 49(4),  
1591 452-456 <https://doi.org/10.1130/G48501.1>.

1592 Shen, J., Yin, R.S., Zhang, S., Algeo, T.J., Bottjer, D.J., Yu, J.X., Xu, G.Z., Penman,  
1593 D., Wang, Y.D., Li, L.Q., Shi, X., Planavsky, N.J., Feng, Q.L., Xie, S.C., 2022.  
1594 Intensified continental chemical weathering and carbon-cycle perturbations  
1595 linked to volcanism during the Triassic–Jurassic transition. *Nat. Commun.* 13(1),  
1596 1-10 <https://doi.org/10.1038/s41467-022-27965-x>.

1597 Shen, S.Z., He, X., Shi, G., 1995. Biostratigraphy and correlation of several Permian–  
1598 Triassic boundary sections in southwestern China. *J. Asian Earth Sci.* 12 (1–2),  
1599 19–30 [https://doi.org/10.1016/0743-9547\(95\)00026-7](https://doi.org/10.1016/0743-9547(95)00026-7).

1600 Shen, S.Z., Crowley, J.L., Wang, Y., Boweig, S.A., Erwin, D.H., Sadler, P.M., Cao,  
1601 C.Q., Rothman, D.H., Henderson, C.M., Ramezani, J., Zhang, H., Shen, Y.A.,  
1602 Wang, X.D., Wang, W., Mu, L., Li, W.Z., Tang, Y.G., Liu, X.L., Liu, L.J., Zeng,  
1603 Y., Jiang, Y.F., Jin, Y.G., 2011. Calibrating the End-Permian Mass Extinction.  
1604 *Science* 334, 1367–1372 <https://doi.org/10.1666/13022>.

1605 Shen, S.Z., Zhang, H., Zhang, Y.C., Yuan, D.X., Chen, B., He, W.H., Mu, L., Lin, W.,  
1606 Wang, W.Q., Chen, J., Wu, Q., Cao, C.Q., Wang, Y., Wang, X.D., 2019. Permian  
1607 integrative stratigraphy and timescale of China. *Sci. China Earth Sci.* 62, 154–  
1608 188 <https://doi.org/10.1007/s11430-017-9228-4>.

1609 Shen, W.J., Sun, Y.G., Lin, Y.T., Liu, D.H., Chai, P.X., 2011. Evidence for wildfire in  
1610 the Meishan section and implications for Permian–Triassic events. *Geochim.*  
1611 *Cosmochim. Acta* 75, 1992–2006 <https://doi.org/10.1016/j.gca.2011.01.027>.

1612 Shen, W.J., Zhang, H., Sun, Y.G., Lin, Y.T., Liang, T., Yang, Z.J., Zhou, Y.Z., 2012.

1613 Evidences for the Permian–Triassic wildfire event: review and appraisal. *Adv.*  
1614 *Earth Sci.* 27 (6), 613–623 [https://doi.org/10.11867/j.issn.1001-](https://doi.org/10.11867/j.issn.1001-8166.2012.06.0613)  
1615 [8166.2012.06.0613](https://doi.org/10.11867/j.issn.1001-8166.2012.06.0613).

1616 Song, H.J., Wignall, P.B., Tong, J.N., Yin, H.F., 2012. Two pulses of extinction during  
1617 the Permian–Triassic crisis. *Nat. Geosci.* 6(1), 52–56  
1618 <https://doi.org/10.1038/NGEO1649>.

1619 Song, H.J., Wignall, P. B., Dunhill, A.M., 2018. Decoupled taxonomic and ecological  
1620 recoveries from the Permo-Triassic extinction. *Sci. Adv.* 4(10), eaat5091  
1621 <https://doi.org/10.1126/sciadv.aat5091>.

1622 Song, Q.Q., Feng, J.P., Yu, J.X., Huang, Q.S., 2013. Study on palaeophytoecology of  
1623 the Dalong Formation (Late Permian) in south Guizhou. *Guizhou Geol.* 30(4),  
1624 255–261 (In Chinese with English abstract).

1625 Song, Q.Q., Yu, J.X., Feng, J.P., Huang, Q.S., 2015. Palaeobotany of the upper  
1626 Permian Dalong Formation (marine facies) in south Guizhou. *Geol. Sci. Technol.*  
1627 *Inf.* 34(1), 63–66 (In Chinese with English Abstract).

1628 Song, T., 2018. Study on the bivalve faunas in Southwestern China during the  
1629 Permian–Triassic transitional time. Doctoral Thesis, China Univ. Geosci. Wuhan  
1630 1–181.

1631 Stanley, S.M., 2009. Evidence from ammonoids and conodonts for multiple Early  
1632 Triassic mass extinctions. *Proc. Natl. Acad. Sci. USA* 106(36), 15264–15267  
1633 <https://doi.org/10.1073/pnas.0907992106>.

1634 Steiner, M.B., Eshet, Y., Rampino, M.R., Schwindt, D.M., 2003). Fungal abundance  
1635 spike and the Permian–Triassic boundary in the Karoo Supergroup (South  
1636 Africa). *Palaeoecol. Palaeogeog. Palaeoclimatol.* 194(4), 405–414  
1637 [https://doi.org/10.1016/S0031-0182\(03\)00230-X](https://doi.org/10.1016/S0031-0182(03)00230-X).

1638 Stevens, L.G., Hilton, J.M., Bond, D.P.G., Glasspool, I.J., Jardine, P.E., 2011.  
1639 Radiation and extinction patterns in Pennsylvanian–Permian floras from North  
1640 China as indicators of environmental and climate change. *J. Geol. Soc.* 168, 607–  
1641 619 <https://doi.org/10.1144/0016-76492010-042>.

1642 Sun, Y.D., Joachimski, M.M., Wignall, P.B., Yan, C.B., Chen, Y.L., Jiang, H.S., Wang,



1643 L.N., Lai, X.L., 2012. Lethally hot temperatures during the Early Triassic  
1644 greenhouse. *Science* 338 (6105), 366–370  
1645 <https://doi.org/10.1126/science.1224126>.

1646 Taylor, T.N., Taylor, E.L., Krings, M., 2009. *Paleobotany, the biology and evolution*  
1647 *of fossil plants*, 2nd ed. Acad. Press, Amsterdam.

1648 Tong, J.N., Chu, D.L., Liang, L., Shu, W.C., Song, H.J., Song, T., Song, H.Y., Wu, Y.Y.,  
1649 2019. Triassic integrative stratigraphy and timescale of China. *Sci. China Earth*  
1650 *Sci.* 62, 189–222 <https://doi.org/10.1007/s11430-018-9278-0>.

1651 Vajda, V., McLoughlin, S., Mays, C., Frank, T.D., Fielding, C.R., Tevywa, A., Lehsten,  
1652 V., Bocking, M., Nicoll, R.S., 2020. End-Permian (252 Mya) deforestation,  
1653 wildfires and flooding—an ancient biotic crisis with lessons for the present. *Earth*  
1654 *Planet. Sci. Lett.* 529, 115875 <https://doi.org/10.1016/j.epsl.2019.115875>.

1655 Visscher, H., Brinkhuis, H., Dilcher, D.L., Elsik, W.C., Eshet, Y., Looy, C.V., Rampino,  
1656 M.R., Traverse, A., 1996. The terminal paleozoic fungal event: evidence of  
1657 terrestrial ecosystem destabilization and collapse. *Proc. Natl. Acad. Sci. USA*  
1658 93(5), 2155–2158 <https://doi.org/10.1073/pnas.93.5.2155>.

1659 Wang, C.J., 2007. Anomalous hopane distributions at the Permian Triassic boundary,  
1660 Meishan, China—evidence for the End-Permian marine ecosystem collapse. *Org.*  
1661 *Geochem.* 38, 52–66 <https://doi.org/10.1016/j.orggeochem.2006.08.014>.

1662 Wang, H., Shao, L., Hao, L.M., Zhang, P.F., Glasspool, I.J., Wheeley, J.R., Wignall,  
1663 P.B., Yi, T.S., Zhang, M.Q., Hilton, J.M., 2011. Sedimentology and sequence  
1664 stratigraphy of the Lopingian (Late Permian) coal measures in southwestern  
1665 China. *Int. J. Coal Geol.* 85, 168–183 <https://doi.org/10.1016/j.coal.2010.11.003>.

1666 Wang, J., Pfefferkorn, H.W., Zhang, Z., Zhou, F., 2012. Permian vegetational Pompeii  
1667 from Inner Mongolia and its implications for landscape palaeoecology and  
1668 palaeobiogeography of China. *Proc. Natl. Acad. Sci. USA* 109, 4927–4943  
1669 <https://doi.org/10.1073/pnas.1115076109>.

1670 Wang, Y., Sadler, P.M., Shen, S.Z., Erwin, D.H., Zhang, Y.C., Wang, X.D., Wang, W.,  
1671 Crowley, J.L., Henderson, C.M., 2014. Quantifying the process and abruptness  
1672 of the end-Permian mass extinction. *Paleobiol.* 40(1), 113–129

1673 <https://doi.org/10.1666/13022>.

1674 Wang, X., Shao, L., Eriksson, K.A., Yan, Z., Wang, J., Li, H., Zhou, R., Lu, J., 2020.

1675 Evolution of a plume-influenced source-to-sink system: An example from the

1676 coupled central Emeishan large igneous province and adjacent western Yangtze

1677 cratonic basin in the Late Permian, SW China. *Earth-Sci. Rev.* 207, 103224

1678 <https://doi.org/10.1016/j.earsci.2020.103224>.

1679 Wang, Z.Q., 1985. Palaeovegetation and plate tectonics: palaeophytogeography of

1680 North China during Permian and Triassic times. *Palaeogeogr. Palaeoclimatol.*

1681 *Palaeoecol.* 49(1–2), 25–45 [https://doi.org/10.1016/0031-0182\(85\)90003-3](https://doi.org/10.1016/0031-0182(85)90003-3).

1682 Wang, Z.Q., 1996. Recovery of vegetation from the terminal Permian mass extinction

1683 in North China. *Rev. Palaeobot. Palynol.* 91, 121–142

1684 [https://doi.org/10.1016/0034-6667\(95\)00069-0](https://doi.org/10.1016/0034-6667(95)00069-0).

1685 Whittaker, R.H., Goodman, D., 1979. Classifying species according to their

1686 demographic strategy. *Am. Nat.* 113, 185–200 <https://doi.org/10.1086/283378>.

1687 Wignall, P.B., 2015. *The Worst of Times: How Life on Earth Survived 80 Million*

1688 *Years of Extinction*. Princeton University Press, pp. 224

1689 <https://doi.org/10.1515/9781400874248>.

1690 Wignall, P.B., Chu, D., Hilton, J.M., Dal Corso, J., Wu, Y., Wang, Y., Atkinson, J.,

1691 Tong, J., 2020. Death in the shallows: The record of Permo-Triassic mass

1692 extinction in paralic settings, southwest China. *Glob. Planet. Change* 189,

1693 103176 <https://doi.org/10.1016/j.gloplacha.2020.103176>.

1694 Wu, Q., Ramezani, J., Zhang, H., Wang, J., Zeng, F.G., Zhang, Y.C., Liu, F., Chen, J.,

1695 Cai, Y.F., Hou, Z.S., Liu, C., Yang, W., Henderson, C.M., Shen, S.Z., 2021.

1696 High-precision U-Pb age constraints on the Permian floral turnovers,

1697 paleoclimate change, and tectonics of the North China block. *Geology* 49(6),

1698 677–681 <https://doi.org/10.1130/G48051.1>.

1699 Xie, S.C., Pancost, R.D., Huang, J.H., Wignall, P.B., Yu, J.X., Tang, X., Chen, L.,

1700 Huang, X.Y., Lai, X.L., 2007. Changes in the global carbon cycle occurred as

1701 two episodes during the Permian–Triassic crisis. *Geology* 35(12), 1083–1086

1702 <https://doi.org/10.1130/G24224A.1>.

- 1703 Xie, S.C., Yin, H.F., Cao, C.Q., Wang, C.J., Lai, X.L., 2009. Episodic changes of the  
1704 earth surface system across the Permian–Triassic boundary: molecular  
1705 geobiological records. *Acta Palaeontol. Sin.* 48(3), 496–506 (In Chinese with  
1706 English abstract).
- 1707 Xiong, C.H., Wang, Q., 2011. Permian–Triassic land-plant diversity in South China:  
1708 was there a mass extinction at the Permian/Triassic boundary? *Paleobiol.* 37(1),  
1709 157–167 <https://doi.org/10.1666/09029.1>.
- 1710 Xiong, C.H., Wang, J.S., Huang, P., Cascales-Minana, B., Cleal, C.J., Benton, M.J.,  
1711 Xue, J., 2021. Plant resilience and extinctions through the Permian to Middle  
1712 Triassic on the North China Block: A multilevel diversity analysis of macrofossil  
1713 records. *Earth-Sci. Rev.* 223, 103846  
1714 <https://doi.org/10.1016/j.earscirev.2021.103846>.
- 1715 Xu, G.Z., Feng, Q.L., Deconinck, J.F., Shen, J., Zhao, T.Y., Young, A.L., 2017. High-  
1716 resolution clay mineral and major elemental characterization of a Permian–  
1717 Triassic terrestrial succession in southwestern China: Diagenetic and  
1718 paleoclimatic/paleoenvironmental significance. *Palaeogeogr. Palaeoclimatol.*  
1719 *Palaeoecol.* 481, 77–93 <https://doi.org/10.1016/j.palaeo.2017.05.027>.
- 1720 Xu, R., Zhu, J.R., Chen, Y., Duan, S.Y., Hu, Y.F., Zhu, W.Q., 1979. China Late  
1721 Triassic Baoding Flora. *Sci. Press* 1–130.
- 1722 Yan, Z.M., Shao, L.Y., Glasspool, I.J., Wang, J., Wang, X.T., Wang, H., 2019.  
1723 Frequent and intense fires in the final coals of the Paleozoic indicate elevated  
1724 atmospheric oxygen levels at the onset of the End-Permian Mass Extinction  
1725 Event. *Int. J. Coal Geol.* 207, 75–83 <https://doi.org/10.1016/j.coal.2019.03.016>.
- 1726 Yang, G.X., 1994. *Palaeobotany*. Geological Publishing House, Beijing (In Chinese).
- 1727 Yang, S.P., 1993. *Paleoecology: principles and methods*. Geol. Publ. Beijing (In  
1728 Chinese).
- 1729 Yang, T.L., 2015. *The Bivalve Fauna From Deep-water Facies of South China During*  
1730 *the Permian–Triassic Interval*. Doctoral Thesis, China Univ. Geosci. Wuhan, pp.  
1731 25–36 (In Chinese with English abstract).
- 1732 Yang, W., Wan, M.L., Crowley, J.L., Wang, J., Luo, X.R., Tabor, N., Angielczyk, K.D.,

- 1733 Castaldo, R., Geissman, J., Liu, F., Roopnarine, P., Sidor, C.A., 2021.  
1734 Paleoenvironmental and paleoclimatic evolution and cyclo- and chrono-  
1735 stratigraphy of Upper Permian–Lower Triassic fluvial-lacustrine deposits in  
1736 Bogda Mountains, NW China—Implications for diachronous plant evolution  
1737 across the Permian–Triassic boundary. *Earth-Sci. Rev.* 222, 103741  
1738 <https://doi.org/10.1016/j.earscirev.2021.103741>.
- 1739 Yang, Y., Sadler, P.M., Shen, S.Z., Erwin, D.H., Zhang, Y.-C., Wang, X.-D., Wang, W.,  
1740 Crowley, J.L., Henderson, C.M., 2016. Quantifying the process or abruptness of  
1741 the end-Permian mass extinction. *Palaeobiology* 40, 113–129  
1742 <https://doi.org/10.1666/13022>.
- 1743 Yang, Z.Y., Zhang, S.X., Yang, J.D., Zhou, H.Q., Cao, H.S., 2000. Stratigraphical  
1744 lexicon of China: Triassic. *Geol. Publ. Beijing* (In Chinese).
- 1745 Yao, Z.Q., 1978. On the age of “Gigantopteris Coal Series” and Gigantopteris flora in  
1746 South China. *Acta Palaeontol. Sin.* 17, 81–89 (In Chinese with English abstract).
- 1747 Yao, Z.Q., Xu, J.T., Zhen, Z.G., Mo, Z.G., 1980. Late Permian biostratigraphy and the  
1748 Permian–Triassic boundary in Western Guizhou and Eastern Yunnan, in: Nanjing  
1749 Institute of Geology and Palaeontology (Ed.), *Stratigraphy and palaeontology of*  
1750 *Late Permian coal-bearing formations in Western Guizhou and Eastern Yunnan.*  
1751 *Sci. Press, Beijing*, pp. 1–69 (In Chinese).
- 1752 Ye, M.N., 1979. On some Middle Triassic plants from Hupeh and Szechuan. *Acta*  
1753 *Palaeontol. Sin.* 18(1), 73–81 (In Chinese with English abstract).
- 1754 Yin, H.F., 1985. Bivalves near the Permian–Triassic boundary in South China. *J.*  
1755 *Paleontol.* 59(3), 572–600.
- 1756 Yin, H.F., Feng, Q.L., Lai, X.L., Baud, A., Tong, J.N., 2007. The protracted Permo-  
1757 Triassic crisis and multi-episode extinction around the Permian–Triassic  
1758 boundary. *Glob. Planet. Change* 55, 1–20  
1759 <https://doi.org/10.1016/j.gloplacha.2006.06.005>.
- 1760 Yin, H.F., Jiang, H.S., Xia, W.C., Feng, Q.L., Zhang, N., Shen, J., 2014. The End-  
1761 Permian regression in South China and its implication on mass extinction. *Earth-*  
1762 *Sci. Rev.* 137, 19–33 <https://doi.org/10.1016/j.earscirev.2013.06.003>.

- 1763 Yin, H.F, Xie, S.C., Luo, G.M., Algeo, T. J., & Zhang, K.X., 2012. Two episodes of  
1764 environmental change at the Permian–Triassic boundary of the GSSP section  
1765 Meishan. *Earth-Sci. Rev.* 115(3), 163–172  
1766 <https://doi.org/10.1016/j.earscirev.2012.08.006>.
- 1767 Yu, J.X., 2008. Floras (macro- and microfloras) and evolutionary dynamics across the  
1768 Permian–Triassic boundary along Guizhou and Yunnan border, South China.  
1769 Doctoral Thesis, China Uni. Geosci. Wuhan & Uni. Pierre et Marie Curie, Paris  
1770 6, 220 pp.
- 1771 Yu, J.X., Broutin, J., Chen, Z.Q., Shi, X., Li, H., Chu, D.L., Huang, Q.S., 2015.  
1772 Vegetation changeover across the Permian–Triassic boundary in Southwest  
1773 China: Extinction, survival, recovery and palaeoclimate: A critical review. *Earth-*  
1774 *Sci. Rev.* 149, 203–224 <https://doi.org/10.1016/j.earscirev.2015.04.005>.
- 1775 Yu, J.X., Broutin, J., Huang, Q.S., Grauvogel-Stamm, L., 2010. *Annalepis*, a  
1776 pioneering lycopsid genus in the recovery of the Triassic land flora in South  
1777 China. *C. R. Palevol.* 9, 479–486 <https://doi.org/10.1016/j.crpv.2010.09.004>.
- 1778 Zhang, K.X., Yu, J.X., Lin, Q.X., Jing, Y.L., Chen, B., 2004. Palynological  
1779 assemblage in section d of Meishan, Changxing, Zhejiang and its significance of  
1780 global correlation. *Earth Sci. J. China Uni. Geosci.* 29 (3), 253–262.
- 1781 Zhang, N., Jiang, H., Zhong, W., Huang, H., Xia, W., 2014. Conodont biostratigraphy  
1782 across the Permian–Triassic boundary at the Xinmin section, Guizhou, South  
1783 China. *J. Earth Sci.* 25(5), 779–786 <https://doi.org/10.1007/s12583-014-0472-0>.
- 1784 Zhang, Z.L., Meng, F.S., Sheng, X.C., 1992. Triassic, in: Wang, X.F., Ma, D.S., Jiang,  
1785 D.H. (Eds.), Hainan Island geology (1) stratigraphic paleontology. *Geol. Publ.*  
1786 Beijing pp. 161–199 (In Chinese).
- 1787 Zheng, R.H., 2011. China pre-Mesozoic structural sequence and lithofacies  
1788 paleogeography atlas. *Geol. Publ. Beijing* (In Chinese).
- 1789 Zhou, Z.Y., 1989. Late Triassic plants from Shaqiao, Hengyang, Hunan Province.  
1790 *Palaeontol. Cathayana* 4, 131–197 <http://ir.nigpas.ac.cn/handle/332004/5891>.
- 1791 Zhou, Z.Y., Li, B.X., 1979. A preliminary study of the Early Triassic plants from the  
1792 Qionghai District, Hainan Island. *Acta Palaeotol. Sin.* 18(5), 444–466 (In

1793 Chinese with English abstract).

1794 Zuazo, V.H.D., Pleguezuelo, C.R.R., 2009. Soil-erosion and runoff prevention by  
 1795 plant covers: A review, in: Lichtfouse, E., Navarrete, M., Debaeke, P., Véronique,  
 1796 S., Alberola, C. (Eds.), Sustainable Agriculture. Springer Dordrecht pp. 65–86  
 1797 [https://doi.org/10.1007/978-90-481-2666-8\\_48](https://doi.org/10.1007/978-90-481-2666-8_48).

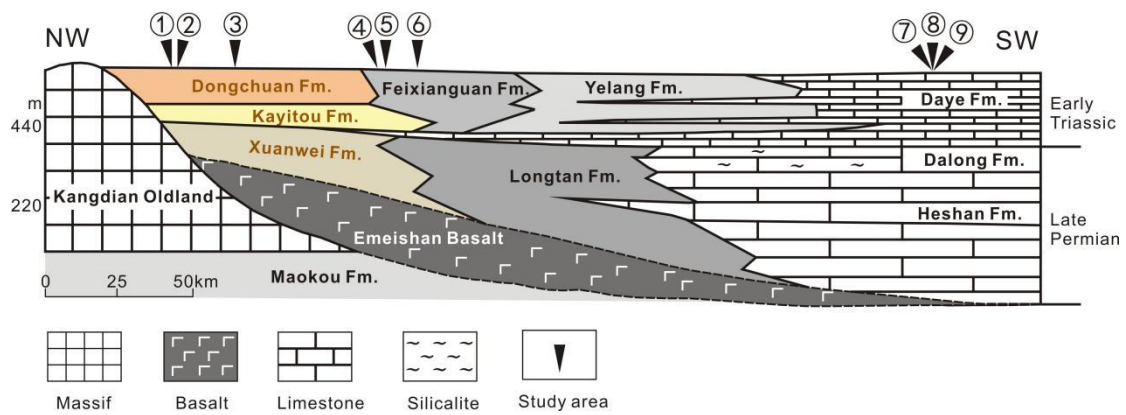
1798

1799 Table and figure captions

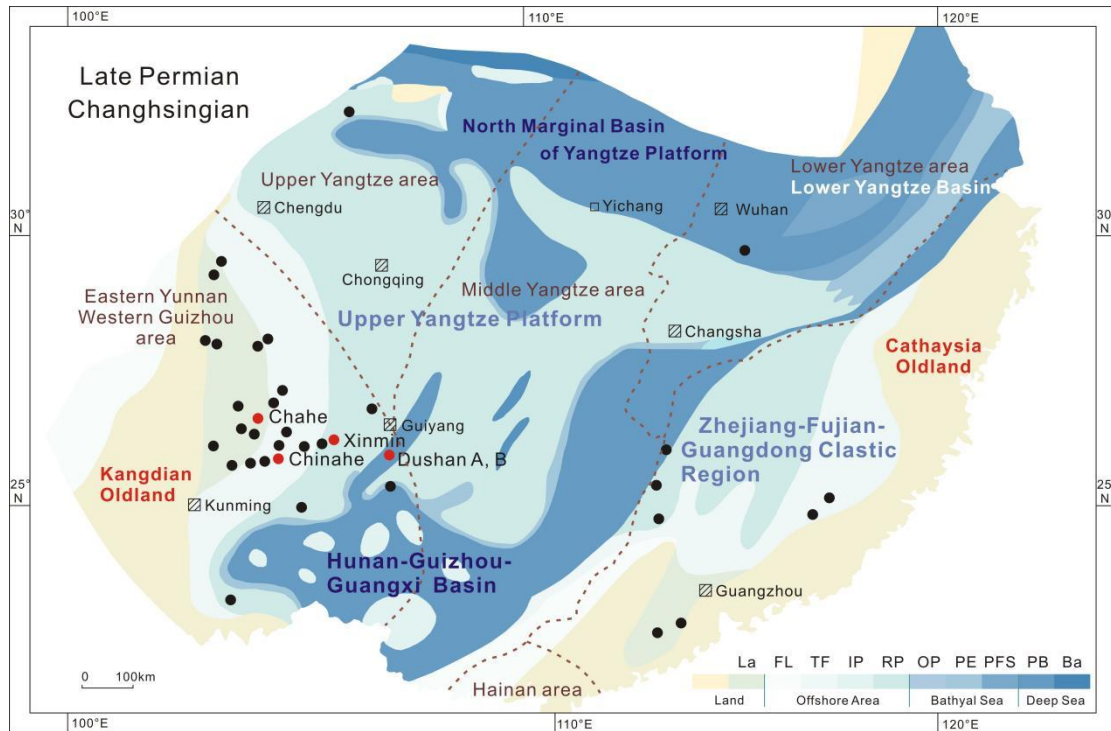
System	Series	Stage/ substages	Lower Yangtze area	Middle Yangtze area	Upper Yangtze area	Eastern Yunnan Western Guizhou area	Hainan area	
Triassic	Upper Triassic	Rhaetian	Lalijian Formation	Wanglongtan Formation	Xujiahe Formation	Baoding F.	Erqiao Formation	
		Norian		Shazhenxi F.	Xiaotangzi Formation	<b>Dajing F.</b>	Huobachong Formation	
		Carnian			<b>Jiuligang Formation</b>	Kuahongdong Formation	<b>Daqiaodi Formation</b>	Banan Formation
	Middle Triassic	Ladinian	Tongtujian Formation	<b>Badong Formation Member 4-5</b>	Huanglianqiao Formation	Bingnan Formation	Falang Formation	
			Yueshan Formation	<b>Badong Formation Member 1-3</b>	Leikoupo Formation	Maantang Formation	Yangliujing Formation	
		Anisian	Dongmaanshan Formation				Guanlin Formation	
	Lower Triassic	Olenekian	Spath. Smith.	Nanlinhu Formation	Jialinjiang Formation	Jialinjiang Formation	Yongningzhen Formation	<b>Lingwen Formation</b>
				Helongshan Formation				
		Induan	Griesb. Dien.	Yinkeng Formation	Daye Formation	<b>Feixianguan Formation</b>		
	PTT							
	Permian	Lopingian	Changhsingian	Changxing Formation	Wujiaping F.	<b>Dalong Formation</b>	Yelang Formation	<b>Kayitou Formation</b>
			Wuchia- pingian	Wujiaping Formation	Heshan F.	<b>Longtan Formation</b>	<b>Xuanwei Formation</b>	<b>Upper Lower</b>
Guadalu- pian		Capitanian					Emeishan Basalt	
		Wordian	<b>Maokou Formation</b>	Gufeng Formation			Maokou Formation	
		Roadian						
Cisura- lian		Kungurian		Qixia Formation			Qixia Formation	
	Artinskian		<b>Liangshan Formation</b>			<b>Liangshan Formation</b>		

1800

1801 **Figure 1.** Correlation of lower Cisuralian to Upper Triassic formations in South China.  
 1802 gray units contain plant fossils, with leaf representing position of separate beds  
 1803 containing plants. Numbers in formations represent: 1. Liangshan section; 2. Maokou  
 1804 section; 3. Longtan and lower Xuanwei section; 4. Chahe and Chinahe sections; 5.  
 1805 Xinmin, Duanshan A and B sections; 6. Chinahe, Mide and Tucheng sections; 7.  
 1806 Lubei, Pojiao and Dongchuan sections; 8. Lingwen section; 9. Hongjiaguan and  
 1807 Furongqiao section; 10. Jiuligang and Daqiaodi sections; 11. Xujaiahe, Dajing, Anyuan,  
 1808 Bagong sections. PTT = Permo-Triassic transition. Figure modified from Yang et al.  
 1809 (2000); Jin et al. (2000), Yu et al. (2015), Tong et al. (2019) and Shen et al. (2019).  
 1810



1812 **Figure 2.** Sketch map of the Permian Changsingian lithofacies in Western Guizhou  
 1813 and Eastern Yunnan, southwestern China. 1. Pojiao section; 2. Lubei section; 3. Chahe  
 1814 section; 4. Chinahe section; 5. Mide section; 6. Tucheng section; 7. Xinmin section; 8.  
 1815 Duanshan A section; 9. Duanshan B section; modified from Yu et al. (2015), Wignall  
 1816 et al. (2020).  
 1817

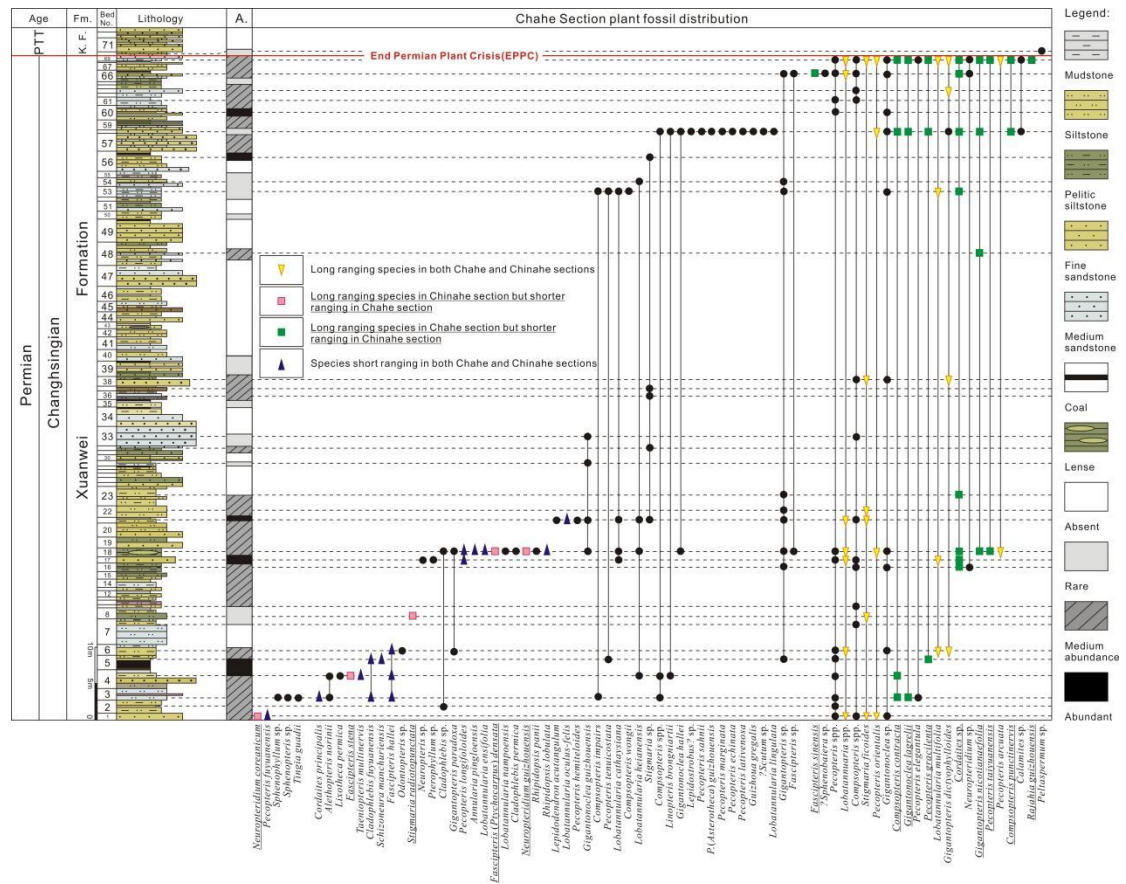


1818

1819 **Figure 3.** Paleogeographic map of South China during the End Permian showing  
 1820 positions of sections studied from the Changhsingian aged Xuanwei and Dalong  
 1821 formations. Red point: studied sections in this paper; Black point: supplementary  
 1822 sections from literature; La = Lacustrine ; FL = Flood land; TF = Tide flat; IP =  
 1823 Isolate platform; RP = Regional platform; OP = Open platform; PE = Platform edge;  
 1824 PFS = Carbonate platform fore slope; PB = Platform basin; Ba = Bathyal sea;  
 1825 modified from Zheng et al. (2011), Yin et al. (2014) and Yu et al. (2015).

1826





1827

1828 **Figure 4.** Plant fossil distributions from the Xuanwei Formation in the Chahe section

1829 (unnormlized). PTT = Permo-Triassic transition; Grib. = Grisbachian; K. F. =

1830 Kayitou Formation; A. = Abundance of plant fossil. The color of the lithology column

1831 shows the real rock color in the field.

1832



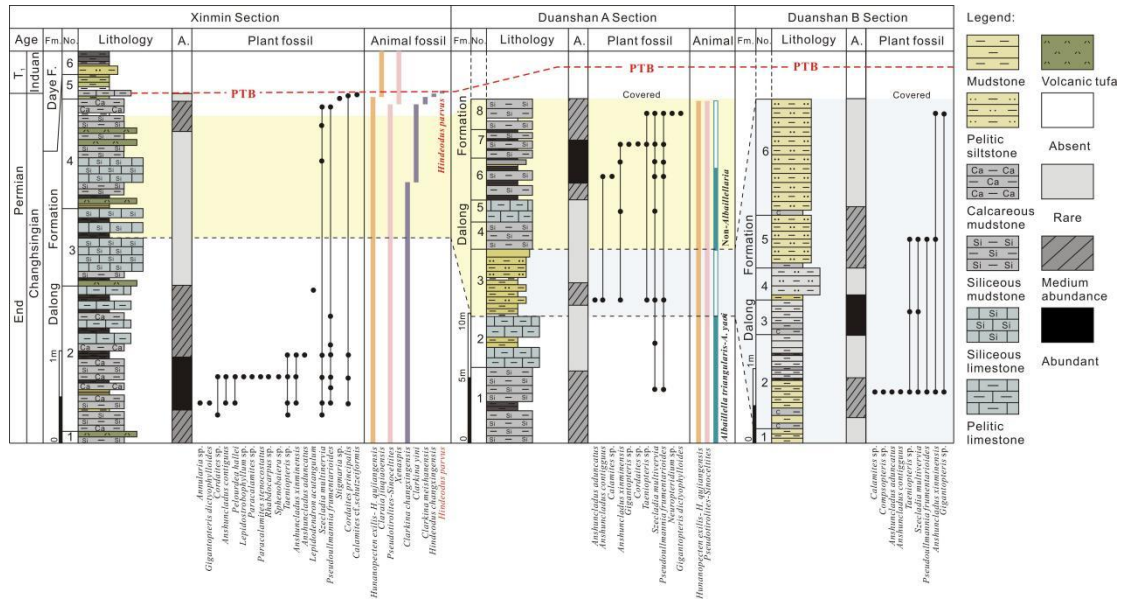


1839

1840 **Figure 6.** Field panorama, sedimentology and representative plant fossils showing  
 1841 preservation condition from the Chinahe section. 1. Strata of the Kayitou Formation; 2.  
 1842 Strata of the upper Xuanwei Formation; 3. Emeishan Basalt with vesicular structure; 4.  
 1843 Boundary between the Emeishan Basalt and the Xuanwei Formation; 5. Panorama of  
 1844 the Chinahe section ranging from the Emeishan Basalt (right) to the Kayitou  
 1845 Formation (left); 6. Conchostraca in the Kayitou Formation; 7. *Tomiostrobus*  
 1846 (= *Annalepis*) layer in the bottom of Kayitou Formation (Bed 26); 8. Abraded  
 1847 *Gigantopteris dictyophylloides* fragments together with *Tomiostrobus* (= *Annalepis*)  
 1848 (Bed 26); 9. Small *Peltaspermum martinsii* together with *Tomiostrobus* (= *Annalepis*)  
 1849 (Bed 26); 10. Broken *Compsopteris* leaf in the upper part of Xuanwei Formation (Bed  
 1850 22); 11. Layer of *Lepidodendron oculus-felis* in middle of Xuanwei Formation (Bed  
 1851 10); 12. *Gigantopteris* fragments occurring from the lower to middle of the Xuanwei  
 1852 Formation (Beds 3–10); 13. Well-preserved leaves with insect feeding trace fossils  
 1853 (bed 2); 14. Complete fern branches in the bottom of Xuanwei Formation (Bed 1).

1854 PTT = Permo-Triassic transition; P = Permian.

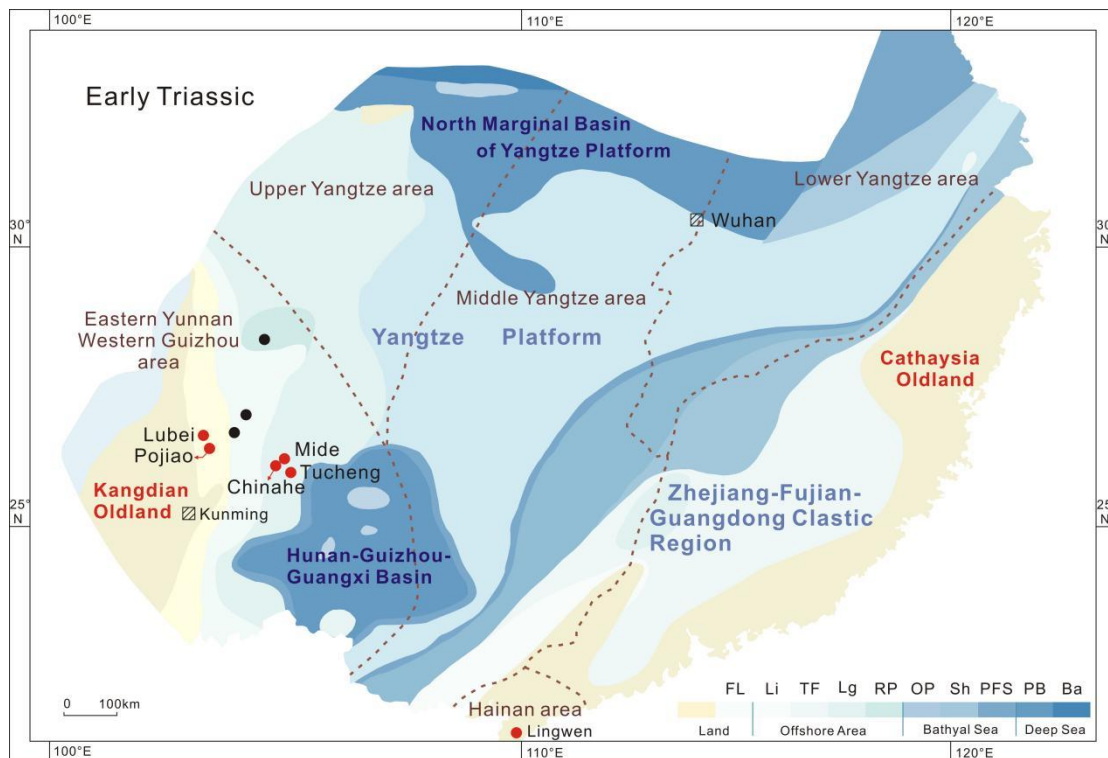
1855



1856

1857 **Figure 7.** Plant and marine animal fossil distributions from the Dalong Formation in  
 1858 the Xinmin, Duanshan A and Duanshan B sections (unnormalized). T<sub>1</sub> = Early  
 1859 Triassic; Fm. = Formation; NO. = Bed number; A. = Abundance of plant fossil; PTB =  
 1860 Permian Triassic boundary. The color of the lithology column shows the real rock  
 1861 color in the field.

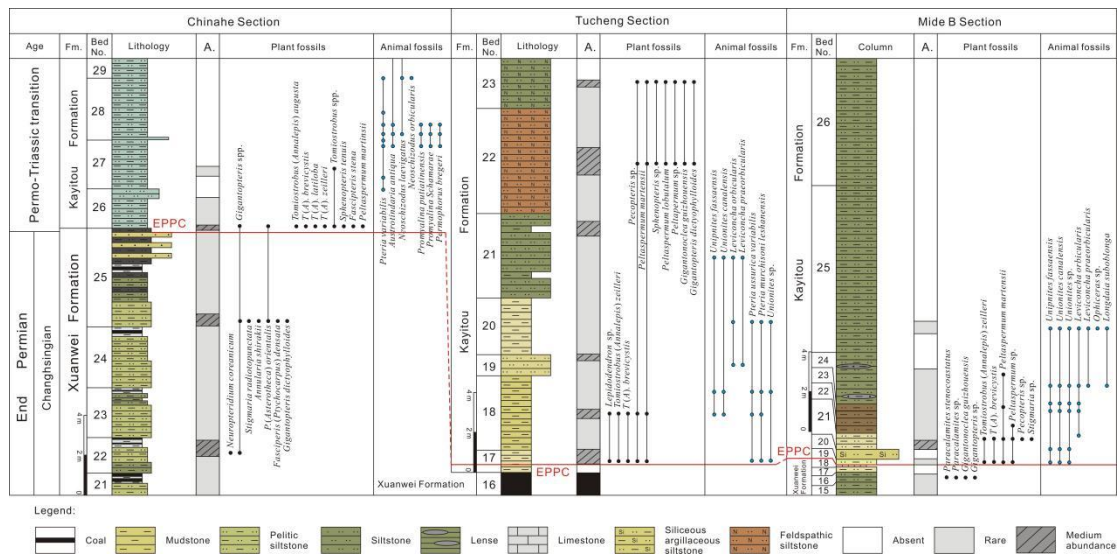
1862



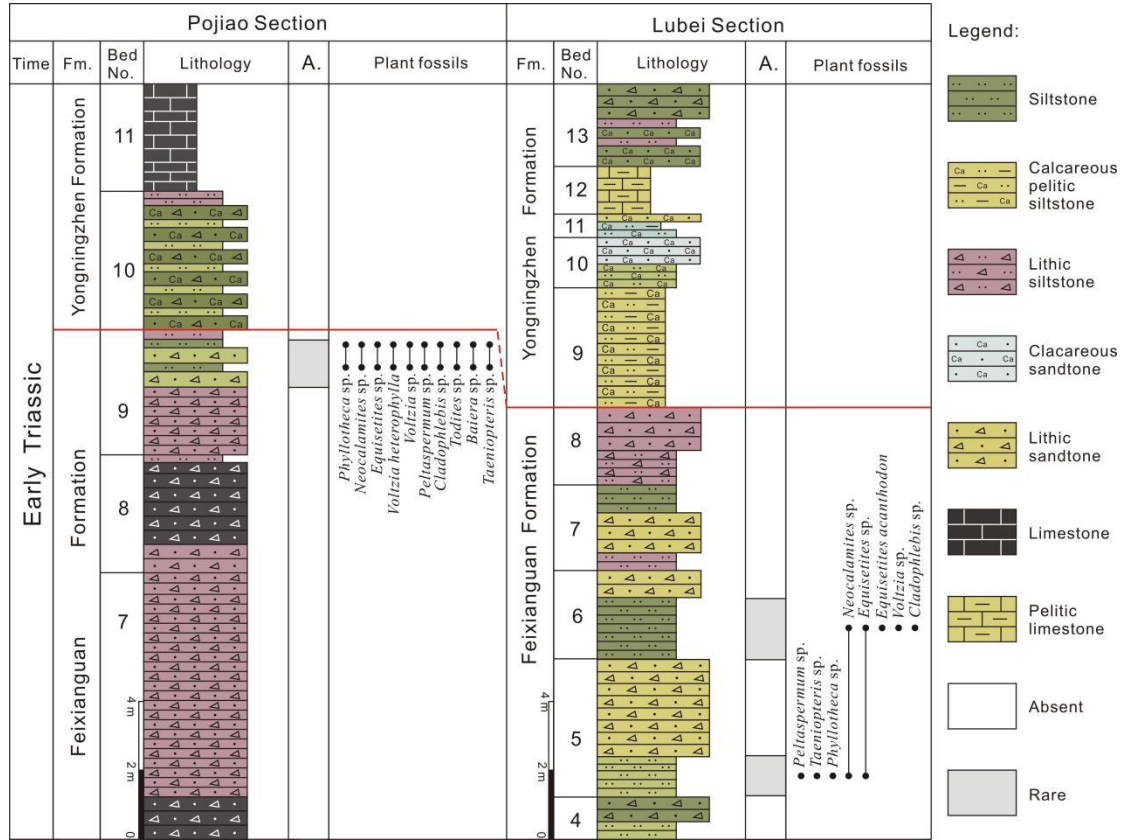
1863

1864 **Figure 8.** Early Triassic paleogeographical map of South China showing locations of

1865 sections containing the Induan Kayitou Formation, Olenekian Feixianguan and  
 1866 Lingwen formations. Red point: studied sections in this paper; Black point:  
 1867 supplementary sections from literature; FL = Flood land; TF = Tide flat; Lg = Lagoon;  
 1868 RP = Regional platform; OP = Open platform; Sh = Shallow sea; PFS = Carbonate  
 1869 platform fore-slope; PB = Platform basin; Ba = Bathyal sea; modified from Zheng et  
 1870 al. (2011) and Yin et al. (2014).  
 1871



1872  
 1873 **Figure 9.** Plant and marine animal fossil distributions from the Kayitou Formation in  
 1874 the Chinahe, Tucheng and Mide sections (unnormalized). Fm. = Formation; NO. =  
 1875 Bed number; EPPC = End Permian Plant Crisis; A. = Abundance of plant fossil. The  
 1876 color of the lithology column shows the real rock color in the field.  
 1877



1878

1879 **Figure 10.** Plant fossil distributions from the Feixianguan Formation in the Lubei and  
 1880 Pojiao sections (unnormalized). Fm. = Formation; NO. = Bed number; A. =  
 1881 Abundance of plant fossil. The color of the lithology column shows the real rock  
 1882 color in the field.

1883



1884

1885 **Figure 11.** Representative plant fossils in Kayitou Formation of Chinahe section (1–8)

1886 and Feixianguan Formation of Lubei and Pojiao section (9–15). 1. Bivalves; 2.

1887 *Tomiostrabus* (= *Annalepis*) spp.; 3. *T. (A.) zeilleri*; 4. *T. (A.) augusta*; 5. *T. (A.)*

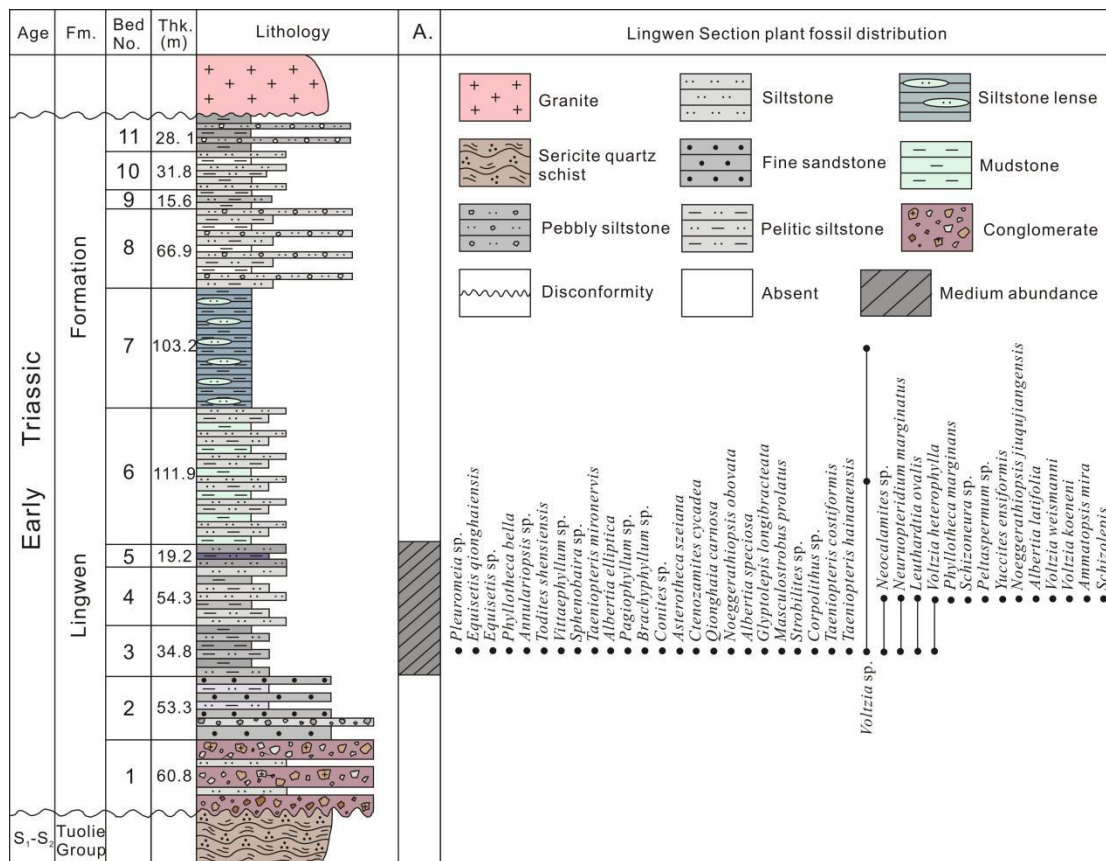
1888 *latiloba*; 6. Unkown index; 7. *Fascipteris stena*; 8. *Peltaspermum martinsii*; 9–12.

1889 *Carpolithus* spp.; 13. *Neocalamites* branches, common in both Lubei and Pojiao

1890 sections; 14. *Voltzia* sp.; 15. Possible fertile spike?; 16. *Peltaspermum* sp.; 17. Fern;

1891 18. *Todites* sp.

1892

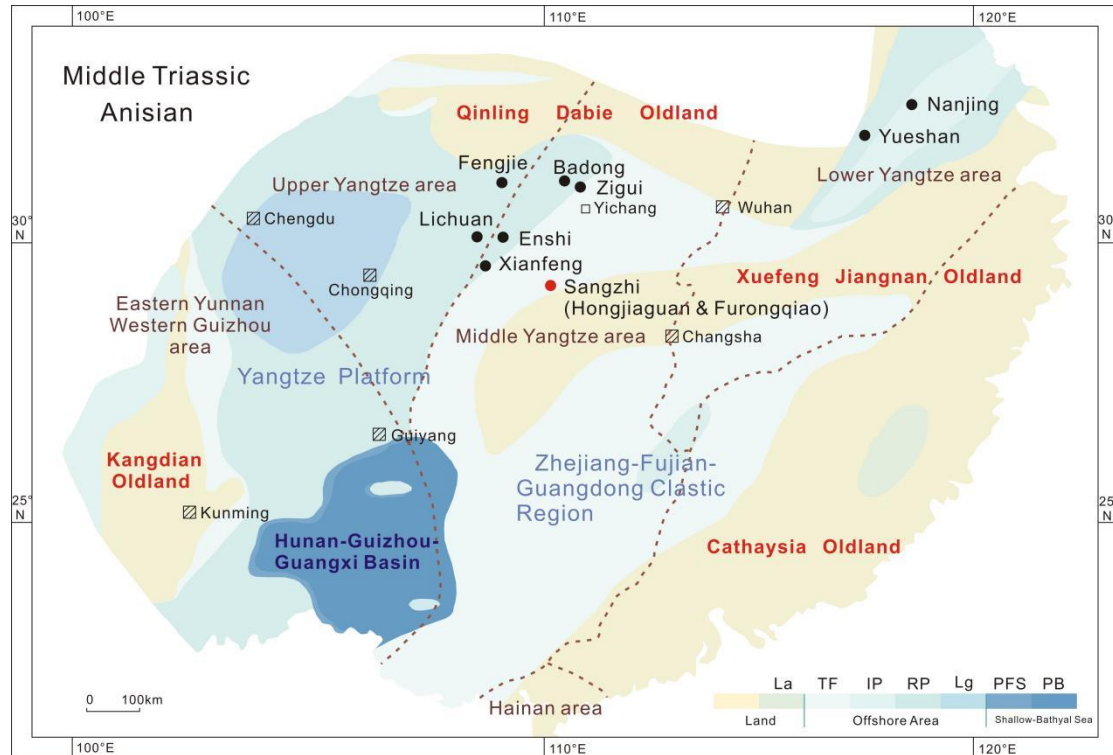


1893

1894 **Figure 12.** Plant fossil distributions from the Lingwen Formation in the Lingwen  
 1895 section (unnormalized). Fm. = Formation; NO. = Bed number; Thk. = Thickness; A. =  
 1896 Abundance of plant fossil. The color of the lithology column shows the real rock  
 1897 color in the field.

1898

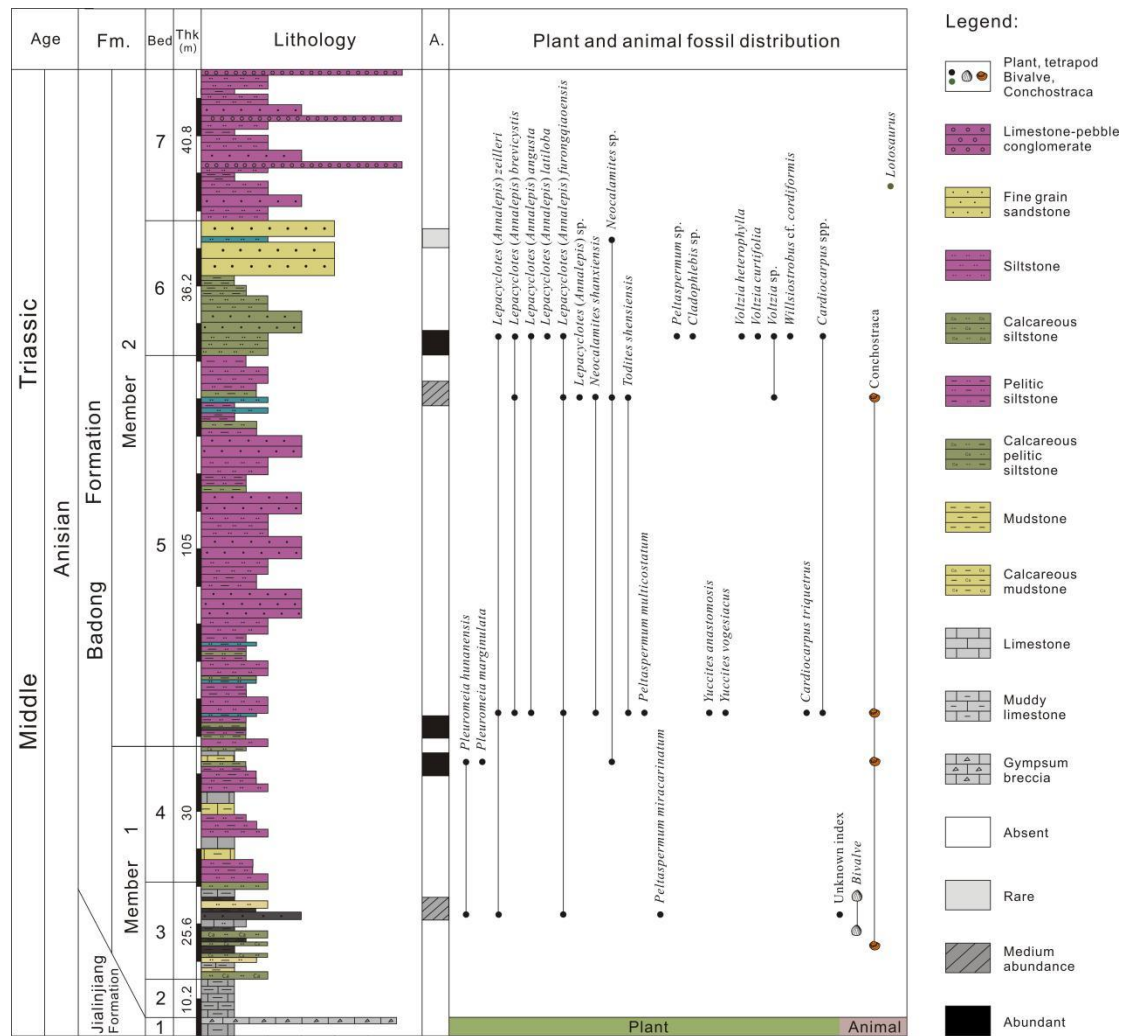




1899

1900 **Figure 13.** Middle Triassic paleogeographic map of South China showing locations  
 1901 for sections of the Badong Formation. Red point: studied sections in this paper; Black  
 1902 point: supplementary sections from literature; La = lacustrine; TF = Tide flat; IP =  
 1903 Isolated platform; RP = Regional platform; Lg = Lagoon; PFS = Carbonate platform  
 1904 fore slope; PB = Platform basin; modified from Zheng et al. (2011).

1905



1906

1907

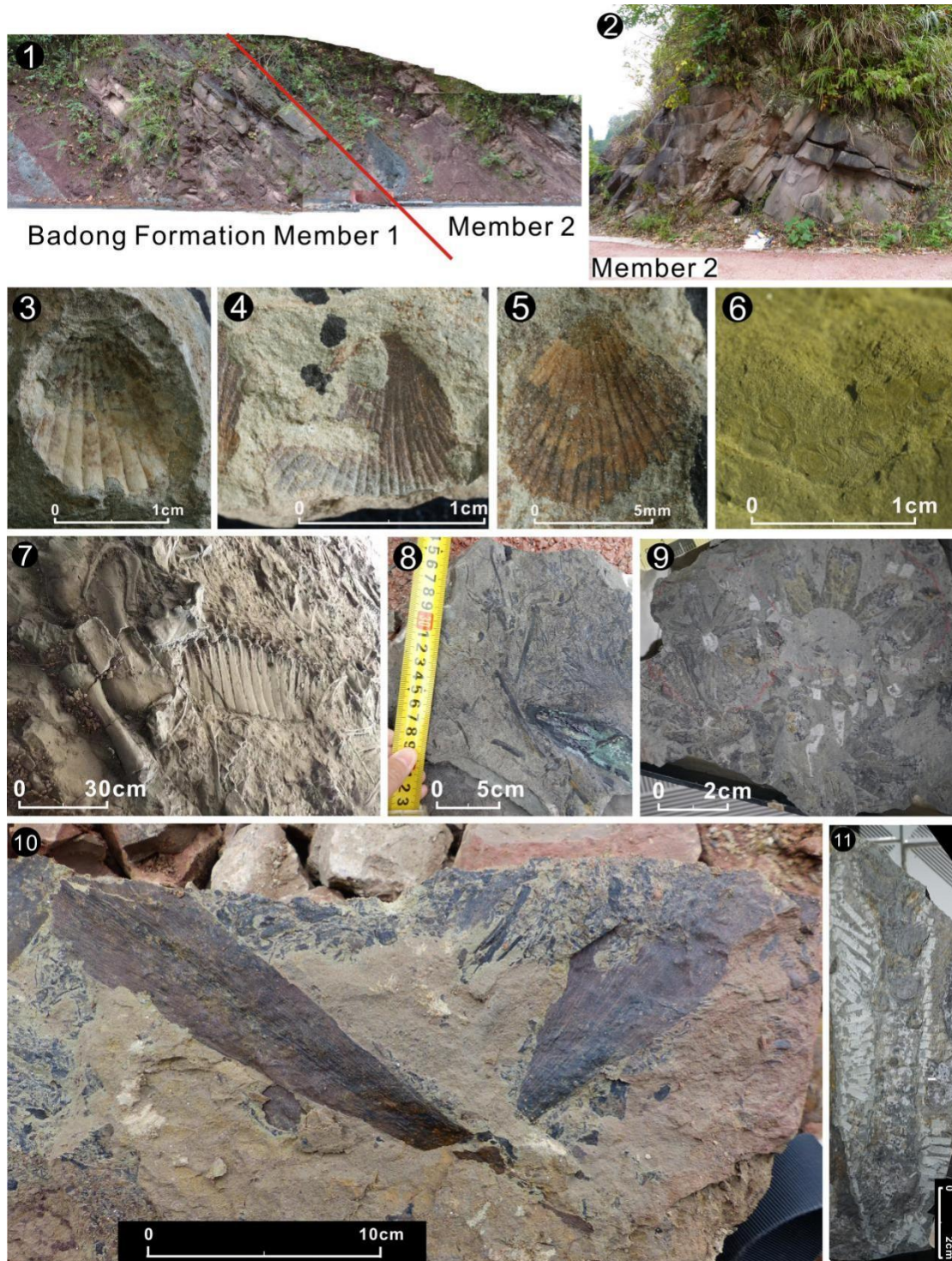
1908

1909

1910

1911

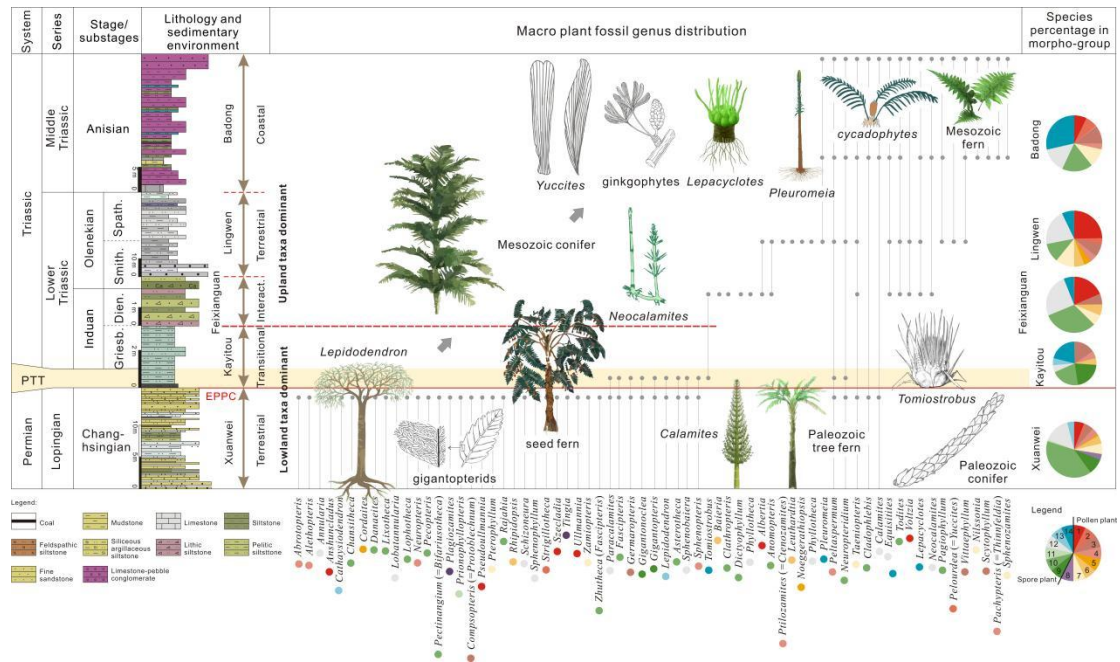
**Figure 14.** Plant fossil distributions from the Badong Formation in the Hongjiaguan and Furongqiao sections (unnormalized). Fm. = Formation; NO. = Bed number; Thk. = Thickness; M. = Mineral; J. = Jialinjiang Formation; A. = Abundance of plant fossil. The color of the lithology column shows the real rock color in the field.



1912

1913 **Figure 15.** Field panorama, sedimentology, representative animal and plant fossils of  
 1914 the Badong Formation from Hongjiaguan and Furongqiao sections. 1. Lithological  
 1915 boundary of Badong Formation Member 1 (left) and Member 2 (right); 2. Thick-  
 1916 bedded sandstone Member 2 (Bed 6 in figure 14); 3. *Myophoria (Costatoria)*  
 1917 *goldfussi*; 4. *Myophoria (Costatoria) goldfussi mansuyi*; 5. *Leptochondria albertii*; 6.  
 1918 *Euestheria* sp.; 7. *Lotosaurus* in Member 2 in Furongqiao village; 8. Long-distance

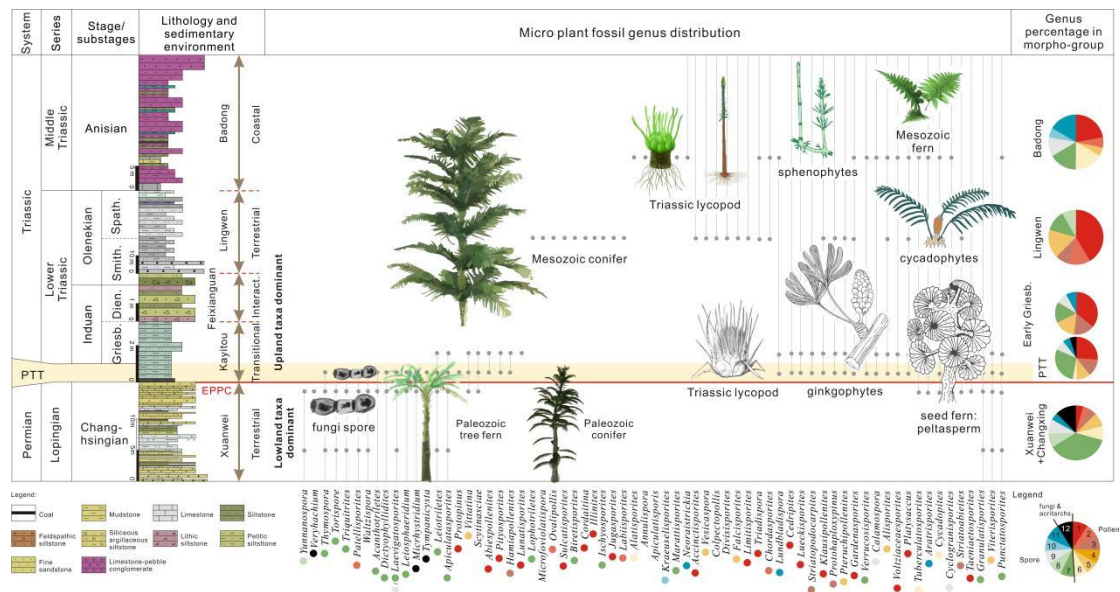
1919 transported plant fragments in sandstone from Member 2; 9 *Lepacyclotes* (= *Annalepis*)  
 1920 *sangzhiensis* in the Hongjiaguan section (collected by Fansong Meng); 10. *Yuccites*  
 1921 sp.; 11. Preserved in-situ *Pleuromeia sanxiaensis* in the Dawotang section, Fengjie,  
 1922 Sichuan (collected by Fansong Meng).  
 1923



1924  
 1925 **Figure 16.** Lithology, sedimentary, macro plant fossil distribution range, floral  
 1926 composition from End Permian Changhsingian to Middle Triassic Anisian in South  
 1927 China area. Kayitou Formation conformably overlies on Xuanwei Formation, while  
 1928 Kayitou, Feixianguan, Lingwen and Badong formation does not directly connect with  
 1929 each other and are divided by dash line. Xuanwei Formation: terrestrial facies;  
 1930 Kayitou Formation: terrestrial marine transitional facies; Feixianguan Formation:  
 1931 terrestrial marine interacting facies; Lingwen Formation: terrestrial facies; Badong  
 1932 Formation: coastal facies. Legend of macro plant morpho group: 1. conifer, 2.  
 1933 gymnosperm, 3. peltasperm, 4. seed fern, 5. cordaites, 6. ginkgophyte, 7. cycadophyte,  
 1934 8. Noeggerathiales, 9. gigantopterid, 10. fern, 11. fern or seed fern, 12. sphenophyte,  
 1935 13. Paleozoic lycopod, 14. Triassic lycopod. All the plant reconstructions are not to  
 1936 scale. Reconstruction of *Lepidodendron*, *Lepacyclotes*, Paleozoic conifer, Paleozoic  
 1937 tree fern and *Calamite* are drawn by Huisu studio, *Tomiostrabus* reconstruction comes  
 1938 from Naugolnykh (2012), ginkgophytes is modified after Zhou (1990), gigantopterids

1939 comes from Yang (1987), others come from Zhen Xu.

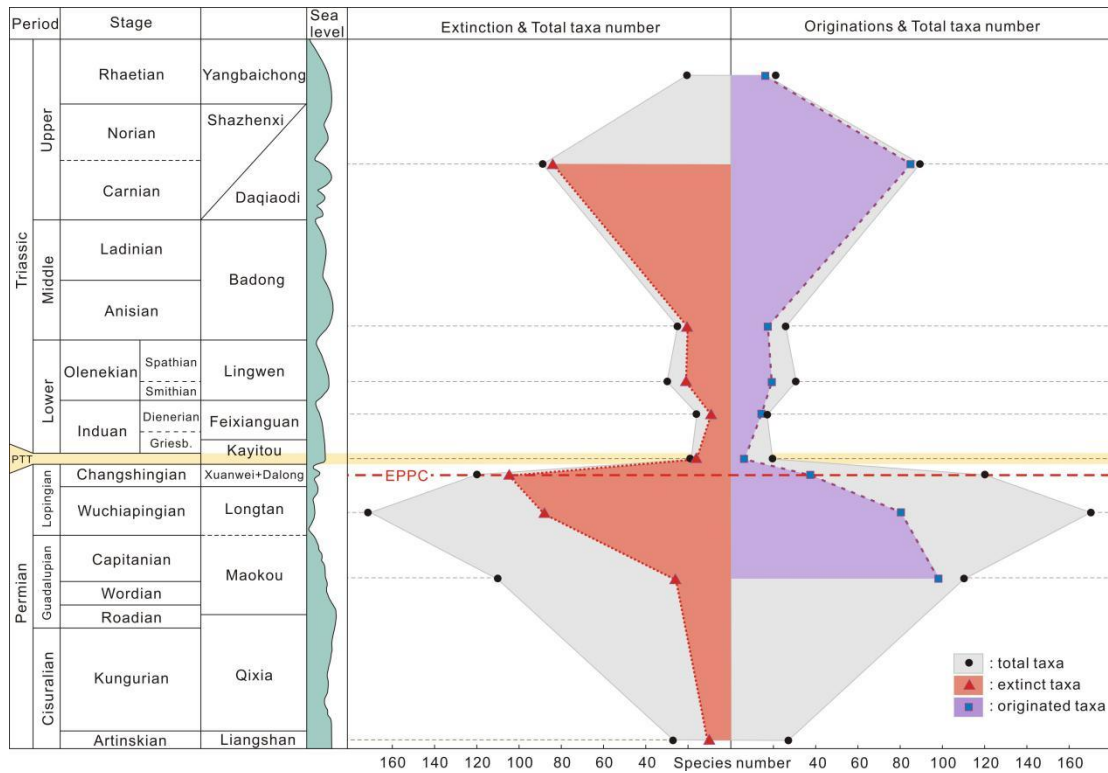
1940



1941

1942 **Figure 17.** Lithology, sedimentary, micro plant fossil distribution range, floral  
 1943 composition from End Permian Changhsingian to Middle Triassic Anisian in South  
 1944 China area. Kayitou Formation conformably overlies on Xuanwei Formation, while  
 1945 Kayitou, Feixianguan, Lingwen and Badong formation does not directly connect with  
 1946 each other and are divided by dash line. Xuanwei Formation: terrestrial facies;  
 1947 Kayitou Formation: terrestrial marine transitional facies; Feixianguan Formation:  
 1948 terrestrial marine interacting facies; Lingwen Formation: terrestrial facies; Badong  
 1949 Formation: coastal facies. Legend of micro plant morpho group: 1. conifer, 2.  
 1950 gymnosperm, 3. peltasperm, 4. cordaites, 5. ginkgophyte, 6. cycadophyte, 7. fern, 8.  
 1951 fern or seed fern, 9. sphenophyte, 10. Paleozoic lycopod, 11. Triassic lycopod, 12.  
 1952 fungi or acritarchs spore. All the plant reconstructions are not to scale. Reconstruction  
 1953 of Middle Triassic lycopod, Paleozoic tree fern are drawn by Huisu studio, Early  
 1954 Triassic lycopod reconstruction comes from Naugolnykh (2012), ginkgophytes is  
 1955 modified after Zhou (1990), peltasperm cone comes from Naugolnykh (2000),  
 1956 Paleozoic conifer comes from Corey A. Ford, others come from Zhen Xu.

1957



1958

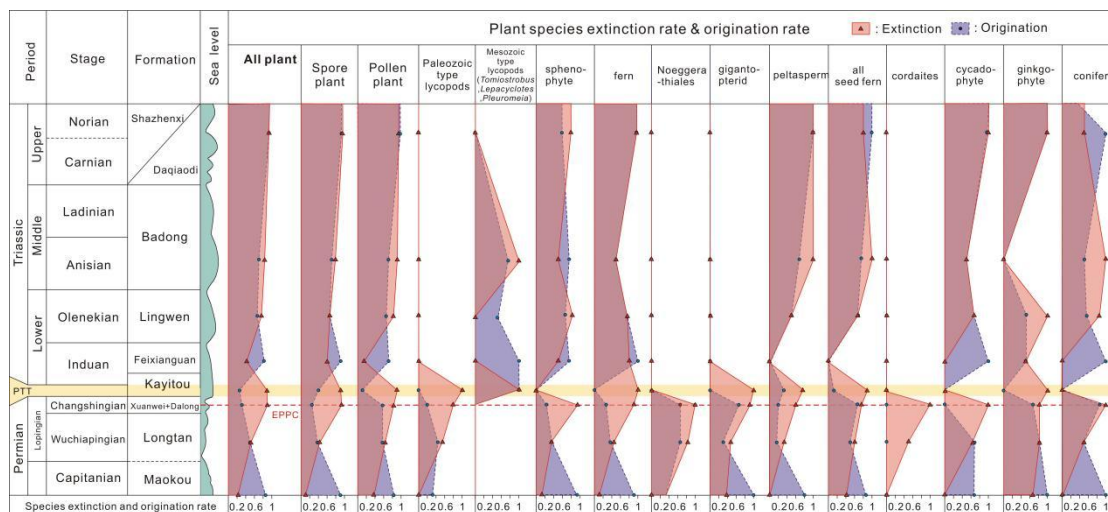
1959 **Figure 18.** Diversity trends for fossil plant species from the Middle Permian Qixia

1960 Formation to the Late Triassic Yangbaichong Formation showing originations,

1961 extinction and total taxon number. PTT = Permo-Triassic transition; Griesb. =

1962 Griesbachian; EPPC = End Permian Plant Crisis.

1963



1964

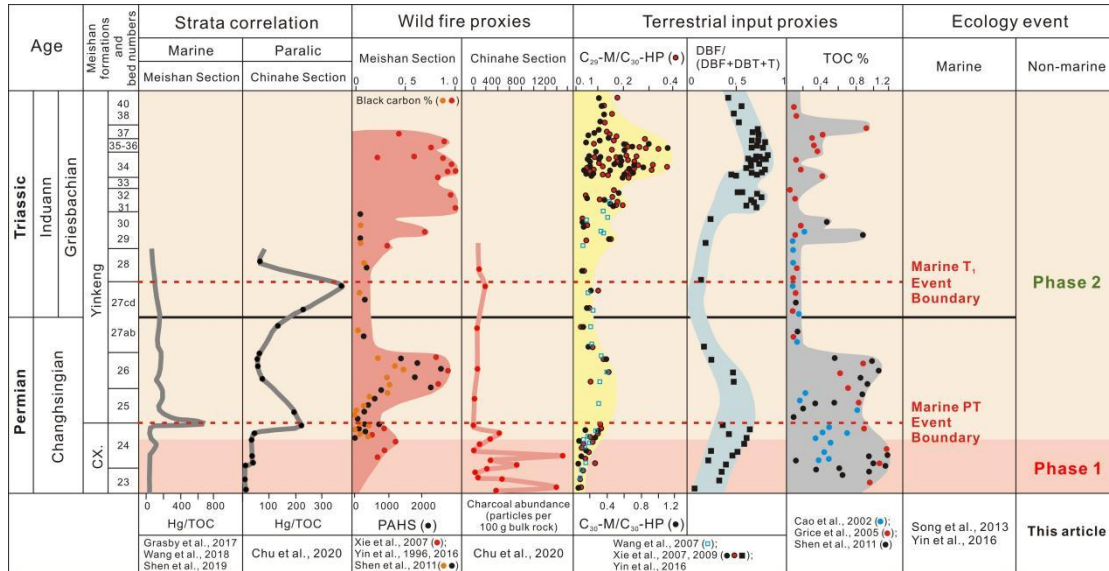
1965 **Figure 19.** Extinction and origination rates from the Middle Permian Maokou

1966 Formation to the Late Triassic Dajing Formation showing origination and extinction

1967 rates for individual plant groups (PTT = Permo-Triassic transition; EPPC = End

1968 Permian Plant Crisis; Red solid line and red area denote extinction rate; purple dashed  
 1969 line and blue–purple area denote origination rates).

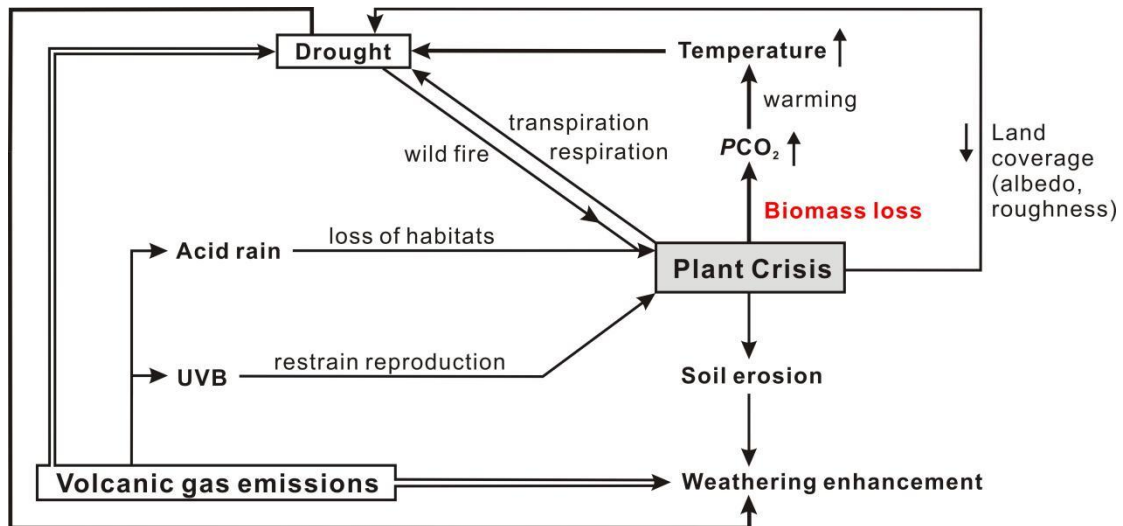
1970



1971

1972 **Figure 20.** High-resolution comparison between terrestrial events and marine  
 1973 feedback from the End-Permian GSSP Meishan section Bed 23 to Early Triassic Bed  
 1974 40. C. X. = Changhsingian; modified from Yin et al. (2016).

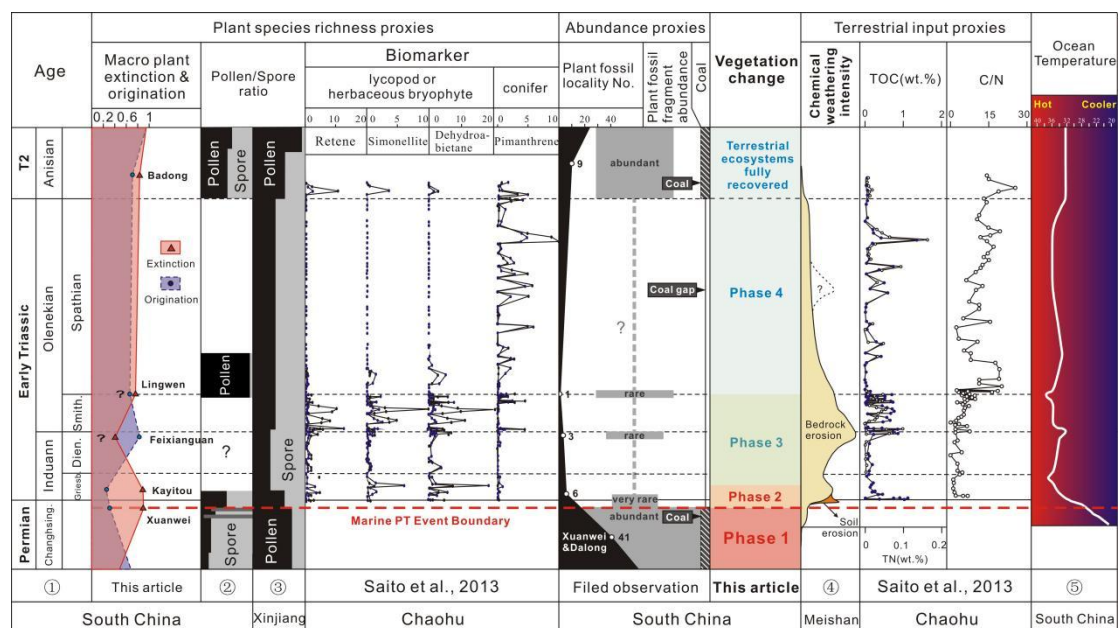
1975



1976

1977 **Figure 21.** Hypotheses for the relationships between environmental changes and plant  
 1978 distribution emphasizing how changes contribute to episodes of plant species richness  
 1979 crisis, and in return causes environmental change.

1980



1981  
 1982 **Figure 22.** Comparison between floral change pattern proxies from macro plant  
 1983 fossils, coal, palynology, biomarker and environment event such as terrestrial input,  
 1984 marine feedback, marine temperature through the End-Permian Changhsingian to  
 1985 Middle Triassic Anisian. Changhsing. = Changhsingian; Griesb. = Griesbachian; Dien.  
 1986 = Dienerian; Smith. = Smithian; T2 = Middle Triassic. (1). Stratal data from Burgess  
 1987 et al. (2014); (2) Palynology data from Changhsingian to Induan of South China from  
 1988 Zhang et al. (2004), Yu et al. (2008), Ouyang et al. (2007), Olenekian Lingwen of  
 1989 South China from Zhang et al. (1992) and Middle Triassic Anisian of South Chin  
 1990 from Qu et al. (1990) and Meng et al. (1995) ; (3) Palynology data of Dalongkou  
 1991 section, Xinjiang Province, from Changhsingian to Anisian from Qu et al. (1986); (4)  
 1992 Chemical weathering rate from Algeo et al. (2011); (5) Oceanic temperature from Sun  
 1993 et al. (2012).

1994

1995



1996

Formation	Stem ( <i>Lepidodendron</i> )	Root ( <i>Stigmaria</i> )	Megasporophyll ( <i>Lepidostrobophyllum</i> )	Cone ( <i>Lepidostrobus</i> )	Species richness	
					Non-normalised	Normalised
Xuanwei	<i>L. acutangulum</i> <i>L. lepidophylloides</i> <i>L. oculus-felis</i>	<i>S. ficoides</i> <i>S. rugulosa</i> <i>S. radiatopunctata</i> <i>S. sp.</i>	<i>L. xiphidum</i>		8	3
Longtan	<i>L. lepidophylloides</i> <i>L. polygonale</i> <i>L. xuanweiense</i> <i>L. emeishanense</i> <i>L. oculus-felis</i>	<i>S. ficoides</i> <i>S. rugulosa</i> <i>S. sp.</i>	<i>L. caudatum</i> <i>L. hastum</i> <i>L. junlianense</i> <i>L. mucronatum</i>	<i>L. acutisquamis</i>	13	5
Maokou	<i>L. asymmetricum</i> <i>L. oculus-felis</i>	<i>S. ficoides</i> <i>S. sp.</i>	<i>L. caudatum</i>		5	2
Qixia	<i>L. asymmetricum</i> <i>L. oculus-felis</i> <i>L. cf. szeianum</i>	<i>S. ficoides</i> <i>S. sp.</i>			5	3

1997

1998 Table 1. organ taxa for stems (*Lepidodendron*), rootstock (*Stigmaria*), sporophylls (*Lepidostrobophyllum*) and cones (*Lepidostrobus*). In each  
 1999 formation, stems represent the best measure of species richness as they present the most reliable features to distinguish species, and in each case  
 2000 show the largest species richness compared to the other organs present. While more species of rootstock are present in the Xuanwei Formation,

2001 we consider this an unreliable measure of species richness. Species delimitation is less reliable in species of *Stigmaria* that have few  
2002 distinguishing features that may vary in different positions across the rooting system. Furthermore, one of the rootstock accounts from the  
2003 Xuanwei Formation has not been identified to the species level (*Stigmaria* sp.) and most likely represents a poorly preserved or incomplete  
2004 specimen of one or more of the other species present. In all cases non-normalised estimates significantly inflate species richness estimates.

2005

2006